

The ECHO of Cell Polarity

Revealing intra- and extracellular factors involved in polarity and axis formation *de novo* in tobacco cells

Zur Erlangung des akademischen Grades einer

DOKTORIN DER NATURWISSENSCHAFTEN

(Dr. rer. nat.)

von der KIT-Fakultät für Chemie und Biowissenschaften

des Karlsruher Instituts für Technologie (KIT)

genehmigte

DISSERTATION

von

M. Sc. Linda Aimee Brochhausen

1. Referent/Referentin: Prof. Dr. Peter Nick
 2. Referent/Referentin: Prof. Dr. Martin Bastmeyer
- Tag der mündlichen Prüfung: 17.10.2017

“The man behind the microscope

Has this advice for you:

Never ask what something Is

Just ask, what does it Do?”

- Hilaire Belloc (1870-1953)

Die vorliegende Dissertation wurde am Botanischen Institut des Karlsruher Instituts für Technologie (KIT) - Universitätsbereich, Lehrstuhl 1 für Molekulare Zellbiologie, im Zeitraum von März 2014 bis September 2017 angefertigt.

Hiermit erkläre ich, dass ich die vorliegende Dissertation, abgesehen von der Benutzung der angegebenen Hilfsmittel, selbständig verfasst habe.

Alle Stellen, die gemäß Wortlaut oder Inhalt aus anderen Arbeiten entnommen sind, wurden durch Angabe der Quelle als Entlehnungen kenntlich gemacht.

Diese Dissertation liegt in gleicher oder ähnlicher Form keiner anderen Prüfungsbehörde vor.

Karlsruhe im September 2017

Danksagung

An dieser Stelle möchte ich mich besonders bei Professor Dr. Peter Nick bedanken, dessen großer wissenschaftlicher Enthusiasmus mich immer zusätzlich motivierte. Professor Dr. Peter Nick gab mir sowohl den Raum frei und selbstständig zu arbeiten, als auch die Möglichkeit, mich jeder Zeit mit Fragen an ihn zu wenden und unterstütze mich dabei ausnahmslos. Für das in mich gesetzte Vertrauen sowie die hervorragende Betreuung während meiner Doktorarbeit möchte ich mich ganz herzlich bedanken.

Mein herzlicher Dank gilt Professor Dr. Martin Bastmeyer für die Übernahme des Korreferats und den weiteren Mitgliedern des Komitees.

Dr. Jan Maisch möchte ich ganz herzlich für die konstruktiven Ratschläge, Anregungen und vielen Bestärkungen während meiner Arbeit danken.

Vielen Dank an alle Kollegen und all die ehemaligen Kollegen des botanischen Instituts, die mich während meiner Arbeit inspiriert haben, für die tolle Arbeitsatmosphäre. My sincere thanks go to all members and alumni of the Botanical Institute I for your inspiration and the amazing working atmosphere! 谢谢!

Ein großes Dankeschön gebührt den technischen Assistenten und auszubildenden Laboranten des Botanischen Instituts für die exzellente Unterstützung im Labor, die den reibungslosen Laboralltag erst ermöglichen.

Many thanks to Dr. Jaideep Mathur, his wife Neeta and the other lab members from the University of Guelph, for the precious advices, great discussions and the time you spend for showing new methods during my stay. You made me feel welcome in Canada from the first moment on.

Für den liebevollen Rückhalt während des Studiums und der Promotion möchte ich nicht zuletzt meiner Familie danken. Dabei bedanke ich mich für die vielen Ratschläge besonders bei meiner Schwester Lucie und bei Maarten. Heel hartelijk bedankt! Von ganzem Herzen möchte ich Christian für die moralische Stärkung während des Studiums und für die Unterstützung unserer gemeinsamen Zukunft danken. Mein größter Dank gebührt meinen Eltern, die mich mit großem Interesse unterstützt haben und immer an mich glaubten. Für die Gewissheit, dass ihr immer hinter mir steht, bin ich unendlich dankbar.

Zusammenfassung

Für alle eukaryotischen Lebewesen spielt die Zellpolarität eine entscheidende Rolle bei unterschiedlichen zellulären Funktionen. Eine fehlerhafte Zellpolarisation kann oftmals mit schweren Krankheitsbildern einhergehen. Den Mechanismus der Polaritätsbildung zu verstehen, stellt daher eine wesentliche Aufgabe in der Grundlagenforschung dar.

Im Gegensatz zu Tieren ist bei Pflanzen die „Direktionalität“ auf einzelne Zellen zurückzuführen. Nach jeder Zellteilung muss sich die „Richtung“ wieder neu aufbauen. Wie die Pflanzenzelle jedoch Polarität und Achse wiederherstellt ist bisher unklar und die zentrale Fragestellung dieser Doktorarbeit. Hierfür wurden extrazelluläre sowie intrazelluläre Faktoren untersucht, welche an der Achsenbildung beteiligt sind. In einem experimentellen System basierend auf regenerierenden Protoplasten konnte die Bildung der Zellachse *de novo* mittels Quantifizierung bestimmter Regenerationsstadien analysiert werden.

Die Kernbewegung und -positionierung sind entscheidend für die Morphogenese der Pflanzenzelle. Um herauszufinden, ob die Kernposition maßgebend für die Polaritätsentwicklung ist, wurden Überexpressionslinien mit fluoreszent markierten extranukleären (perinuklearer Aktinkorb, KCH Kinesine) sowie intranukleären (Histon H2B) Faktoren untersucht, welche auf die Kernpositionierung wirken. Zeitrafferaufnahmen früher Regenerationsstadien zeigten jedoch entgegen anfänglicher Annahmen, dass eine zentrale Kernposition keine Voraussetzung für die Ausbildung einer Zellachse ist. Zusätzlich enthüllten die quantitative Analyse und Identifikation des Kernproteoms Unterschiede in der Histonmenge dieser transgenen Überexpressionslinien im Vergleich zu nicht transformierten Zellkernen. Obwohl die Kernposition und Zellachsenbildung nicht direkt miteinander verknüpft sind, sind beide Phänomene eindeutig von extra- und intranukleären Faktoren abhängig, welche sich auf die sogenannte „*Tensegrity*“, d.h. das mechanische Zusammenspiel von Spannung („*tension*“) und Zusammenhalt („*integrity*“) des Cytoskeletts, auswirken. Mittels verschiedener Überexpressionslinien und pharmakologischer Untersuchungen konnte die Rolle der (i) Dynamik des Cytoskeletts, (ii) Motorproteine sowie von (iii) Histonen und (iv) Kernmembranproteinen in Bezug auf die Achsenbildung aufgedeckt werden. Zudem konnte mittels Nanofasern, welche entweder geordnet ausgerichtet oder ungeordnet waren, erstmals gezeigt werden, dass auch die Strukturen von extrazellulären Faktoren wie RGD Peptiden an der pflanzlichen Zellachsenbildung beteiligt sind.

Zusammengefasst wurden diese Ergebnisse schlussendlich in einem Modell, bei welchem retrograde Signale für die Polaritätsbildung erforderlich sind. Diese Signale wandern über das dynamische Cytoskelett vom Zellkern nach außen zur Plasmamembran und wieder zurück von der Zellwand in Richtung des Zellkerns. Aus diesem Modell ergeben sich neue Impulse, um in Zukunft lokale Unterschiede in der Dynamik des Cytoskeletts und dessen Motorproteine während der Achsenregeneration mittels modernsten mikroskopischen Methoden zu detektieren.

Betrachtet man das Gesamtbild, führten die Ergebnisse dieser Doktorarbeit zu einem universellen Konzept, welches für alle eukaryotischen Reiche Gültigkeit besitzen könnte und besagt, dass die Zellpolarität basierend auf der mechanischen „*Tensegrity*“ und chemischen Signalwirkung von einem engen und kontinuierlichen Zusammenspiel der Extrazellulären Matrix, des Cytoskeletts, Hormonen und anderen Signalmolekülen, sowie Organellen (kurz: ECHO-Prinzip) reguliert würde. Gelangen die Signale zum Zellkern antwortet dieser möglicherweise wie bei einem Echo und die Signale werden zurück zur Plasmamembran transportiert.

Abstract

Within all prokaryotic kingdoms cell polarity plays an indispensable role for various cellular functions. Failure in cell polarity can often result in serious diseases. Thus, understanding the mechanism behind polarity formation assigns a fundamental task to basic research.

In contrast to mammalian cells, directionality is a fixed characteristic of plant cells. However, after division, this “direction” must be re-established. How cells acquire polarity and axis presents a central question of plant morphogenesis and represents the aim of this study. Therefore, the role of extracellular as well as intracellular candidates for axis formation was analyzed by using an experimental system based on regenerating protoplasts, where the induction of a cell axis *de novo* can be followed by quantification of specific regeneration stages.

Nuclear migration and positioning are crucial for the morphogenesis of plant cells. The potential role of nuclear positioning for polarity induction was addressed by using overexpression of fluorescently tagged extranuclear (perinuclear actin basket, KCH kinesins) as well as intranuclear (histone H2B) factors of nuclear positioning. Time-lapse series of the early stages of regeneration showed that a central nuclear position is not a prerequisite for axis formation. Additionally, sophisticated quantification methods combined with computational analysis of nuclear proteome indicated differences in histone abundance of these transgenic overexpression lines, where nuclear migration was altered compared to the non-transgenic nuclei. Although nuclear positioning and cell axis formation were uncoupled, both phenomena are clearly dependent on the extra- and intranuclear factors affecting cytoskeletal tensegrity. Via different overexpression lines and pharmacological approaches, this study revealed how (i) cytoskeletal dynamics and (ii) motor proteins, as well as (iii) histones and (iv) nuclear membrane proteins are involved in axis formation. Further, it was demonstrated for the first time in plants that the structural organization of extracellular factors such as RGD peptides is significantly involved in axis formation, indicated by using aligned and unaligned nanofibers.

Together, these findings were integrated into a model where retrograde signals are required for polarity induction. These signals travel via the cytoskeleton from the nucleus towards targets at the plasma membrane and back from the cell wall towards the nucleus. To refine this model, advanced microscopy techniques such as color recovery after photoconversion

should be used in the future, as it would unravel local differences in dynamics of the cytoskeleton and motor proteins.

Drawing the bigger picture, the results of this thesis lead to a general concept that could be valid for all eukaryotic kingdoms. It claims that cell polarity might be regulated by the close interplay of extracellular matrix, cytoskeleton, hormones and other signaling molecules, and organelles (abbreviated as the ECHO-principle) based on a mechanical tensegral mechanism together with chemical signaling. Received at the nucleus, extracellular signals could be “echoed” back to the plasma membrane.

Table of contents

Danksagung	IX
Zusammenfassung.....	XI
Abstract	XIII
List of abbreviations	XVII
1 INTRODUCTION.....	1
1.1 Back to basics – Lost and found of plant cell polarity	1
1.2 Factors of nuclear migration and their role in cell polarity	2
1.2.1 Is the moving nucleus a pacemaker for cell polarity?	2
1.2.2 Kinesin with a calponin-homology domain – KCH walking around the nucleus... 3	
1.2.3 Perinuclear basket – An actin basket wrapping the nucleus	4
1.2.4 From extranuclear to intranuclear factors – Manipulation of nuclear architecture	5
1.3 Differences in nuclear proteome or two peas in a pod?	6
1.4 Hunting for further factors involved in directional axis formation	6
1.4.1 Need for speed – Cytoskeletal dynamics and motors.....	7
1.4.2 Myosin XI – Molecular motor moving along microfilaments.....	8
1.4.3 It’s all about connection – Revealing the LINC between intra- and extranuclear factors.....	8
1.5 From outer space – From intracellular to extracellular candidates	11
1.6 Scope of the Dissertation.....	11
2 MATERIAL AND METHODS.....	15
2.1 Cell lines, protoplast generation, and manipulation of regeneration.....	15
2.1.1 Cell lines and cultivation.....	15
2.1.2 Generation and regeneration of protoplasts	17
2.1.3 Chemical treatments of regenerating protoplasts.....	17
2.2 Analysis of nuclei	18
2.2.1 Isolation of nuclei	18
2.2.2 Protein separation	19
2.2.3 Proteomics – Tandem mass spectrometry.....	20
2.2.4 Data processing – From matrix to heat map.....	20
2.3 Generation of RGD peptides and nanofibers	22
2.3.1 Electrospinning the nanofibers	23
2.3.2 Surface modification of PCL nanofibers	24
2.3.3 Regeneration of protoplasts on RGD plotted nanofibers	24
2.4 Microscopy and quantifications	25
3 RESULTS	27
3.1 Nuclear position can be separated from axis formation	28
3.2 Nuclear proteomes of H2B-mEos and Lifeact-psRFP differ compared to BY-2 wildtype	30
3.3 Cytoskeletal dynamics, motors as well as intranuclear factors are involved in axis formation	37
3.3.1 Classification of different regeneration stages	37

3.3.2	The perinuclear basket, actin dynamic, and motor protein myosin XI are involved in axis formation	39
3.3.3	Microtubules and their motor proteins are involved in axis formation	47
3.3.4	The interior of the nucleus and its membrane proteins affect axis formation ..	51
3.3.5	Summing up.....	55
3.4	Aligned structures of RGD peptides promote axis formation	57
3.5	Summary.....	60
4	DISCUSSION	63
4.1	Polarity and its link to nuclear migration	64
4.1.1	A central position of the nucleus is not a prerequisite for polarization	64
4.1.2	Nuclear positioning depends on perinuclear actin, KCH, and chromatin structure	67
4.2	Nuclear migration and its link to nuclear proteome	69
4.3	Polarity depends on tensegrity and intracellular logistics	71
4.4	Polarity and its link to external structures	78
4.5	Conclusion and the ECHO of cell polarity	81
4.6	Outlook	85
4.6.1	How to make intracellular dynamic visible and measurable?	85
4.6.2	Translation to the protoplast system	86
5	APPENDIX.....	89
5.1	Vectors of myosin lines.....	89
5.2	Protein analysis of BY-2 WT, H2B-mEos, and Lifeact-psRFP nuclei.....	91
5.3	Regeneration analysis – Additional diagrams and figures	99
5.4	SEM analysis of aligned and unaligned nanofibers	106
5.5	ECHO research – Four key players, three kingdoms, two mechanisms, one concept	108
5.6	Supplemental experimental procedure	109
6	ACKNOWLEDGEMENTS.....	111
7	REFERENCES.....	113

List of abbreviations

AF	actin filament
BY-2	<i>Nicotiana tabacum</i> L. cv. Bright Yellow 2
CSC	cellulose synthase complex
DCB	2,6-Dichlorobenzonitrile
EB	end-binding protein
ECHO	extracellular, cytoskeleton, hormones and signaling molecules, organelles
ECM	extracellular matrix
GFP	green fluorescent protein
H2B	histone 2B
INM	inner nuclear membrane
KCH	Kinesin with calponin homology domain
LINC	Linker of nucleoskeleton and cytoskeleton
LFQ	label-free quantification
MS	Murashige and Skoog medium
MS/MS	Tandem Mass Spectrometry
MT	microtubules
Nt	<i>Nicotiana tabacum</i>
ONM	outer nuclear membrane
Os	<i>Oryza sativa</i>
PCL	polycaprolactone
psRFP	photoswitchable red fluorescent protein
RGD	arginine-glycine-aspartate amino acid sequence
SDS-PAGE	sodium dodecyl sulfate polyacrylamide gel electrophoresis
SUN	Sad1 and UNC-84 homology
WIP	WPP (tryptophan-proline-proline motif) domain-interacting protein
WIT	WPP (tryptophan-proline-proline motif) domain-interacting tail-anchored protein
WT	wildtype

1 INTRODUCTION

Looking out of the window one can observe that from huge trees to little grasses, the roots of plants always grow into the earth and shoots in the opposite direction. But how does a single plant cell manage to tell its direction? How cells acquire polarity and axis remains a central question of plant morphogenesis and development.

For all eukaryotic organisms from yeast to mammals polarity plays an important role in morphogenesis (Schierenberg 1987; Nick and Furuya 1992; St Johnston and Nüsslein-Volhard 1992; Goodner and Quatrano 1993; Verde *et al.* 1995; Madden and Snyder 1998; Lyczak *et al.* 2002; Roignot *et al.* 2013), migration (Etienne-Manneville and Hall 2001), pathogen response, and in the immune system (Schmelzer 2002; Lipka and Panstruga 2005; Billadeau *et al.* 2007). Failure in polarity formation leads to serious consequences, which can result in cancer (Wodarz and Nathke 2007; Lee and Vasioukhin 2008; Ellenbroek *et al.* 2012). Therefore, understanding the mechanism behind polarity formation represents a fundamental task in basic research.

Whilst polarity in animals is usually systemic in nature and is generated through the interaction of different cell types, plant polarity seems to be rooted directly within the individual cell (Vöchting 1878). Thus, directionality is a fixed characteristic of plant cells. Axis and polarity are mostly inherited from the maternal cell (Nick 2011), raising the question of how polarity and axis are established *de novo*.

1.1 Back to basics – Lost and found of plant cell polarity

A classic system for polarity induction has been the *Fucus* zygote (Goodner and Quatrano 1993; Hable and Hart 2010). Similar cases of symmetrical, and freely accessible cells, which undergo formative divisions, are rare in higher plants.

As alternative to study polarity induction *de novo*, polarity can be artificially eliminated by digesting the cell wall with cellulases. This approach yields protoplasts, which, in most cases, are round and appear to have lost axis and polarity. Nevertheless, they can be induced to regenerate complete plants, as has been demonstrated for the first time in tobacco (Nagata

and Takebe 1970). Tobacco BY-2 (Bright Yellow 2) cell cultures provide a perfect model system since their ability to generate multicellular cell files with a clear axis and polarity is a characteristic feature of these cultures (Nagata *et al.* 1992; Nick 2010). Upon standardization of the protoplast system, Zaban *et al.* (2013) were able to generate quantitative data on the temporal patterns of regeneration due to classification into distinct stages. The synthesis of a new cell wall marks the transition to the first important stage of regeneration and proceeds, within a few minutes, after a long preparatory phase. During this preparatory phase, the nucleus migrates actively. This indicates that nuclear migration is linked with the induction of polarity in axis.

1.2 Factors of nuclear migration and their role in cell polarity

Nuclear migration has been described in great detail for many different organisms such as *Drosophila melanogaster*, *Saccharomyces cerevisiae*, *Aspergillus nidulans*, and *Caenorhabditis elegans* (for review see Morris 2000; Morris 2003). The molecular components responsible for positioning and movement of the nucleus are moderately conserved among these well-characterized model organisms and comprise dynein, dynactin, as well as other microtubule and actin linker proteins.

1.2.1 Is the moving nucleus a pacemaker for cell polarity?

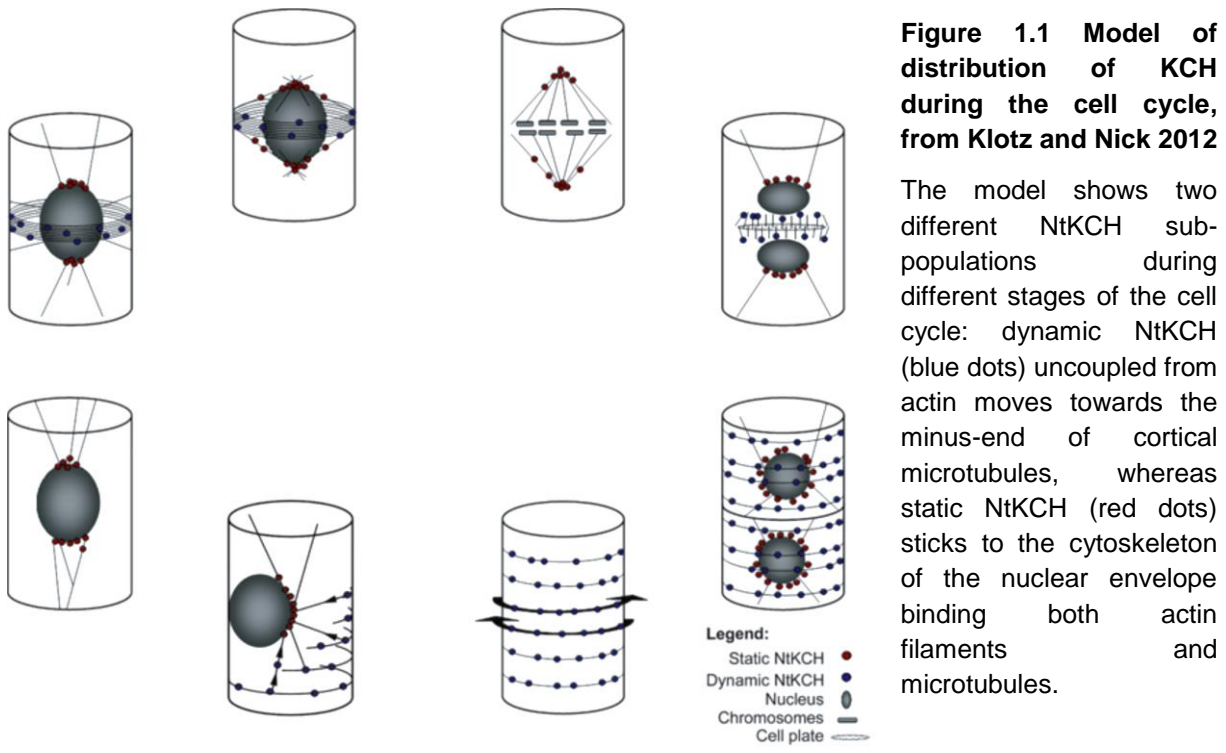
Nuclear migration also plays a pivotal role for a wide range of several cellular processes in plants. These include development of pollen tubes, trichomes, and root hairs, symbiotic and pathogenic plant-microbe interactions, responses to mechanical and blue light stimuli, and symmetric, as well as asymmetric cell divisions (for review see Griffis *et al.* 2014). As characterized for stomatal development, pre-mitotic nuclear migration is linked to the position of asymmetric division planes that are oriented with respect to the polarity of the mother cells (for review see Smith 2001). Several examples exist demonstrating the importance of nuclear positioning for symmetry and plane of the ensuing cell division, although the mechanistic link between nuclear migration and the induction of cell axiality is far from being understood.

In the experimental protoplast regeneration model mentioned above (Zaban *et al.* 2013), the re-establishment of a cell wall is heralded by a phase of vivid nuclear motility, where the

nucleus is searching for a central position, similar to the situation when a vacuolated cell prepares for cell division. Here, the position of the nucleus determines the division plane while cytoplasmic strands rearrange in a pattern predicting the site of the prospective cell plate (for review see Nick 2008). Both cytoskeletal elements - actin filaments as well as microtubules - participate in nuclear migration and tethering (Katsuta and Shibaoka 1988). Unlike nuclear positioning in fungi and insects, plants lack dynein and thus a dynactin complex. Therefore, they must employ other proteins for the dynamic cross-link of actin and microtubules in pre-mitotic nuclear migration.

1.2.2 Kinesin with a calponin-homology domain – KCH walking around the nucleus

In fact, a plant-subgroup of the kinesin-14 family, the KCH kinesins (for ‘kinesins containing a calponin-homology domain’) were identified as microtubule-actin filament cross-linkers (for review see Schneider and Persson 2015). As these motor proteins are capable of minus-end directed movement, the KCHs might be the functional homologs of dyneins. In addition to the characteristic microtubule-binding kinesin motor domain, KCH-proteins possess a conserved calponin-homology (CH) domain, well known as actin binding motif from a variety of actin-associated proteins such as α -actinin, spectrin and fimbrin. Thus, KCHs mediate between both cytoskeletal elements and bind to both elements of the cytoskeleton. Both the rice member OsKCH as well as the tobacco member NtKCH have been shown to modulate premitotic nuclear positioning in tobacco BY-2 (Frey *et al.* 2010; Klotz and Nick 2012). To understand the role of nuclear migration in cell polarity, two facts of KCH play an important role: KCH exists in two functionally different sub-populations, either uncoupled from actin in a mobile form that moves along microtubules of the interphase cortex and the phragmoplast, or coupled to actin in a static form in the premitotic radial array of cytoplasmic microtubules (see Figure 1.1 from Klotz and Nick 2012). This actin-bound form of KCH also accumulates on the nuclear envelope prior to the onset of mitosis, suggesting a role of actin-linked KCH for nuclear positioning.



1.2.3 Perinuclear basket – An actin basket wrapping the nucleus

In animal cells, the nuclear envelope is structured by a subtending nuclear lamina, which is highly important for nuclear positioning and movement. Several proteins link the lamins to the cytoskeleton (Malone *et al.* 1999; Lee *et al.* 2002). However, nuclear lamins have remained elusive in plant cells so far. Instead, a perinuclear actin basket has been reported (Wang and Nick 1998). Recently, this perinuclear actin basket was specifically visualized by a tetrameric Lifeact fused to a photoswitchable red fluorescent protein (Lifeact-psRFP). The yeast peptide Lifeact is well known to bind to a ubiquitous motif in F-actin. In Durst *et al.* (2014) it was fused to a tetrameric photoswitchable red fluorescent protein (psRFP, Fuchs 2011). Due to its large size, this fusion construct should be sterically prevented from binding to actin via the Lifeact motif, when the actin filament is densely decorated with actin-binding proteins, whereas the construct should readily bind to uncovered actin (see Figure 1.2). Using this marker, z-stacks of the actin basket were collected by PALM in a resolution of 20 nm (Durst *et al.* 2014). Super-resolution microscopy showed that the perinuclear actin cage was wrapped around the nuclear envelope in a lamellar fashion.

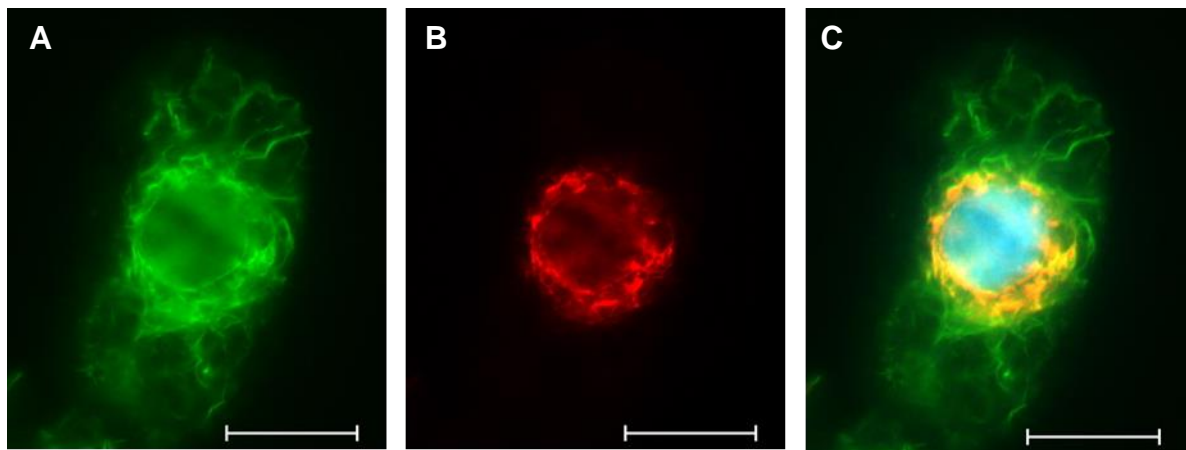


Figure 1.2 Visualization of actin filaments in Lifact-psRFP BY-2 cells by stably expressed Lifact-psRFP and AlexaFluor®488 phalloidin

Whole Lifact-psRFP BY-2 cell; green channel: AlexaFluor®488 phalloidin (A); red channel: Lifact-psRFP (B); (C) merge of (A) and (B), yellow signal marks colocalization, blue visualizes the nucleus, stained with Hoechst 33528. Scale bars: 20 μm . Published in Durst *et al.* 2014.

1.2.4 From extranuclear to intranuclear factors – Manipulation of nuclear architecture

Apart from extranuclear factors, the question arises if the interior of the nucleus might influence nuclear migration as well.

Within the nucleus, the DNA is wrapped around dimers of core histones (H2A, H2B, H3 and H4) forming the nucleosome, the structural unit of chromatin. Among all eukaryotic organisms histones are highly conserved and the most abundant proteins in the nucleus. Besides their role in DNA packaging, histones also play a role in the regulation of gene expression due to their modifications, acetylation, and methylation (for review see Rosa and Shaw 2013; Jiang and Berger 2017). The structure of the chromatin should influence nuclear migration as well. In fact, epigenetic changes in histone packaging can result in changes of nuclear architecture (Bartova *et al.* 2008). Overexpression of core histones such as in the line H2B-mEos (Wozny *et al.* 2012) might be used to test this assumption, which has not been addressed experimentally, so far.

1.3 Differences in nuclear proteome or two peas in a pod?

Indeed, this study will reveal alterations of nuclear migration as a result of manipulation of the three factors described above affecting extranuclear components (KCH, nuclear basket) as well as intranuclear components (H2B). These observations stimulate the question whether these manipulated nuclei differ in terms of their protein level compared to the non-transformed nuclei. As mentioned before, epigenetic changes in histone packaging can result in changes of nuclear architecture. This might be visible by a changed abundance of histones.

So far, plant nuclei have been characterized in *Arabidopsis thaliana* in response to stress (Calikowski *et al.* 2003) or to a modest number of proteins in rice (Khan *et al.* 2005; Petrovska *et al.* 2015). Although nuclear proteomics represents a major future field, a complete plant nuclear proteome has not been characterized to date. So far, the question if a changed nuclear migration leads to changed nuclear protein composition has never been addressed.

Biochemical approaches together with bioinformatical techniques in the field of nuclear proteome allow us to gain a deeper understanding of the function of the nucleus. Tandem mass spectrometry (MS/MS) represents a sophisticated tool for protein quantifications and enables highly probable identifications. Hitherto, the analysis and presentation of the huge data sets remained the bottleneck. However, the latest computational analysis tools enable clear illustrations of differences in protein abundances by generating heat maps (Tyanova *et al.* 2016). Using these tools, the nuclear proteome of overexpression lines can be compared to non-transformed lines to see if the histone amount has changed.

1.4 Hunting for further factors involved in directional axis formation

Since the nuclear migration might influence cell polarity, factors involved in nuclear migration could also play a role in axis formation itself. Therefore, this leads to two possible scenarios: 1.) Promotion or failure in axis formation could be a causality of an altered nuclear position or 2.) these factors act independently on nuclear migration and on axis formation at the same time. To confirm one of these hypotheses, previously mentioned key players (in connection with their role in nuclear migration), plus additional candidates including cytoskeletal

dynamics, the actin motor and nuclear membrane proteins, have to be investigated to understand their role in axis formation.

1.4.1 Need for speed – Cytoskeletal dynamics and motors

One of these candidates involved in nuclear migration is the cytoskeleton. However, cell shape and axis are maintained by the cytoskeleton as well. In animals, cells are shaped by the property of tensegrity (combination of tension and integrity). This neologism indicates the ability of the cytoskeleton to confer both traction and tension forces (Ingber 2003a, 2003b; Nick 2013). Yet, how does a cell expand in a certain direction with the tensegral framework and how can the axis be re-established after cell division? Furthermore, the plant cytoskeleton needs to sense and react to abiotic and biotic stimuli constantly and rapidly (Qiao *et al.* 2010; Smertenko and Franklin-Tong 2011). This is only possible due to the high cytoskeletal dynamic, which is defined by the rate of polymerization and depolymerization. The differences in polymerization and depolymerization rate between the two ends of actin filaments or microtubules lead to their polar structure (for reviews see Lee and Dominguez 2010 and Nick 2011). The overexpression of motor proteins, e.g. the microtubule motor protein kinesin KCH, could influence axis formation by binding and altering of microtubules (Klotz and Nick 2012).

Additionally, the dynamic or stability of the cytoskeletal components is influenced by actin-binding proteins (ABP) or microtubule-associated proteins (MAP) respectively, which are both responsible for crosslinking and bundling (Staiger *et al.* 2010; Akhmanova and Steinmetz 2015). Studies suggest that actin-binding proteins could differ in their decoration of actin subpopulations. The specific binding of Lifeact fused to the big tetramer might also influence stability of the perinuclear actin basket (Durst *et al.* 2014). Therefore, overexpression of the nuclear basket composed of cross-linked actin filaments might also influence cell axes. The manipulation of stabilization and destabilization is possible with cytoskeletal drugs, for instance by using Phalloidin, which binds filamentous actin; Latrunculin B, which sequesters G-actin; or Oryzalin, which eliminates dynamic microtubules via binding to α -tubulin (Maisch *et al.* 2009; Klotz and Nick 2012; Durst *et al.* 2014; Zaban *et al.* 2013).

The plant motor proteins consisting of kinesins and myosins present further proteins binding to the cytoskeleton. Using the cytoskeleton as the railway for the transport of their cargos,

the direction of the transport is determined by the polarity of the respective cytoskeletal element.

1.4.2 Myosin XI – Molecular motor moving along microfilaments

Whereas actin is a highly-conserved protein among all eukaryotic species, myosins arise in a high diversity. However, they show similarities in their structural organization. The fastest plant myosin is myosin XI. It consists of a motor domain with ATPase activity, an actin binding motif, IQ-domains that bind myosin light chains, and the tail domain which is responsible for binding the cargo (for review see Buchnik *et al.* 2015). Several studies have shown that myosins play a role in cell polarity of root hair, pollen tubes and mosses (Lenartowska and Michalska 2008; Vidali *et al.* 2010; Park and Nebenführ 2013). In moss *Physcomitrella patens* knock down of myosin XI resulted in a loss of cell polarity (Vidali *et al.* 2010). This in turn raises the question if overexpression of myosin XI leads to a promotion of cell polarity.

1.4.3 It's all about connection – Revealing the LINC between intra- and extranuclear factors

Since the cytoskeleton (with its nuclear basket, cytoskeletal dynamics and linkage via motor proteins) as well as intranuclear factors (involving the histone packaging) are assumed to be involved in axis formation, the question arises where the connection of the cytoskeleton and the inner nucleus can be found. If the nuclear migration is changed due to altered nuclear architecture, axis formation and cell shape could be altered as well. And if so, there must be a connection to the cytoskeleton via nuclear membrane proteins. To test this hypothesis to a larger extent, the role in axis formation of the nuclear membrane proteins should be studied in addition to those previously presented key players.

In fact, in animal cells so-called “linker of nucleoskeleton and cytoskeleton” (LINC) complexes that link histones with the cytoskeleton have been identified within the nuclear membrane. They are responsible for chromosome segregation, nuclear shape and nuclear migration during the development or in response to stress (Starr 2009, 2011). The LINC complex in metazoans consists of inner nuclear membrane (INM) proteins with Sad1/ Unc-84 domains (SUN) that interact with lamin and proteins of the outer nuclear membrane (ONM) with Klarsicht/ANC-1/Syne homology domains (KASH), which connect the ONM to the cytoskeleton

(Wilhelmsen *et al.* 2006; Schneider *et al.* 2008; Razafsky and Hodzic 2009; Starr 2009). SUN proteins interact with intranuclear components, while KASH proteins recruit cytoplasmic elements (Crisp *et al.* 2006; Starr 2011; Zhou and Meier 2013). SUN proteins are highly conserved among eukaryotes. In contrast, KASH domain proteins as described in metazoans have been elusive in plants so far. Nevertheless, homologs called tryptophan-proline-proline (WPP)-interacting protein (WIP) have been identified (Zhou *et al.* 2012; Tamura *et al.* 2013). Another protein has been identified that interacts with the WPP domain, called the WPP domain-interacting tail-anchored (WIT) protein. These WIT proteins also interact with myosin XI-I and thus connect the nuclear envelope to actin filaments (Tamura *et al.* 2013). The complex formed by WIT, WIP and SUN might be analogous to the metazoan LINC complex (Figure 1.3).

LINC complexes in animals receive great attention in current research. In contrast, analogous studies in plant cells are relatively at the beginning and still hypothetical.

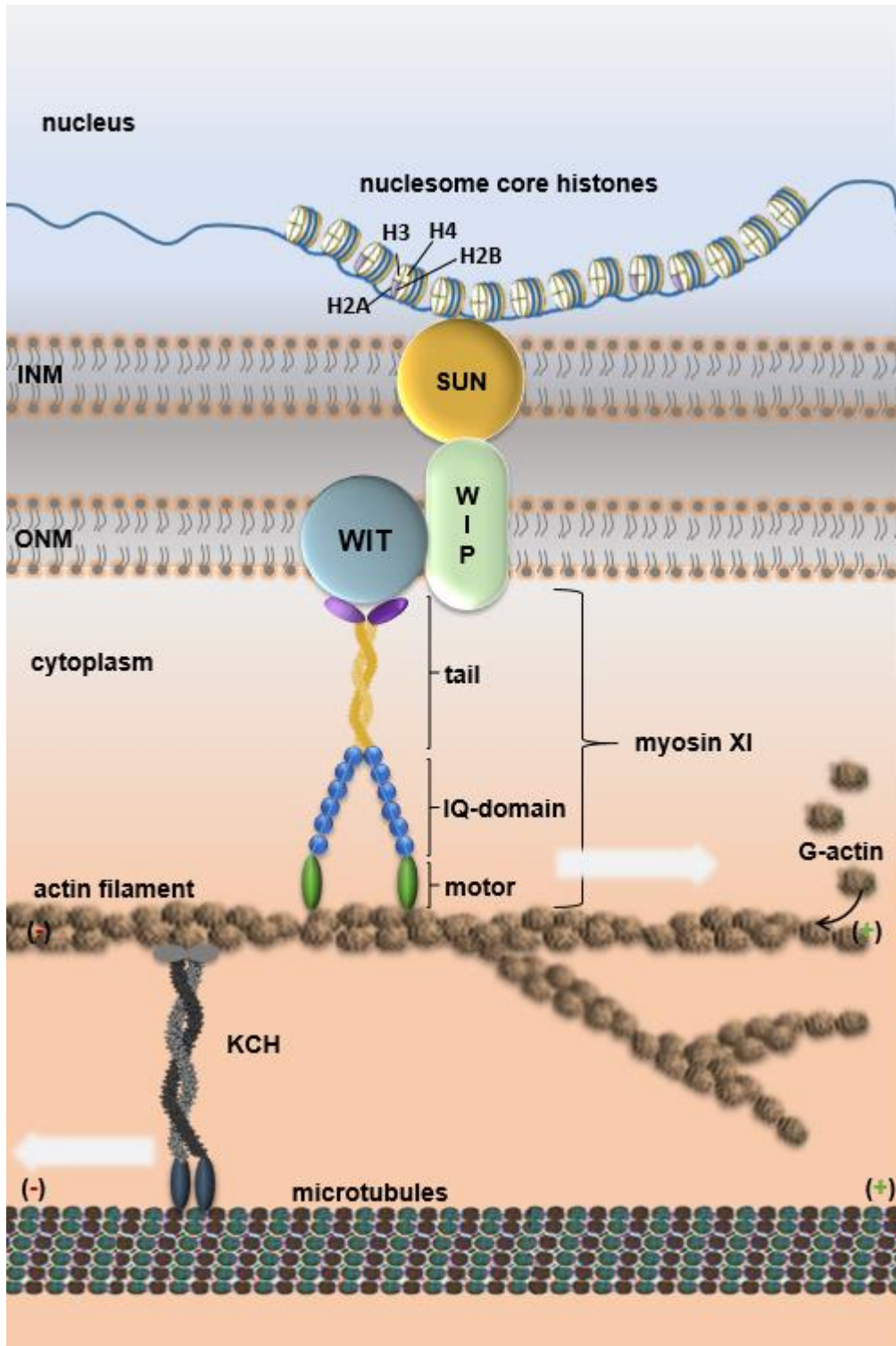


Figure 1.3 Model of the connection between interior of the nucleus and the cytoskeleton

From the nucleus to the cytoplasm: The DNA wraps around four core histones (H2A, H2B, H3, H4), which are responsible for DNA packaging and intranuclear architecture. Histones are connected to SUN proteins. SUN proteins at the inner nuclear membrane (INM) and WIP create a bridge and are connected with WIT at the outer nuclear membrane (ONM). WIT presents the cargo for Myosin XI, consisting of tail, IQ and motor domain walking along actin filaments towards the (+) end (movement indicated by the white arrow). The calponin homology domain of KCH is able to bind to actin. However, KCH binds to microtubules as well and walks towards the (-) end of microtubules (indicated by the white arrow).

1.5 From outer space – From intracellular to extracellular candidates

So far, intracellular factors involved in nuclear migration and polarity formation have been presented. Furthermore, the link between intranuclear and extranuclear factors has been illustrated above. Finally, the fact that extracellular factors and their links to intracellular factors might also influence directional axis formation, will be introduced in the final part of the introduction.

The extracellular matrix (ECM) composed of polysaccharides and proteins is well-studied for animal cells. The ECM serves as structural support and is also required for mechanical signaling, growth, defense, and development (for review see Lee and Streuli 2014). Transmembrane proteins such as integrins are able to bind to proteins of the ECM. It has been shown that removal of integrin encoding genes leads to loss of polarity (Bombardelli *et al.* 2010; Akhtar and Streuli 2013). Integrins recognize ECM proteins such as fibronectin due to recognition sites consisting of three amino acids: arginine, glycine, and aspartic acid (RGD motif). Recently, it has been shown that patterning of ECM proteins can influence cell polarity (Autenrieth *et al.* 2016). In the field of plants, the presence of integrins or fibronectin remained elusive so far. However, previous studies have revealed that RGD peptides play an important role in plant cell polarity (Zaban *et al.* 2013). Whether the pattern of RGDs influences polarity in plant cells has never been tested until now.

1.6 Scope of the Dissertation

Directionality is a fixed characteristic in plant cells. Cell polarity and axis formation are crucial for the morphogenesis of plant cells. How cells acquire polarity and axis presents a central question of plant morphogenesis. Therefore, the potential role of extracellular as well as intracellular factors for axis formation was investigated by using an experimental system based on regenerating protoplasts. Here, the induction of a cell axis *de novo* can be followed by quantification of specific regeneration stages. This study covers different influences on polarity from intranuclear proteins through extranuclear candidates and organelles to extracellular peptides.

This work aimed to answer four interconnected questions:

- a) Is the position of the nucleus a prerequisite for axis formation?

The intensive nuclear movements observed during the first day of protoplast regeneration (Zaban *et al.* 2013) indicate a link between nuclear positioning and the formation of axis and polarity. In this current work, the hypothesis was tested whether the nuclear position is a prerequisite for the re-establishment of axis and polarity. To address this, the nuclear migration was manipulated on a genetic level by overexpression of fluorescently tagged players of nuclear movement (Lifeact-psRFP, GFP-NtKCH, and H2B-mEos). By overexpression of these components, both extranuclear (perinuclear actin basket, KCH) as well as intranuclear (histone H2B) factors supposed to act on nuclear movement were tested. The effect of these manipulations on nuclear migration was followed via time-lapse studies and was then compared with respect to their impact on polarity and axis formation by quantitative analysis of the regeneration pattern.

- b) Does the nuclear proteome differ in H2B-mEos and Lifeact-psRFP compared to the non-transgenic cell line?

The first results reveal an altered nuclear migration behavior in the H2B-mEos and Lifeact-psRFP cell line. It leads to the question whether their nuclear proteome is different compared to the nuclei of non-transformed cells. This could become visible in a changed histone abundance. Therefore, this section aimed to find differences in the histone quantity of the two transgenic lines compared to the wildtype. To test this, the nuclei were isolated, followed by a biochemical approach to separate proteins with subsequent tandem MS analysis in order to identify and quantify the proteins. This was completed through a computational analysis to process the data and generate heat maps for clear illustrations of differences.

- c) Which role do intracellular factors play in axis formation?

Further, the results revealed that induction and manifestation of cell axes can be uncoupled from nuclear positioning, but both phenomena depend on factors that affect cytoskeletal tensegrity (perinuclear actin basket, KCH), as well as on factors acting on chromatin structure. Therefore, the aim was to investigate additional intracellular candidates involved in axis formation for a better understanding of the mechanism behind cell axis formation *de novo* and the interplay of extra- and intranuclear factors. These selected intranuclear and extranuclear factors were manipulated genetically via overexpression, or pharmacologically via drug treatment and the regeneration of BY-2 protoplasts subsequently quantified.

Chromatin consisting of core histones can bind to SUN proteins of the inner nuclear membrane (INM), which are connected via the WIP/WIT bridge to the outer nuclear membrane (ONM). Therefore, an overexpression line of the core histone H2B as well as of the nuclear membrane protein WIT was used in this study to test their role in axis formation *de novo*. In turn, WIT serves as cargo for myosin XI. The motor domain of myosin XI is able to bind to actin and moves towards the plus end of actin filaments. To test the influence of myosin XI in axis formation, two overexpression lines were used. Moreover, actin dynamic was manipulated via cytoskeletal drugs and the perinuclear actin basket was manipulated via overexpression of Lifeact-psRFP. Due to its calponin homology domain, KCH is capable of binding both actin and microtubules. In this study, an overexpression line of KCH was used and microtubule drugs were applied. Together, these factors are physically linked (see Figure 1.3). The goal was to reveal the respective role in cell axis formation one by one and ultimately discuss its functional interplay.

d) Does the orientation of extracellular structures affect axis formation?

The final section aimed to provide insight into the role of extracellular structures in cell polarity. In addition to intracellular factors, another goal was to gather information about extracellular factors with their structural arrangement and their consequential impact on axis formation. To gain a comprehensive overview of the mechanism of polarity formation, peptides with RGD sequences were plotted on nanofibers with either aligned or unaligned orientation. Three days after regeneration on the respective surfaces, cells were quantified according to their regeneration stage.

2 MATERIAL AND METHODS

2.1 Cell lines, protoplast generation, and manipulation of regeneration

2.1.1 Cell lines and cultivation

BY-2 (*Nicotiana tabacum* L. cv Bright Yellow 2) suspension cell lines (Nagata *et al.* 1992) were cultivated in liquid medium containing 4.3 g/L Murashige and Skoog (MS) salts (Duchefa Biochemie, The Netherlands), 30 g/L sucrose, 200 mg/L KH_2PO_4 , 100 mg/L (myo)-inositol, 1 mg/L thiamine, and 0.2 mg/L 2,4-D, pH 5.8. Cells were subcultivated weekly, inoculating 1.0 to 1.5 mL of stationary cells into fresh medium (30 mL) in 100 mL Erlenmeyer flasks under sterile conditions with the laminar flow hood (Hera guard Thermo Scientific, Heraeus, Hanau, Germany). The cell suspensions were incubated in darkness at 26°C under constant shaking on a KS260 basic orbital shaker (IKA Labortechnik, Germany) at 150 rpm. All experiments were performed using cells after 3 d of subcultivation.

In addition to the non-transformed BY-2 wildtype (WT), transgenic lines were used in this study that expressed the actin binding protein Lifeact in fusion with a photoswitchable red fluorescent protein (Lifeact-psRFP, Durst *et al.* 2014), a myosin line where specific domains of myosin XI were overexpressed in fusion with GFP (GFP-Myo I+IQ and GFP-Myo TailN, Qiong Liu, Appendix Figure 5.1 and 5.2 pp. 89), a kinesin with a calponin homology domain in fusion with GFP isolated either from *Nicotiana tabacum* or from *Oryza sativa* (GFP-NtKCH and GFP-OsKCH, Frey *et al.* 2009, Klotz and Nick 2012), a microtubule end-binding protein (EB1) fused to GFP (EB1-GFP, Qiong Liu), a histone marker fused to a photoconvertible protein (H2B-mEos, Wozny *et al.* 2012), and a nuclear membrane protein binding to actin via myosin XI isolated from *A. thaliana* in fusion to GFP (GFP-AtWIT, Qiong Liu), all under the control of a constitutive cauliflower mosaic virus (CaMV) p35S promotor. Additionally, a free GFP line was used as a control (K. Schwarzerová, Charles University, Prague, Czech Republic). The media for the transgenic cell lines were complemented with either 30 mg/L hygromycin (H2B-mEos), or 40 mg/L hygromycin (Lifeact-psRFP), 25 mg/L kanamycin (freeGFP), 50 mg/L kanamycin (GFP-

MATERIAL AND METHODS

NtKCH, GFP-OsKCH, GFP-Myo M+IQ, GFP-Myo TailN, GFP-AtWIT, EB1-GFP), respectively. All the transgenic lines used in this study together with the represented color bars appearing in the result part are listed for an overview in the following table.

Table 2.1 Transgenic lines used in this study

This table lists the transgenic lines with associated color coding (CC) used in the diagrams of the result part, abbreviations used in the following description, full name, applied antibiotic and concentration, and source of construct and cell line.

CC	Abbreviation	Name	Antibiotic	Source
	Lifeact-psRFP	Lifeact fused to photoswitchable red fluorescent protein	40 mg/L hygromycin	Durst <i>et al.</i> (2014)
	GFP-Myo+IQ	Green fluorescent protein fused to motordomain plus IQ domain of Myosin XI-I	50 mg/L kanamycin	Q. Liu, Karlsruhe Institute of Technology, Karlsruhe, Germany
	GFP-Myo TailN	Green fluorescent protein fused to Tail on N-terminus of Myosin XI-I	50 mg/L kanamycin	Q. Liu, Karlsruhe Institute of Technology, Karlsruhe, Germany
	GFP-EB1	Green fluorescent protein fused to end binding protein 1 of microtubules	50 mg/L kanamycin	Q. Liu, Karlsruhe Institute of Technology, Karlsruhe, Germany
	GFP-NtKCH	Green fluorescent protein fused to Kinesin with a chalponin homology domain isolated from <i>Nicotiana tabacum</i>	50 mg/L kanamycin	Frey <i>et al.</i> (2009), Klotz and Nick (2012)
	GFP-OsKCH	Green fluorescent protein fused to Kinesin with a chalponin homology domain isolated from <i>Oryza sativa</i>	50 mg/L kanamycin	Frey <i>et al.</i> (2009), Klotz and Nick (2012)
	FreeGFP	Free green fluorescent protein	25 mg/L kanamycin	K. Schwarzerová, Charles University, Prague, Czech Republic

■	GFP-AtWIT	Green fluorescent protein fused to WPP domain-interacting tail-anchored protein isolated from <i>Arabidopsis thaliana</i>	50 mg/L kanamycin	Q. Liu, Karlsruhe Institute of Technology, Karlsruhe, Germany
■	H2B-mEos	Histone H2B fused to monomeric Eos	30 mg/L hygromycin	Wozny <i>et al.</i> (2012)

2.1.2 Generation and regeneration of protoplasts

The protocol was adapted from Kuss-Wymer and Cyr (1992) and Zaban *et al.* (2013) with minor modifications. Aliquots of 4 mL were harvested under sterile conditions 3 d after subcultivation and digested for 1 h at 26°C in 4 mL enzyme solution of 1% (w/v) cellulase YC (Yakuruto, Tokyo) and 0.1% (w/v) pectolyase Y-23 (Yakuruto, Tokyo) in 0.4 M mannitol at pH 5.5 under constant shaking on a KS260 basic orbital shaker (IKA Labortechnik) at 100 rpm in petri dishes of 90 mm diameter. After digestion, protoplasts were collected by 500 rpm for 5 min in fresh reaction tubes. The protoplast sediment was carefully resuspended in 10 mL of FMS wash medium (4.3 g/L MS-salts, 100 mg/L (myo)-inositol, 0.5 mg/L nicotinic acid, 0.5 mg/L pyridoxine-HCl, 0.1 mg/L thiamine, and 10 g/L sucrose in 0.25 M mannitol). After three washing steps, protoplasts were transferred into 4 mL FMS-store medium (FMS wash medium complemented with 0.1 mg/L 1-naphthaleneacetic acid (NAA), and 1 mg/L benzylaminopurine). Protoplasts were incubated in the dark at 26°C without shaking in petri dishes (50 mm diameter). To prevent evaporation, the petri dishes were sealed with Parafilm®M (Bemis Company Inc., Neehna WI, USA).

2.1.3 Chemical treatments of regenerating protoplasts

To manipulate microtubules during the regeneration of the protoplasts, the FMS-store medium of the non-transgenic wildtype BY-2 cell line as well as the transgenic line GFP-NtKCH, were complemented with 500 nM of Oryzalin (Sigma-Aldrich, Neu-Ulm, Germany). Alternatively, actin drugs such as 100 nM Latrunculin B (Sigma-Aldrich), or 100 nM Phalloidin (Sigma-Aldrich) were added to the FMS-store medium of the wildtype BY-2 cell line to see the effect of stabilization and destabilization on regeneration. Additionally, Lifeact-psRFP was completed with 100 nM Latrunculin B. Further, 75 nM 2,6 Dichlorobenzonitrile (Sigma-Aldrich) were added to the FMS-store medium of the non-transgenic wildtype to get an idea of the

function of the cell wall in regeneration. To get an overview, the used chemicals are summarized in the table given below together with the color used in the diagrams in the results part.

Table 2.2 Chemicals used in this study

This table lists the chemicals used in this study together with their associated color coding (CC), applied concentration, stock solution and further dilution.

CC	Name	Concentration	Stock solution
	Oryzalin	500 nM	10 mM in DMSO dilution to 10 μ M in ddH ₂ O
	Phalloidin	100 nM	12 μ M in ddH ₂ O
	Latrunculin B	100 nM	10 mM in DMSO dilution to 10 μ M in ddH ₂ O
	2,6 Dichlorobenzonitrile (DCB)	100 nM	10 mM in DMSO dilution to 10 μ M in ddH ₂ O

2.2 Analysis of nuclei

In order to test whether the nuclei of Lifeact-psRFP and H2B-mEos differ compared to BY-2 WT in the protein content, the nuclei were isolated from protoplasts, their proteins separated via SDS-PAGE and subsequently analyzed as described in the following chapter.

2.2.1 Isolation of nuclei

To isolate the nuclei, the protocol was adapted from Saxena *et al.* (1985) with some modifications. After three washing steps, protoplasts were collected by 500 rpm for 5 min and the supernatant was discarded. Protoplast sediment was carefully resuspended in 800 μ L of 4°C cold Nuclei Isolation Buffer (NIB containing 0.2 M sucrose, 10 mM 2-N-Morpholino ethane sulphonic acid (MES), 0.1 mM spermine, 2.5 mM ethylenediaminetetraacetic acid (EDTA), 2.5 mM dithiothreitol (DTT), 10 mM NaCl, 10 mM KCl and 0.1% Triton X-100 with pH adjusted to 5.3 via KOH). To achieve deplasmolysis, protoplasts were incubated in NIB for 10 minutes on ice. Protoplasts were resuspended on ice to allow disruption of the protoplasts. The suspension was subsequently filtered through a set of three filters (Franz Eckert GmbH, Waldkirch, Germany, mesh size: 100 μ m, 50 μ m and finally 20 μ m). The nuclei were centrifuged at 500 rpm for 10 min at 4°C and filtered again through 20 μ m mesh. Finally, nuclei were collected by centrifugation at 500 rpm for 10 minutes and the pellet was resuspended

in 0.5 mL NIB without Triton X- 100 and either stored at -20°C or directly loaded on SDS-gel. An aliquot of $10\ \mu\text{L}$ was used to calculate the total number of nuclei. On average, the method achieved 100,000 nuclei/ μL .

To illustrate the entire procedure the following Figure 2.1 outlines the method of isolating the nuclei together with previous protoplast isolation. Isolated nuclei were used for further protein analysis.

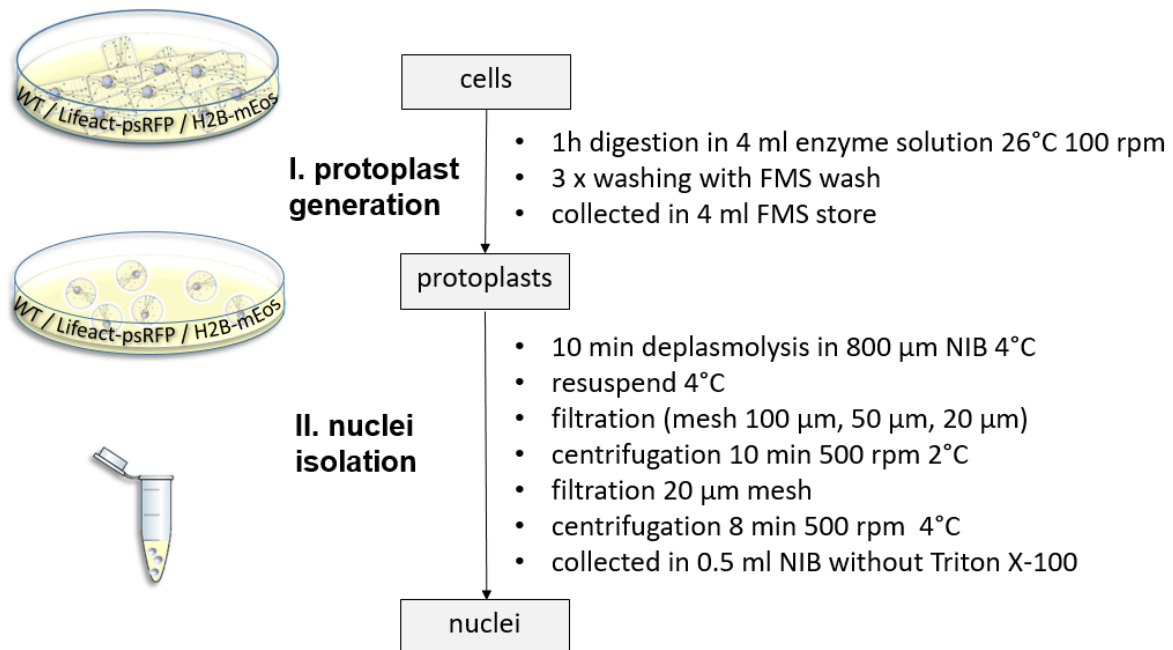


Figure 2.1 Summary of generation of protoplasts with subsequent isolation of the nuclei

The flow chart summarizes the individual working steps from three days old BY-2 WT, BY-2 Lifeact-psRFP, or BY-2 H2B-mEos cells to single nuclei and gives an overview of the entire process. I.) protoplast generation was carried out at 26°C . II.) nuclei isolation was carried out at 4°C . For detailed description and buffer compositions, see text in 2.1.2 and 2.2.1.

2.2.2 Protein separation

In order to separate the proteins, sodium dodecyl sulfate polyacrylamide gel electrophoresis (SDS-PAGE) was carried out according to Laemmli (1970) consisting of 10% stacking and 4% separation gel.

To see differences of the nuclei and their attached nuclear baskets, $20\ \mu\text{L}$ of nuclei suspension (containing approximately 2,000,000 nuclei) of BY-2 Lifeact-psRFP, H2B-mEos and WT as well

as a high molecular weight marker SDS6H2 (Sigma-Aldrich, Munich, Germany) were supplemented with 10 μ M sample loading buffer. After denaturation at 95°C for 10 min, samples were subsequently loaded on gel in Atto mini Page system (Atto, Tokyo, Japan). The gel was run at 25 mA for 90 min. Finally, gels were stained in Coomassie staining solution (0.04% [w/v] Brilliant Blue R, 40% [v/v] methanol, 10% [v/v] acetic acid) for 120 min and afterwards destained in 30% [v/v] ethanol supplemented with 10% [v/v] acetic acid for 20 min.

2.2.3 Proteomics – Tandem mass spectrometry

Protein analysis was performed by the group of Dr. Achim Treumann at the department of Proteomics and Proteome analysis, Newcastle University, UK. Label-free analysis was done by using a method that is based on integration of the peptide peaks at MS1 level (LFQ quantitation) in MS analysis as described in Azimifar *et al.* (2014).

The lanes of the SDS-gel of BY-2 wildtype, Lifeact-psRFP, and H2B-mEos nuclei were excised, samples homogenized and proteins were digested with trypsin at 37°C overnight. For LC-MS/MS analysis, peptides were analyzed via a Q-Exactive mass spectrometer (Thermo Fisher Scientific, Lutterworth, UK). This was coupled to an EASY-nLC 1000 UHPLC system (Thermo Fisher Scientific) with a nanoelectrospray ion source. Full-scan MS spectra (300 to 1,750 m/z) were acquired as the following: resolution 70,000 at 200 m/z, 20 ms maximum injection time, 3×10^6 charges. In order to perform label-free quantification the precursors were isolated from a 2.2 m/z window and a fixed first mass of 100 m/z. MS/MS spectra (17,500 at 200 m/z) were obtained with a maximum injection time of 120 ms and a target value of $1e^5$ charges.

Subsequently, raw MS data were processed by MaxQuant (Cox and Mann 2008). Peak lists were searched against the UniProt (2017) FASTA database of *Nicotiana tabacum*. Using a target-decoy approach, proteins and peptides were identified with a reversed database. Final quantification was operated by MaxQuant with default settings.

2.2.4 Data processing – From matrix to heat map

After protein identification and quantification via tandem MS raw data organized in a matrix format were processed further to visualize differences in nuclear protein content by creating heat maps. As an outline of the process see the following Figure 2.2.

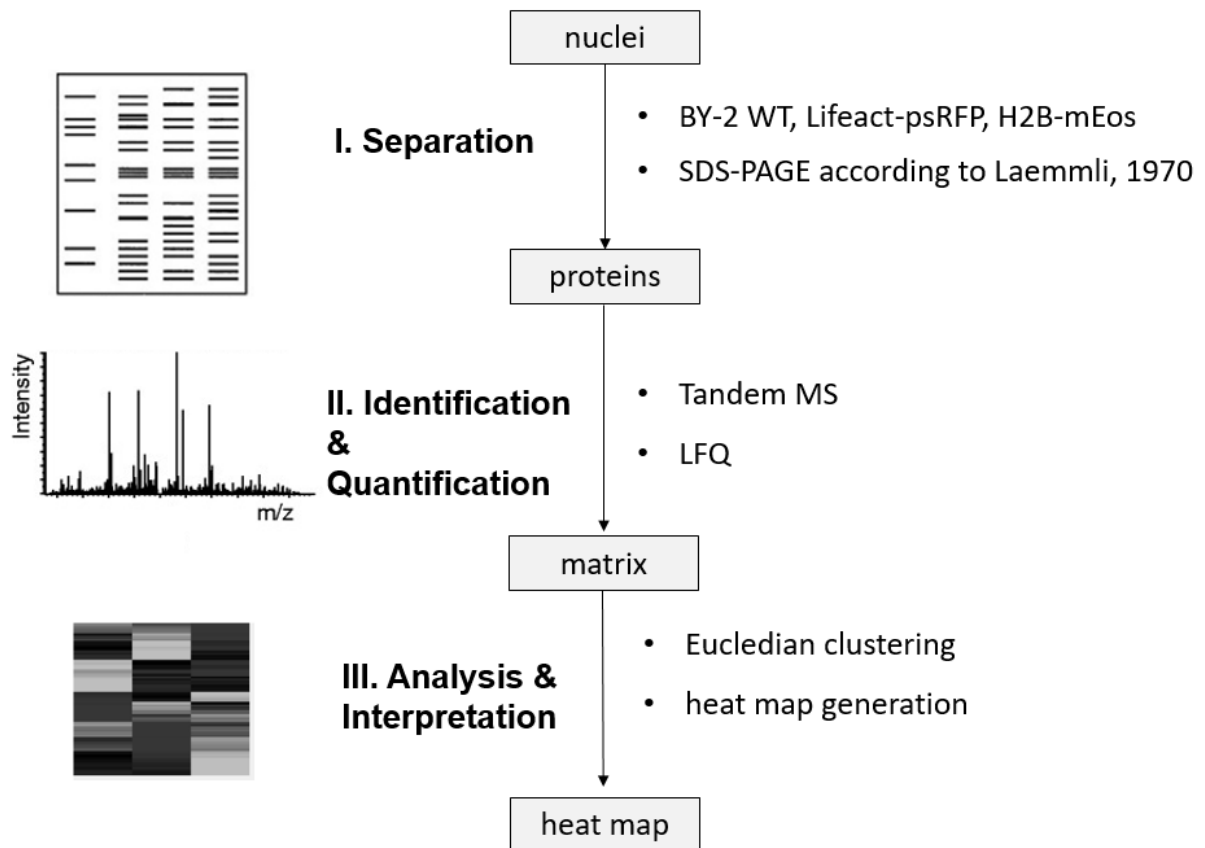


Figure 2.2 Protein separation, quantification and interpretation

Workflow top down from protein separation through quantification to final data processing. To separate the proteins from isolated nuclei, SDS-PAGE was performed according to Laemmli (1970) for BY-2 WT, Lifeact-psRFP and H2B-mEos nuclei. The group of Dr. Treumann performed tandem mass spectrometry with label-free quantification (LFQ). Raw data can then be analyzed and the heat map can be generated. For detailed description see text in 2.2.4.

For downstream analysis of the quantitative protein abundance data generated via tandem mass spectrometry (performed by the department of Proteomics and Proteome analysis, Newcastle University, UK) a recently investigated program called Perseus was used (Tyanova *et al.* 2016).

First data were filtered by deleting artefactual proteins identified either randomly or due to contaminants as a consequence of probe manufacturing (certain, BTA, etc.). Proteins, which were not identified within all three samples (WT, Lifeact-psRFP, and H2B-mEos) were sorted out (see Appendix Figure 5.4 p.92 and Table A 5.1 pp.93). To also include proteins with low abundance a log₂ transformation of the quantification was performed next. This resulted in a

Gaussian distribution of the data. However, proteins with only very weak evidence were sorted out in the subsequent step. Then, low values for proteins that were not consistently detected were computed from normal distribution using the Gaussian curve with the value of 1.8 for standard deviation. This was followed by normalization with z-scores for every selected protein. Using the z-normalization each raw data score was converted into a standardized value with a mean of 0 and a standard deviation of 1. Therefore, the effect of different scales (due to different ranges of intensities along all proteins) was eliminated. This enables direct comparison analysis of the three samples for all proteins as a general form of normalized distance function, which utilizes Euclidean distance measure. Finally, Euclidean clusters were generated for proteins that behave similarly when the three different samples were compared. Different protein abundance can be visualized by a heat map. Mapping was generated by the following color key (Figure 2.3). Value 0 denotes no difference (black). High abundance increases in their red intensity whereas low abundance leads to a green color presented in the heat map.

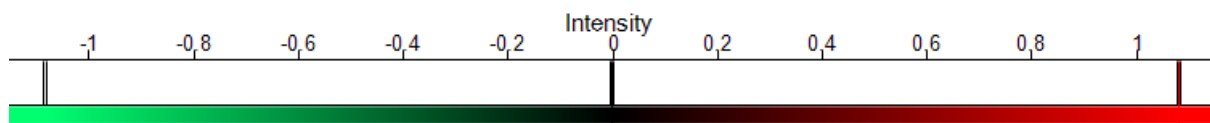


Figure 2.3 Color Key

Used color gradient for intensity after z-normalization and direct comparison between the three cell lines. Black denotes no difference (0), red shows high abundance, green low abundance.

2.3 Generation of RGD peptides and nanofibers

In order to detect the influence of extracellular organization, RGD peptides were plotted on either aligned or unaligned nanofibers on which protoplasts regenerated for three days before observation.

PCL nanofiber mats with aligned or unaligned plotted peptides were designed by Dr. Renee Goreham together with Prof. Dr. Thomas Nann at the Alan MacDiarmid Institute, Victoria University of Wellington, New Zealand. Methods were adapted from Mattanavee *et al.* (2009).

2.3.1 Electrospinning the nanofibers

The following protocol was described by Dr. Renee Goreham. Electrospun polycaprolactone nanofiber mats were spun using the electrospinning set-up (Figure 2.4). 12% [w/w] polycaprolactone (PCL) solution was made up in 50:50 [v/v] dichloromethane and N,N'-dimethylformamide. A blunt 20-gauge stainless steel hypodermic needle (0.91 mm) was used as a nozzle.

The target plate was wrapped in aluminum foil around a rotating cylinder (diameter of 15 cm and rotating speed of 50 rpm). The distance between the needle and the drum was 10 cm. A direct current potential of 21 kV was applied creating positive polarity on the electrode (needle) and the fibers were collected on the drum (grounded). To gain aligned structures of the nanofibers, a rotating speed of 1400 rpm was applied. The feed rate of the PCL solution was 1 mL/h after continuous spinning for 6-8 h. Scanning electron microscopy (SEM) was used to image the nanofibers that determined the average diameter and uniformity (see Appendix 5.4 SEM analysis; Figure 5.13 and Figure 5.14 pp.106).

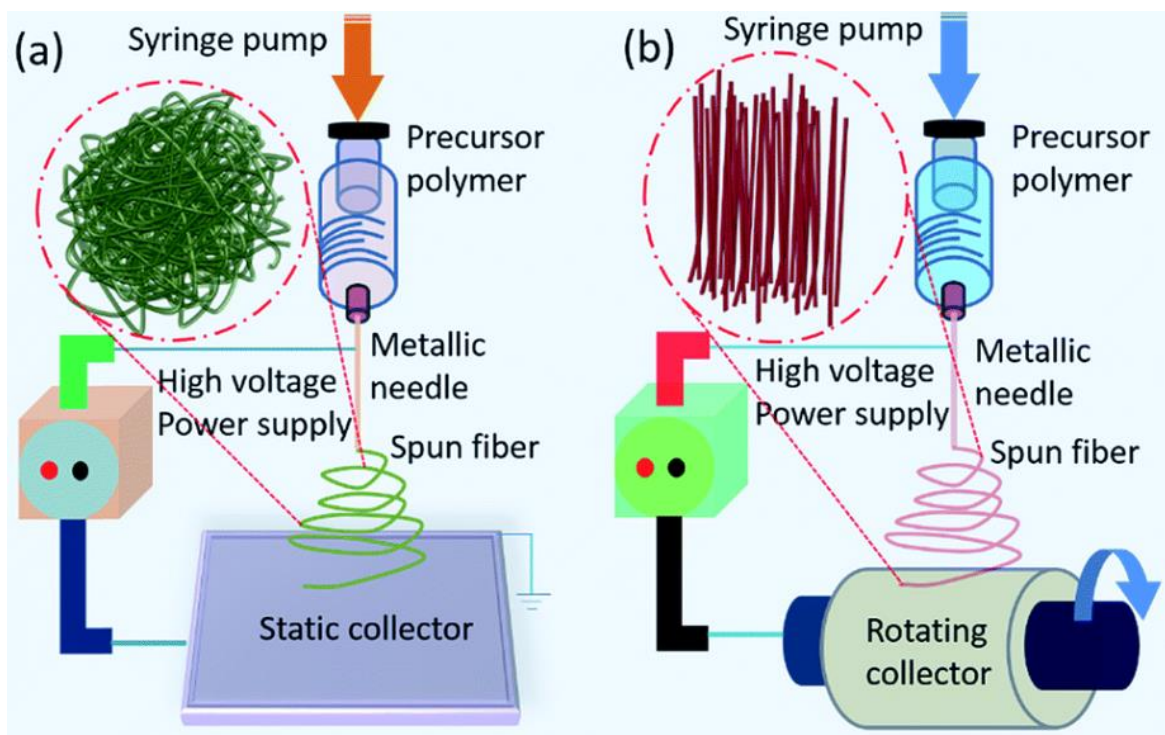


Figure 2.4 Schematic representation of electrospinning set-up

Schema is adapted from Mondal and Sharma (2016). An electric force is generated to draw charged threads of a polymer such as PCL. The nano-sized threads arrive on a collector. Aligned and unaligned patterns are generated by a rotating (b) or static collector (a).

2.3.2 Surface modification of PCL nanofibers

Once the PCL fibers have been synthesized, they were cut into 1 cm diameter round disks and placed into a 24-well plate.

1. Unaligned NFs modified RGD
2. Unaligned NFs modified DGR
3. Unaligned NFs
4. Aligned NFs modified RGD
5. Aligned NFs modified DGR
6. Aligned NFs

The PCL nanofibers were immersed into an ethanolic aqueous solution (1:1 [v/v]) for 2-3 h and then washed with ample amounts of DI water. 1, 6-hexadecylamine in isopropyl solutions (10% [w/w]) were used to aminolyze the PCL scaffold (Figure 2.5) for 8 h at 37 °C.

The aminolyzed scaffolds were then rinsed with DI water for 24 h at RT to remove unreacted 1, 6-hexadecylamine and dried under vacuum at 30 °C until the weight remained unchanged. N,N'-disuccinimidylcarbonate (DSC; 0.1 M) in dimethylsulfoxide solution in the presence of trimethylamine (0.1 M) was used to activate the PCL scaffold for 60 min at ambient temperatures. The activated scaffolds were then immersed in 1 mg/mL YGRGDSP or YGDGRSP (Margarette Brimble; Auckland University) at ambient temperatures for 24 h and subsequently rinsed for an additional 24 h in DI water.

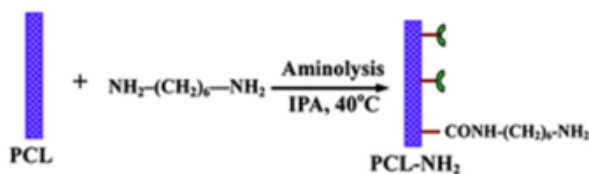


Figure 2.5. Aminolysis of PCL using a diamine according to Yuan *et al.* (2012)

Blue represents the PCL nanofibers before (left) and after aminolysis (right)

2.3.3 Regeneration of protoplasts on RGD plotted nanofibers

In order to analyze the effect of RGD peptides plotted on aligned or unaligned nanofibers on axis formation during regeneration, each 1 cm diameter disk was transferred to one well of Lab-Tek™ 24-well chamber (Nunc GmbH & Co. KG Thermo Fischer Scientific, Langenselbold, Germany), respectively. After generation of protoplasts (described in 2.1.2, p.17) 1 mL of the

4 mL protoplasts FMS-store suspension was dropped on each disk. Protoplasts on the disks were incubated in the dark at 26°C without shaking. To prevent evaporation, the Lab-Tek™ 24-well chambers were sealed with Parafilm®M (Bemis Company Inc., Neehna WI, USA). Shortly before observation, cells were stained with 100 µg/mL Fluorescein diacetate (FDA, Sigma-Aldrich, Neu-Ulm, Germany) to distinguish the cells from the noisy background generated from the nature of the fibers.

2.4 Microscopy and quantifications

To analyze temporal patterns of regeneration for different transgenic BY-2 lines and drug-treated cells in comparison to non-transformed and untreated BY-2 cells, 15 µL of the respective protoplast suspension was carefully mounted on slides using silicone imaging spacers (Secure-Seal, Sigma-Aldrich, Neu-Ulm, Germany) to safeguard the protoplast from bursting. For detection, the regenerated cellulosic cell wall was stained by Calcofluor White (1 volume of 0.1% w/v) according to Maeda and Ishida (1967) and Nagata and Takebe (1970). Regeneration was followed for one week under an AxioImager Z.1 microscope (Zeiss, Jena, Germany) equipped with an ApoTome microscope slider for optical sectioning and a cooled digital CCD camera (AxioCam MRm) recording the cells through differential interference illumination with a 20x/0.75 plan-apochromat objective and the Calcofluor White signal through the filter set 49 (excitation at 365 nm, beam splitter at 395 nm, and emission at 445 nm).

To gain more details of either the isolated nuclei or the nanofibers, an Axio Observer Z1 microscope (Zeiss, Jena, Germany) with a spinning-disc device (YOKOGAWA CSU-X1 5000) was used. Differential interference contrast (DIC) images were obtained with a 20x/0.8 or 63x/1.44 oil objective. Additionally, with the Ar-Kr laser with 488 nm excitation for H2B-mEos and 561 nm excitation for Lifeact-psRFP images of the transgenic lines were captured.

Images were processed and analyzed using the AxioVision software (Rel. 4.8.2) (Zeiss, Jena, Germany). To ensure unbiased acquisition of images, the MosaiX-module sampling system (Zeiss, Jena, Germany) was employed, automatically recording individual cells and assembling a large panel of cells covering an area of 5 × 5 mm consisting of 266 individual images.

Individual stages as defined in Figure 3.5 (p.38) were scored from those composite images. Stages were defined as follows: stage 1 round, no cell wall; stage 2 cell wall present upon staining with Calcofluor White; stage 3 ovoid shape, stage 4 elongated with a ratio of longer axis to shorter axis of >2.0 , stage 5 tripolar shape. Frequency distributions were calculated from 3,000 individual cells per time point from three independent biological replications, error bars represent standard errors of the mean (SE), significance of indicated differences was tested by a paired, two-sided t-test. Frequency distributions for protoplasts growing on RGD treated surfaces were calculated from 1,000 individual cells (200 cells per disk) from two independent biological replications, error bars represent standard errors of the mean (SE), significance of indicated differences was tested by a paired, two-sided t-test.

To follow the regeneration of individual cells, 45 μL of the protoplast suspension was filled in each 4-well Nunc™ Lab-Tek™ II Chamber Slide™ (Nunc GmbH & Co. KG Thermo Fischer Scientific, Langenselbold, Germany). The suspension was then embedded in 400 μL liquefied FMS-store medium complemented with 0.1% Agarose (Sigma-Aldrich Chemie GmbH, Steinheim, Germany) to avoid that cells drifted out of focus during recording. Subsequently, the chambers were wrapped with Parafilm®M (Bemis Company Inc., Neehna WI, USA) to maintain humidity, followed by a short centrifugation step with 500 rpm for 1 min (Concentrator 5301, Eppendorf, Hamburg, Germany). Nuclear movement and regeneration of the protoplasts were observed using an AxioObserver Z1 microscope (Zeiss, Jena, Germany). A selected position was defined in x, y and z-axis with the AxioVision software (Rel. 4.8.2, Zeiss, Jena, Germany), and every 3 min an image was recorded automatically with a 20x/0.8 plan-apochromat objective and differential interference contrast illumination. To generate movies, single pictures were compiled into one avi-video using Image J (National Institutes of Health, Bretehesda, USA). For each cell line 10-20 individual cells were recorded from two or three independent biological replications.

3 RESULTS

The following results will be presented in four main sections.

The first part focuses on nuclear migration and its role in axis formation. It will answer the question whether the nuclear position is a prerequisite for axis formation. To test the hypothesis that the nucleus must be at the cell center to start axis formation, nuclear migration and axis formation of three transgenic lines were analyzed via time-lapse studies of regenerating protoplasts. In these three transgenic cell lines, the nuclear positioning from the cell periphery to the cell interior was altered. These results indicated differences in nuclear migration behavior leading to the next investigation.

The second part focuses on the role of nuclear protein content in nuclear migration. Histone abundance might be changed in the transgenic cell lines where nuclear migration was altered. To test this hypothesis, a proteomic approach was used. To this end, the nuclei were isolated, and their proteins separated via SDS-PAGE. Proteins were then quantified via tandem MS and completed by computational analysis to generate heat maps and thus enable clear illustrations of differences in protein abundance.

The third part focuses on the role in polarity and axis formation of the two cytoskeletal elements actin and microtubules, their motor proteins myosin and kinesin, the interior of the nucleus, i.e. histone packaging, and its connection to the cytoskeleton via the SUN WIP WIT bridge. This was tested both on a genetic level with different transgenic overexpression lines and additionally on a pharmacological level with various cytoskeletal drugs by quantitative analysis of regenerating protoplasts.

The fourth part focuses on the role of extracellular components in polarity and axis formation. Not only intracellular factors are involved in axis formation. Which influence the external environment has, and even more precise: which role its structure plays in axis formation, will be addressed in the last part of the results. Therefore, RGD peptides and its reverse sequence DGR were plotted on aligned or unaligned nanofibers on which the protoplasts regenerate. Three days later the regeneration pattern was analyzed.

Finally, the results are summarized at the end of this chapter.

3.1 Nuclear position can be separated from axis formation

In the first chapter of the results part, the role of the nuclear migration in polarity and axis formation is tested. Therefore, the nuclear migration was manipulated on a genetic level by overexpression of fluorescently tagged players of nuclear movement (Lifeact-psRFP, GFP-NtKCH, and H2B-mEos). By overexpression of these components, both extranuclear (perinuclear actin basket, KCH) as well as intranuclear (histone H2B) factors supposed to act on nuclear movement were tested.

In order to investigate the question whether nuclear position is required for the formation of axis and polarity, time-lapse studies were conducted (Figure 3.1). From previous data, it was evident that the early stages of regeneration were the most significant, since after one day the regeneration patterns in the three transgenic lines already clearly differed from the situation in the non-transformed line. Therefore, the initial phase of nuclear migration and polarity formation during the first day in individual cells was followed. These differences became detectable from around 9 h after regeneration, which was therefore scrutinized as critical time point. Representative images from these time-lapse series of the three transgenic lines compared to the non-transformed line are shown in Figure 3.1.

At the onset of regeneration ($t = 0$ h), the nucleus of the non-transformed cell line was elliptical in shape and located at the periphery (Figure 3.1 A, white arrow). It should be noted that protoplasts were generated at the peak of the proliferation phase, three days after subcultivation, which means that prior to cell-wall digestion, most nuclei were in the cell center (Appendix Figure 5.12 p.105). After 9 h of regeneration, the nucleus began to round up and to shift slowly from the cell wall to the cell center (Figure 3.1 B, white arrow). The cell was still round with no indications of changes in size or shape at this stage. After one day, the nucleus had reached the cell center and the cell expanded symmetrically (Figure 3.1 C, dashed yellow arrows), but no indications of cell axis or polarity were detectable.

To test for a potential influence of the perinuclear actin basket on nuclear migration and the formation of axis and polarity, Lifeact-psRFP cells were analyzed. Here, the nucleus was already tethered at the cell center $t = 0$ h, i.e. straight at the end of cell-wall digestion, and it was not elliptic, but round (Figure 3.1 D, white arrow). At 9 h, axis formation had already

started (Figure 3.1 E, dashed yellow arrow), and the nucleus was still positioned in a central position (Figure 3.1 E, white arrow). At 24 h, the cells were clearly ovoid, i.e. axis manifestation had continued (Figure 3.1 F). The nucleus, still positioned at the cell center, had become enlarged after 24 h (Figure 3.1 F, white arrow).

Since the nucleus is moved via interaction of actin filaments and microtubules, a cell line was investigated that overexpresses the class-XIV kinesin KCH. Similar to the non-transformed line, in GFP-NtKCH the nucleus was positioned at the periphery at the onset of regeneration, and the protoplast was round (Figure 5 G, white arrow). At 9 h, axis formation had already initiated (Figure 3.1 H, dashed yellow arrow). The nucleus, however, was moving slower than in the non-transformed cell line and hence was still located at the periphery (Figure 3.1 H, white arrow). Only at 24 h, the nucleus had ultimately reached the cell center, while axis formation had already proceeded further (Figure 3.1 I, white arrow).

To probe for potential alterations of chromatin structure, the H2B-mEos cell line was investigated. At the end of cell-wall digestion ($t = 0$ h), the nucleus was located at the periphery, similar to the situation in the non-transformed control (Figure 3.1 J, white arrow). At 9 h, the cell already started to elongate (Figure 3.1 K, dashed yellow arrow), although the nucleus was still at the periphery. Interestingly, the nucleus was partially separated into two interconnected lobes (Figure 3.1 K, white arrows). At 24 h, these two lobes had again merged into one complete nucleus, which slowly moved into the cell center (Figure 3.1 L, white arrow). At this time, axis manifestation had already started.

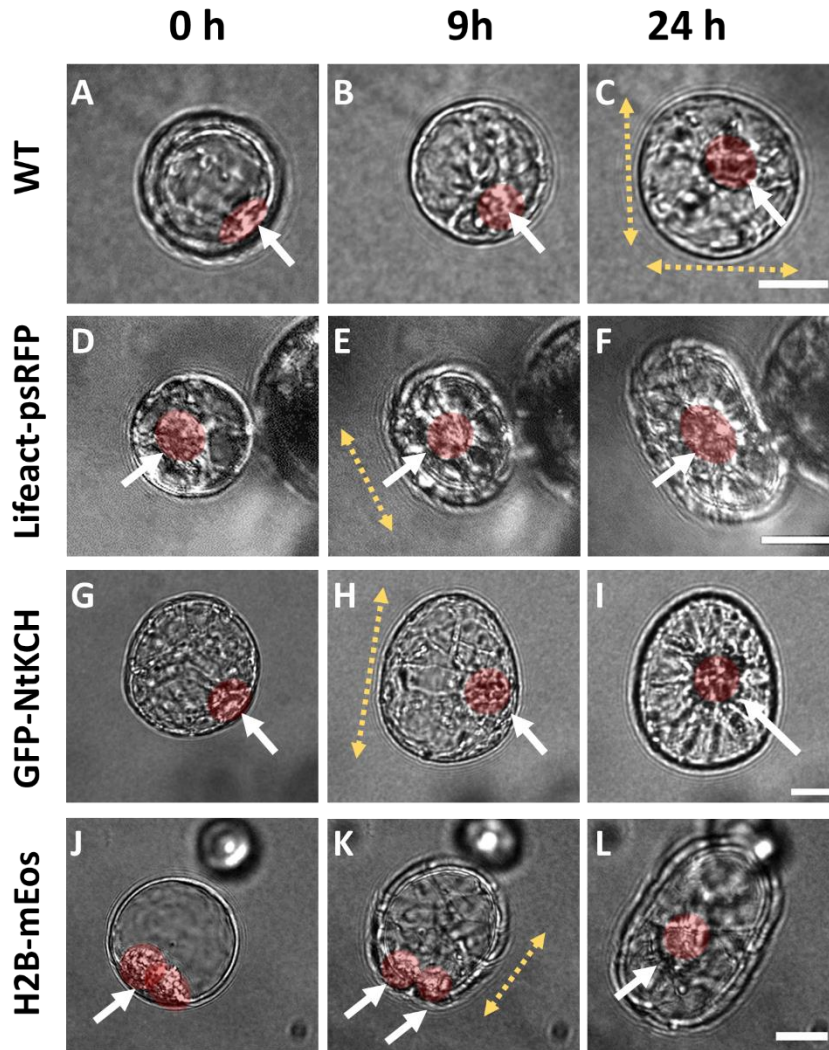


Figure 3.1 Time-lapse series after protoplast generation

Representative images from time-lapse series recorded from individual cells at 0 hours (A,D,G,J), 9 hours (B,E,H,K), and 24 hours (C,F,I,L) after generation of protoplasts, respectively for non-transformed BY-2 WT (A,B,C), Lifeact-psRFP (D,E,F), GFP-NtKCH (G,H,I), and H2B-mEos (J,K,L). The nucleus is shaded in red, and indicated by white arrows. Yellow arrows indicate the orientation of the ensuing axis formation. Scale bars: 20 μm .

3.2 Nuclear proteomes of H2B-mEos and Lifeact-psRFP differ compared to BY-2 wildtype

Since nuclear migration is clearly altered by overexpression of Lifeact-psRFP, there could be differences in the composition of nuclear proteins compared to non-transformed BY-2 wildtype. Additionally, H2B-mEos showed altered behavior in nuclear positioning. For the latter, an altered nuclear shape has also been observed. To answer the question if the nuclear proteome of these two overexpression lines differ from the wildtype, nuclei of both transgenic lines were isolated and their identified proteins were compared to non-transformed WT nuclear proteins. Since the previous results indicate an altered nuclear architecture, changes

in histone abundance could be possible. Therefore, this part aimed to find differences in the histone quantity of the two transgenic lines compared to the wildtype.

In order to analyze their protein content, nuclei had to be isolated together with their strongly attached nuclear basket (Figure 3.2 A, B, C). The characteristic signal of actin originating from the nuclear basket wrapping the nucleus was still visible (Figure 3.2 C). Likewise, the characteristic labeling of the histones within the nucleus was still visible for H2B-mEos nuclei (Figure 3.2 D, E, F). Overall, the isolated nuclei were still intact and their overexpressed fusion proteins still detectable.

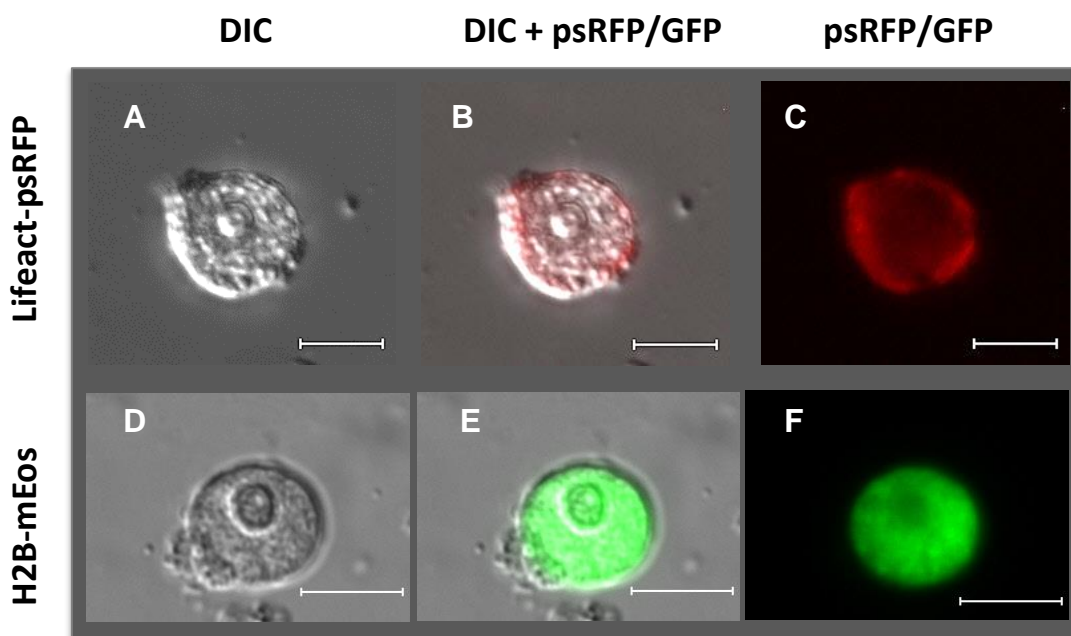


Figure 3.2 Images of transgenic nuclei together with their fluorescent signal after isolation process

Representative images of isolated nuclei of BY-2 Lifeact-psRFP (A,B,C) and BY-2 H2B-mEos (D,E,F) after isolation process in DIC (A,D), merge of red channel and DIC (B) or green channel and DIC (E) and fluorescent signal in the red channel (C) or green channel (F). Scale bars: 10 μ m.

After nuclear isolation, proteins were separated via SDS-PAGE (see Appendix Figure 5.3 p.91). Due to the high amount of proteins no differences in protein composition are detectable in the SDS-PAGE. Thus, proteins were identified via tandem mass spectrometry and label-free quantification. In order to visualize the results, raw data matrices were transformed into heat maps via a sophisticated computational analysis program called Perseus (Tyanova *et al.* 2016).

RESULTS

In the following paragraph, information will be filtered starting from an overview over all identified proteins to ultimately five selected proteins of interest. These are selected based on their relevance to histone packaging and higher abundance compared to wildtype.

In total, 435 proteins were identified within the three nuclear isolation solutions. Proteins, which were not identified within all three samples (WT, Lifeact-psRFP, and H2B-mEos) were sorted out beforehand (see visualization via Venn diagram in Appendix 5.4 p.92 and discarded proteins listed in Table A 5.1 pp.93). The intensities for identified proteins in H2B-mEos, Lifeact-psRFP and wildtype were classified regarding to their frequency. To also maintain proteins with low appearance, a log₂ transformation of the raw data was performed. This resulted in a Gaussian distribution of the data (see Appendix Figure 5.5 A p.95). In order to compare the results of three different cell lines to a standard normal deviation, z-normalization was carried out (see Appendix Figure 5.5 B p.95).

Next, clustering of proteins that behave similarly when compared was performed following Euclidean distance, leading to 8 big clusters (Figure 3.3 left side ①-⑧). Different protein abundance can be visualized by a heat map (Figure 3.3 right side): High abundance increases red intensity whereas low abundance leads to a green color in the heat map. Since this study aims to find proteins that are different in their abundance in both transgenic lines compared to the wildtype, the results will further focus on proteins that are more abundant in both of the two mutant samples (Figure 3.3 left side, ① first cluster in purple, highlighted via blue background). Noteworthy the core histone H2B that is expected to be more abundant for the H2B-mEos overexpression line is also classified in cluster ①. Therefore, the first cluster was further examined.

In this cluster, the same proteins are more abundant (visible by the red color) in H2B-mEos (Figure 3.3 right side, left lane), and in Lifeact-psRFP (Figure 3.3 right side, middle lane) in contrast to wildtype (Figure 3.3 right side, right lane), visible by the green color of the heat map.

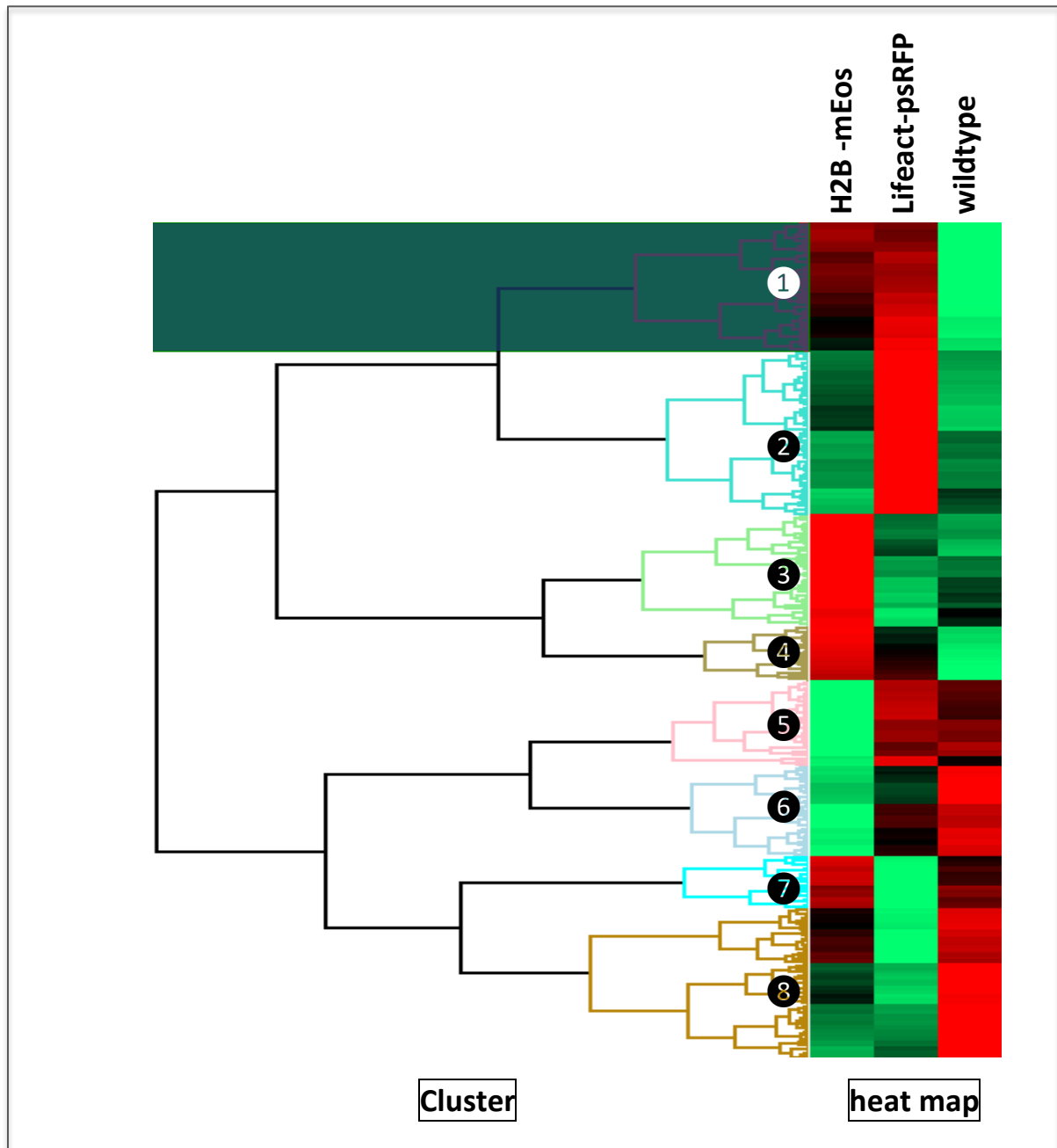


Figure 3.3 Overview of the heat map following the Euclidean clustering of H2B-mEos, Lifeact-psRFP, and WT

Proteins were clustered according to their Euclidean distance. Groups are reduced to 8 clusters (visible via different colors and numbers ①-⑧). A heat map was generated when the three different samples of H2B-mEos, Lifeact-psRFP, and wildtype were compared. Mapping was visualized by the color key (see Figure 2.3 p.22). High abundance increases red intensity whereas low abundance leads to a green color in the heat map.

The blue background visualizes the first cluster (①), proteins that are more abundant in the transgenic lines compared to wildtype).

RESULTS

Since this study aimed to find proteins that are more abundant in the transgenic lines, the cluster shown in blue was chosen for further investigation. In this cluster 69 proteins of the transgenic line behaved in a similar way when compared to the wildtype (Figure 3.4). The identifications of the proteins are shown by the FASTA headers (see Appendix Table A 5.2 pp.96). In the upper two thirds of the heat map, the proteins are more abundant in H2B-mEos and Lifeact-psRFP, indicated by the red color, whereas the same proteins are depleted in wildtype (indicated by the green color). However, the lower third of the map reveals only slight differences of protein amount in H2B-mEos compared to wildtype (black color), whereas the same proteins are clearly more abundant in Lifeact-psRFP (red color).



Figure 3.4 “Zoom-in”: Heat map of proteins that are more abundant in transgenic lines

Names of the proteins of the chosen cluster were presented in FASTA-format. All FASTA names of 69 proteins identified in cluster ① are listed in Table 5.1 (see Appendix pp.96). Mapping was visualized by the color key (see Figure 2.3 p.22). High abundance is visualized by a red color whereas low abundance is visualized by a green color in the heat map.

A few proteins in cluster ① are known as non-nuclear proteins, for example isocitrate dehydrogenase (see Appendix Table A 5.2 pp.96). The appearance of these proteins is the result of cellular contamination: small cytoplasmic proteins were isolated and filtered together with the nucleus. Some identified proteins such as ATPases and proteasomes (see Appendix Table A 5.2 pp.96) are commonly localized in both the nucleus and the cytoplasm. Following the scope of the dissertation, this work will not concentrate on these proteins; Since the previous results in 3.1 revealed different nuclear migration behavior and an altered nuclear shape in the transgenic cell lines, the histone packaging and abundance might be different compared to the non-transformed nuclei. This could be the reason for a changed nuclear architecture. To test this, five proteins were selected in the next step from the cluster ① for detailed analysis, which are histones or histone related proteins: linker histone H1, linker histone H1C, core histone H2B, plus the two enzymes histone deacetylase, and importin (Table 3.1). Positive values indicate high abundance of the protein, whereas negative values indicate low abundance. It needs to be noted that the values are unitless since this method allows accurate comparison but gives no conclusion of the total amount of protein detected.

The linker histone H1 is more abundant in H2B-mEos (+0.62) and Lifeact-psRFP (+0.53) compared to WT (-1.15). Its variant linker histone protein H1C is also more abundant in both of the transgenic cell lines (about +0.45 and +0.69, respectively) compared to the non-transgenic line (-1.14). As expected, the core histone H2B is more abundant in the H2B-mEos overexpression line (+0.52). However, it is also more abundant in Lifeact-psRFP (+0.63). The normalized intensity calculated of these proteins in wildtype is about -1.15. Also, histone deacetylase is found to be more abundant in H2B-mEos (-0.10) than in WT (-0.94). However, the frequency of histone deacetylase is much higher in Lifeact-psRFP (+1.05) compared to both (WT and H2B-mEos). Further, importin is found more often for both transgenic lines H2B-mEos (+0.63) and Lifeact-psRFP (+0.53) in comparison to wildtype (-1.15).

Table 3.1 Selected proteins: LFQ intensities for respective cell line

The table shows the normalized intensities for five different proteins based on label-free quantification (LFQ). Name of the protein is given in FASTA-format below the table with Sequence ID of the UniProtKB, Protein name, OS (Organism Name), GN (Gene Name), PE (Protein Existence), SV (Sequence Version). The values after normalization with z-score for each protein found in the H2B-mEos line, Lifeact-psRFP line, and the non-transformed wildtype are given in the table.

Protein	LFQ intensity mEos-H2B	LFQ intensity Lifeact-psRFP	LFQ intensity wildtype
#1	0.6219	0.5316	-1.1535
#2	0.4541	0.6924	-1.1465
#3	0.5214	0.6315	-1.1529
#4	-0.1041	1.0480	-0.9439
#5	0.6250	0.5283	-1.1533

NAMES of the selected proteins in FASTA format

#1: Q9SLS1|Q9SLS1_TOBAC **Histone H1** OS=Nicotiana tabacum GN=NtH1 PE=2 SV=1

#2: Q9SWA4|Q9SWA4_TOBAC **Histone H1C** OS=Nicotiana tabacum GN=H1c PE=2 SV=1;

#3: A8J6V0|A8J6V0_TOBAC **Histone H2B** OS=Nicotiana tabacum GN=NtH2B2 PE=2 SV=1

#4: E1U7Y2|E1U7Y2_TOBAC **Type 2 histone deacetylase a** OS=Nicotiana tabacum GN=HD2a
PE=2 SV=1

#5: A0A076L4P6|A0A076L4P6_TOBAC **Importin** subunit alpha OS=Nicotiana tabacum PE=2
SV=1

3.3 Cytoskeletal dynamics, motors as well as intranuclear factors are involved in axis formation

Since the results in 3.1 revealed that induction and manifestation of cell axes can be uncoupled from nuclear positioning, in this chapter the role of intracellular factors in polarity and axis formation will be investigated. Therefore, intracellular factors were altered on a genetic level by overexpression and additionally on a pharmacological level by drug treatments. Subsequently, the regeneration patterns of the protoplasts were compared to the non-transformed untreated BY-2 WT cell line.

To quantify the observations of regenerating protoplasts, the classification of regeneration stages will be presented and described first. Afterwards, in the second sub section, cytoskeletal elements together with their motor proteins assumed to be involved in axis formation will be analyzed. It starts with the analysis of the influence of a perinuclear actin basket, stabilization and destabilization of actin filaments and their motor protein myosin XI in axis formation. This part continues with the influence of microtubules plus their special motor protein kinesin KCH that connects actin with microtubules. Eventually, the effect on axis formation of the interior of the nucleus (DNA packaging) and its connection to the cytoskeleton via the nuclear membrane protein WIT will be presented. Since many different candidates were tested, a short overview of the impact on cell polarity of these factors will be given at the end of this section.

3.3.1 Classification of different regeneration stages

In order to follow the formation of polarity and axis *de novo*, a staging system modified from Zaban *et al.* (2013) was used to generate quantitative data on the temporal patterns of regeneration (Figure 3.5).

Based on delineated differences in cell shape and cell-wall reformation, the cells were clearly assigned to one of five stages schematically represented in Figure 3.5. Stage 1, prevailing at the end of digestion (defined as $t = 0$), comprised round, completely symmetrical protoplasts lacking any indications for axis or polarity. The nucleus is mostly ovoid in shape and placed at the periphery. Subsequently, the nucleus moves from the periphery of the cell towards the

cell center and becomes spherical. About 12–24 h later, a new cell wall has been first synthesized as visualized by staining with Calcofluor White. These cells still show radial symmetry and are classified into stage 2. Between day 1 and day 2 of regeneration, cell shape changes distinctly, and a clear cell axis emerges leading to an ovoid shape. The presence of a cell axis represents the criterion for stage 3. Subsequently, this axis becomes manifest as cell elongation. Cells, where the long axis has reached a length, which is more than twice as long as the short axis, fall into stage 4. At this stage, some of the cells already begin to divide axially, producing the pluricellular files characteristic of tobacco suspension cells. These files are indistinguishable from those derived from walled cells. During this final step of regeneration, the nucleus is still tethered at the cell center and has become elliptic, in which its longer axis is parallel to the elongation axis. Failure in axis manifestation leads to cells in which a third pole emerges. These aberrant tripolar cells are defined as stage 5. In these cells, the position of the nucleus does not follow any obvious rule.

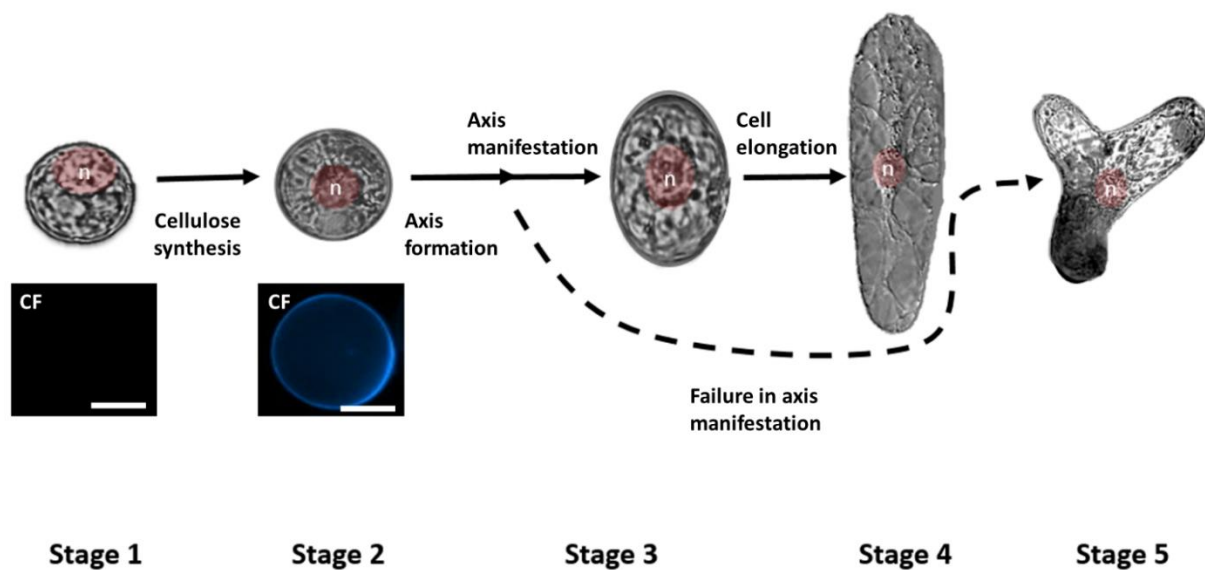


Figure 3.5 Classification of different regeneration stages

Classification into distinct stages (according to Zaban *et al.* 2013) used for the current study to follow nuclear position (highlighted in red) in the context of axis formation. Stage 1 is defined by the absence of the cell wall. The protoplasts are completely spherical, the nucleus (n) is mostly located at the periphery. Stage 2 is defined by the presence of the cell wall which can be visualized by staining with Calcofluor White (CF, scale bars: 20 μm). Cells are still symmetrical. Stage 3 is defined by a break of radial symmetry. A clear axis emerges and axis becomes manifest. Stage 4 is defined by the elongated cell axis. Stage 5 occurs if axis manifestation is disturbed (dashed line) and tripolar structures are generated.

The relative frequencies of these five different stages were scored over time. In order to understand the role of the cytoskeleton, its motor proteins, and the interior of the nucleus, in addition to the non-transformed BY-2 cell line, different transgenic cell lines were used. These included a perinuclear actin marker line (Lifeact-psRFP), a class XIV-kinesin overexpression line (GFP-NtKCH), two cell lines where parts of myosin XI were overexpressed (GFP-Myo M+IQ, GFP-Myo TailN), a histone marker line (H2B-mEos), and a nuclear membrane protein overexpression line (GFP-AtWIT). Besides transgenic manipulation, the regeneration of the protoplasts was altered by a pharmacological approach using Latrunculin B, Phalloidin, and Oryzalin, and then quantified and compared to the non-treated BY-2 cell line in the following bar charts.

3.3.2 The perinuclear basket, actin dynamic, and motor protein myosin XI are involved in axis formation

Since the cytoskeletal element actin is indispensable for cell polarity in many different organisms, the role in axis formation in the BY-2 protoplast system of a perinuclear actin basket (via overexpression of Lifeact-psRFP), the dynamic of actin (via treatment with Phalloidin, Latrunculin B), and its functional motor protein myosin XI (via overexpression of GFP-Myo M+IQ and GFP-Myo TailN) will be presented here.

Since the formation of a cell axis is preceded by the formation of a new polarity (Zaban *et al.* 2013), in the following, for pragmatic reasons, the term axis formation will mainly be used in the following, implying that polarity induction has been successfully completed, when a cell axis becomes visible.

3.3.2.1 Overexpression of the perinuclear actin marker Lifeact-psRFP promotes axis formation, but perturbs axis manifestation

To reveal the role of the perinuclear basket in axis formation, a transgenic line Lifeact-psRFP was used, in which only the actin filaments of this perinuclear cage are labelled via a photoswitchable red fluorescent protein. The temporal pattern of regeneration in the Lifeact-psRFP line was compared to the situation in the non-transformed BY-2 wildtype cell line (Figure 3.6).

RESULTS

Already after the first day of regeneration, the majority of the transgenic cells had formed a new cell wall, thus entering stage 2. Only some 10% were still lacking a cell wall, which was in sharp contrast to non-transformed cells, where around 60% of the cells still had not generated a cell wall. A significant fraction (30%) of the Lifeact-psRFP cells had even already passed the transition to stage 3, which is defined by an ovoid cell shape, compared to only 5% in the non-transformed cell line. Even at day 2 of regeneration, the transgenic lines remained ahead with more than 40% of the cells in stage 3 in comparison to about 25% in the non-transformed cell line. At this time point, first deviations from the normal sequence of events became detectable: more than 40% of the Lifeact-psRFP cells started to divide prematurely (in stage 3), although axis manifestation had not yet initiated, which was different from the non-transformed control (see Appendix Figure 5.6 p.99). Also, in many cells, during day 3 after regeneration, a second competing axis was observed, leading to a significantly higher frequency of tripolar structures (stage 5), compared to the non-transformed cell line. Although the initial course of regeneration was accelerated in the transgenic line, the transition from stage 3 to 4 (axis manifestation, normally at day 4) was not (indicating that the transgenic cells required more time to leave stage 3). From day 5, the frequency distributions of transgenic line were not distinguishable from those of the non-transformed controls, indicating that the transition from stage 3 to 4 was not arrested, but just delayed by overexpression of the transgene.

Thus, axis formation was significantly promoted by the Lifeact-psRFP cell line, whereas the final step of regeneration (axis manifestation) was delayed. The latter correlated with a higher frequency of aberrant tripolar structures in the transgenic line compared to the non-transformed cell line.

To test whether these deviations are a consequence of overexpression *per se*, a cell line, where free GFP was overexpressed under the same promotor (CaMV-35S) was employed. The regeneration pattern of this 35S::GFP line was exactly the same as that of non-transformed controls (see Appendix Figure 5.7 p.100) suggesting that the effects observed in the Lifeact-psRFP line were specific to the overexpression of the perinuclear actin marker.

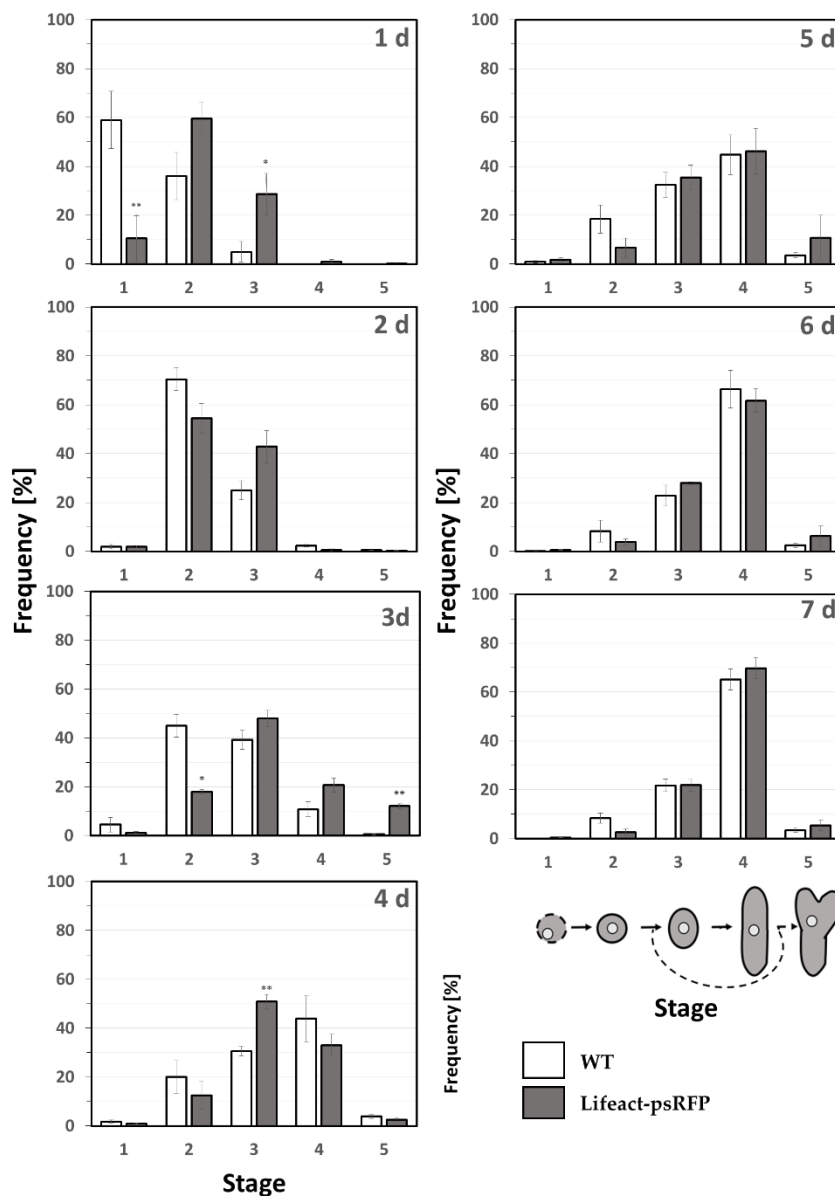


Figure 3.6
Frequency distributions of regeneration stages in BY-2 Lifact-psRFP

Frequency distributions of the different regeneration stages for different time points after protoplast preparation in BY-2 Lifact-psRFP (gray bars) compared to non-transformed BY-2 (WT, white bars). Stages are indicated schematically. Frequency distributions were calculated from 3,000 individual cells per time point from three independent biological replications. Error bars show standard errors of the mean (SE). Asterisks represent significance of indicated differences as tested by a paired, two-sided t-test (*P < 5%, **P < 1%).

3.3.2.2 Stabilization of actin promotes axis formation, destabilization causes a delay in cell wall synthesis but not in axis formation nor in axial cell expansion

To investigate the role of the dynamic of all actin filaments on axis formation in this modified system, actin drugs like Phalloidin, which stabilizes actin, and Latrunculin B, which is known for its destabilization effect, were applied to the BY-2 WT cell line and compared to the non-treated BY-2 WT protoplasts (Figure 3.7).

After treatment with 100 nM Phalloidin in the BY-2 WT cell line similar to the previous results of Lifact-psRFP cell line, the early phases of regeneration were promoted. At day 1, already 30% of the Phalloidin treated cells had advanced to stage 3 and more than 20% even

RESULTS

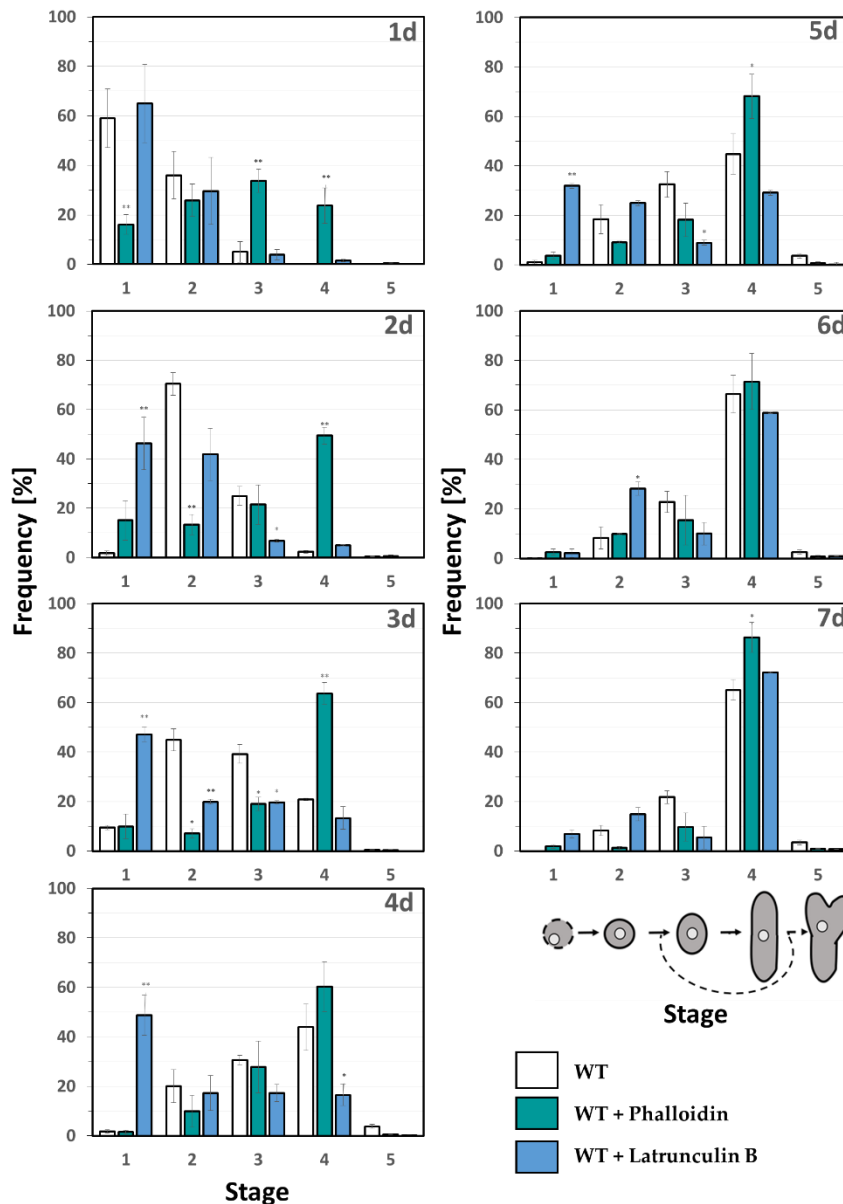
developed further to the final stage 4 in comparison to less than 5% to 0% in non-treated cells. This means that most of the Phalloidin treated cells had built an axis by this time and were elongating. In contrast, treatment with 75 nM Latrunculin B, which is known for its destabilization function of actin, did not show significant differences to non-treated cells so far. At day 1 most of the Latrunculin B treated cells were still in stage 1, e.g. had not generated a new cell wall, and only about 30% were categorized as stage 2.

During day 2 and 3 after regeneration, the frequency of cells in stage 4 increased rapidly in the Phalloidin treated cells compared to the untreated cells. At day 3, already 60% of the cells treated with Phalloidin were elongated, i.e. they had expressed their axis, whereas only 10% of the non-treated cells had reached this stage 4. This means that at day 3, most of the Phalloidin treated cells had already fully regenerated from round protoplasts to elongated cells. Meanwhile, Latrunculin B treated cells revealed to have troubles with continuing to stage 2, which is defined as the stage of cell wall formation. At day 2, still more than 40% remained in stage 1, whereas none of the non-treated cells remained in stage 1 but continued further to stage 2 (70%). At day 3 and 4 over 40% of the Latrunculin B treated cells had not built a cell wall and remained in stage 1. This delay means that Latrunculin B treated cells struggled with the first step, which is cell wall formation.

From day 5 onwards, the frequency distributions of actin drug treated cells began to look similar to the non-treated cells, indicating that transition from stage 1 to 2 was delayed by Latrunculin B, but on the other hand, the transition from 2 to 3 and 4 was not delayed by Latrunculin B.

Thus, cell wall and axis formation were significantly promoted by Phalloidin, whereas cell wall formation, but not axis formation, was significantly delayed by Latrunculin B. However, with the low concentrations of actin drugs applied, no disruption of polarity in terms of the appearance of stage 5 cells has been observed.

To sum up, stabilization of actin via low concentrations of Phalloidin significantly promoted all steps of regeneration (cell wall synthesis, axis formation and elongation). In contrast, destabilization of actin filaments via Latrunculin B caused a delay in cell wall synthesis. However, cell elongation was not negatively affected by low concentrations of Latrunculin B.



3.3.2.3 Destabilization of the perinuclear actin cage in Lifact-psRFP causes a similar phenotype as in the non-transgenic line

Next, to see if the destabilizing effect of Latrunculin B can be rescued by the perinuclear basket marker line, 75 nM Latrunculin B was applied to the transgenic cell line Lifact-psRFP and directly compared to the non-treated WT and non-treated Lifact-psRFP as well as to the 75 nM Latrunculin B treated non-transformed WT (Figure 3.8).

After the first day of regeneration, the distribution of BY-2 WT, Latrunculin B treated WT and Latrunculin B treated Lifact-psRFP appeared to be similar. About 60% did not generate a new

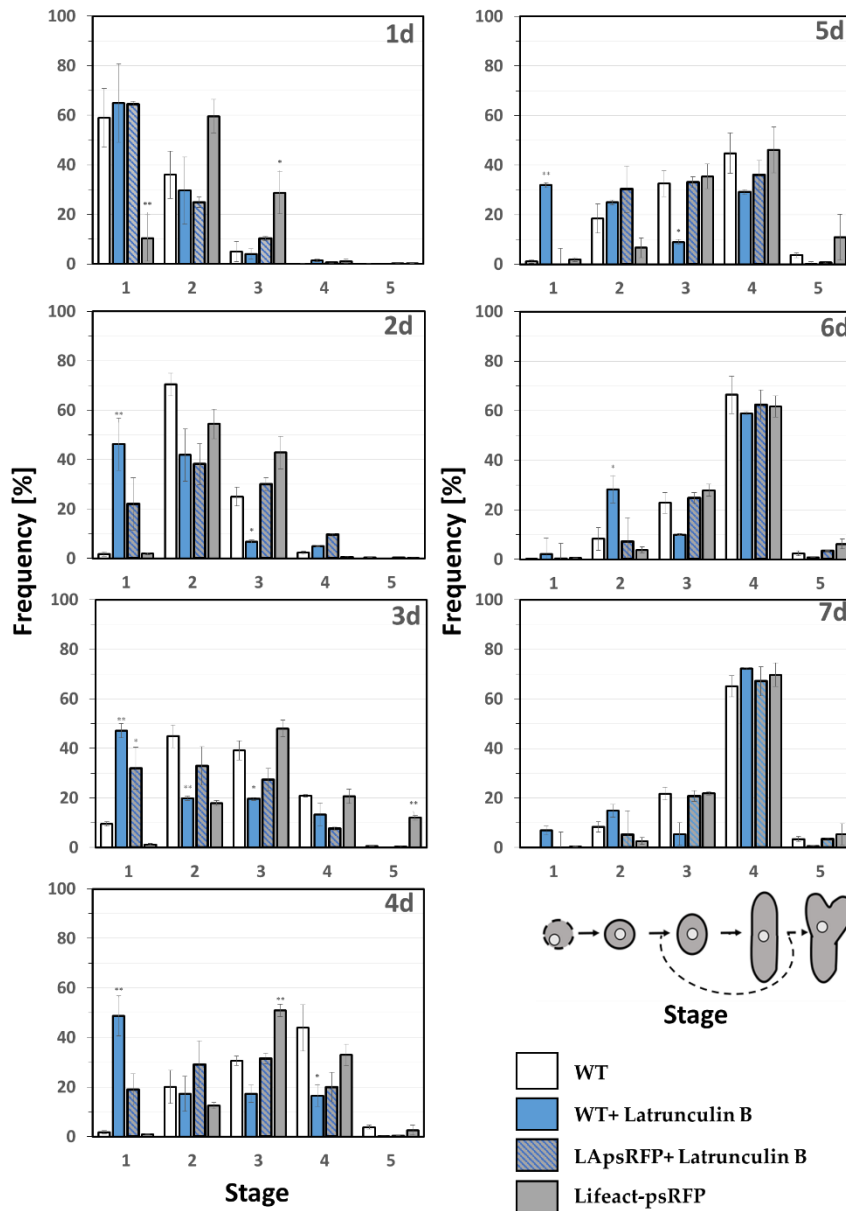
RESULTS

cell wall yet, whereas the majority of the untreated Lifact-psRFP had already formed a new cell wall.

At day 2 more than 40% of the Latrunculin B treated WT protoplasts still remained in stage 1, and thus had not built a cell wall. In contrast, in Latrunculin B treated Lifact-psRFP only half of this amount (20%) were lacking a new cell wall. About 30% of the Latrunculin B treated Lifact-psRFP cells had even passed the transition to stage 3, which is defined by an ovoid cell shape. This frequency showed the average of the stage 3 distribution of untreated WT (above 20%) and untreated Lifact-psRFP cells (above 40%), meaning that axis formation in Latrunculin B treated Lifact-psRFP was still slightly but not significantly delayed compared to untreated WT. However, axis formation was not delayed compared to untreated WT.

The pattern of regeneration of Latrunculin B treated Lifact-psRFP on day 3 stayed nearly the same as on day 2. During day 4 the number of protoplasts in stage 1 of Latrunculin B treated Lifact-psRFP cell decreased to less than 20%. Another 20% of Latrunculin B treated Lifact-psRFP cells reached the final stage 4, whereas more than 40% of non-treated WT cells were already elongated. This low frequency of stage 4 cells in Latrunculin B treated Lifact-psRFP resulted from the delay in transition from stage 1 to 2, since from day 5 the frequency distributions of the transgenic line were not distinguishable from those of the non-transformed and non-treated controls. Therefore, transition from stage 1 to 2 was not arrested, but just slightly delayed compared to the Latrunculin B treated WT. Whilst the regeneration pattern of Lifact-psRFP showed the occurrence of tripolar structures on day 3 and 5, it should be emphasized that Lifact-psRFP after Latrunculin B treatment does not show tripolar cells at any time point.

In summary, cell wall synthesis was just slightly retarded by Latrunculin B in the Lifact-psRFP cell line but not significantly compared to BY-2 WT, whereas axis formation and elongation were not delayed any more compared to the untreated, non-transformed cell line. Additionally, the appearance of tripolar structures was no longer observed for Lifact-psRFP after treatment with Latrunculin B.



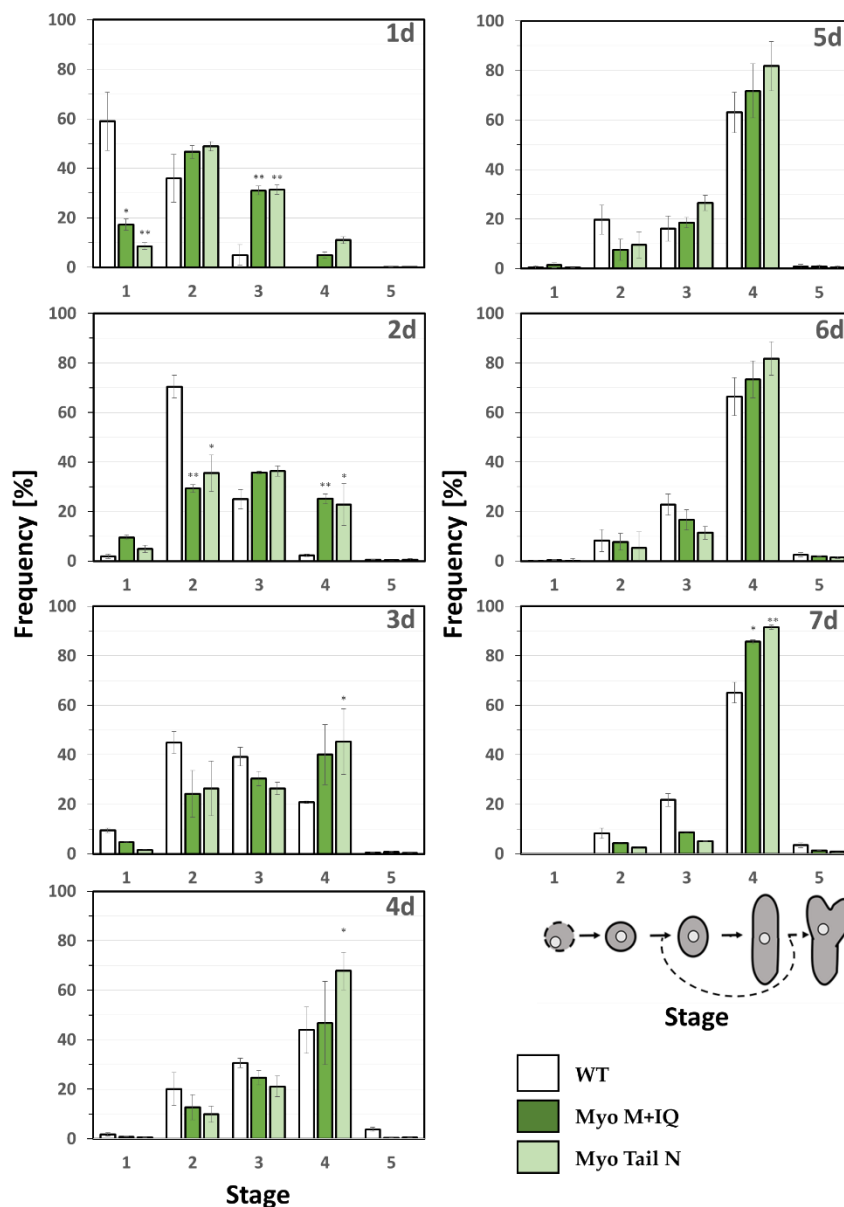
3.3.2.4 Overexpression of myosin XI promotes axis formation

Since the influence of actin dynamic in regeneration has been tested, the effect of the motor proteins that run along actin filaments was analyzed. Therefore, two transgenic lines were used, in which a part of the motor protein myosin XI was overexpressed. Either the motor domain plus the IQ motif of the myosin XI, or the TailN domain of myosin XI was overexpressed, and the respective regeneration pattern was compared to the non-transformed WT (Figure 3.9).

RESULTS

As a consequence of overexpressing GFP-Myo M+IQ and GFP-Myo TailN early phases of regeneration were promoted. At day 1, less than 20% of the transgenic cells were in stage 1 in comparison to about 60% in non-transformed cells. Whereas around 30% of the transgenic GFP-Myo M+IQ as well as GFP-Myo TailN cells continue to stage 3, and thus built an axis, only some 5% of non-transgenic cells had reached this stage. During day 2 and 3 after regeneration, the frequency of cells in stage 4 increased faster in the GFP-M+IQ and GFP-TailN line compared to the non-transformed line. At day 2, already 20% of the manipulated cells were elongated, rising to around 40% at day 3, whereas less than 5% of the non-transformed cells had reached this stage 4 at day 2 and nearly 20% at day 3. During day 3 and 4 the frequency of stage 4 increased further in both transgenic cell lines. At day 5 no transgenic cells were observed in stage 1 and only less than 10% were in stage 2 compared to 20% of non-transgenic cell in stage 2. At days 6 and 7 the frequency of cells in stage 4 increased further. More than 80% of cells of both the myosin overexpression lines reached the final stage of regeneration at day 7. Besides, barely any tripolar structures were observed in the treated or non-treated line.

Overall, the regeneration was clearly faster in both the overexpression lines, which can be attributed to an accelerated axis formation.



3.3.3 Microtubules and their motor proteins are involved in axis formation

In addition to actin, microtubules present the second part of the cytoskeletal elements in plant cells and are involved in cell expansion as well as nuclear migration. In the following section, charted data will be presented of a special member of the class-XIV kinesins with a calponin homology domain (GFP-NtKCH), which can bind to both actin and microtubules. Finally, results gathered from an Oryzalin treatment in BY-2 WT protoplasts will be presented.

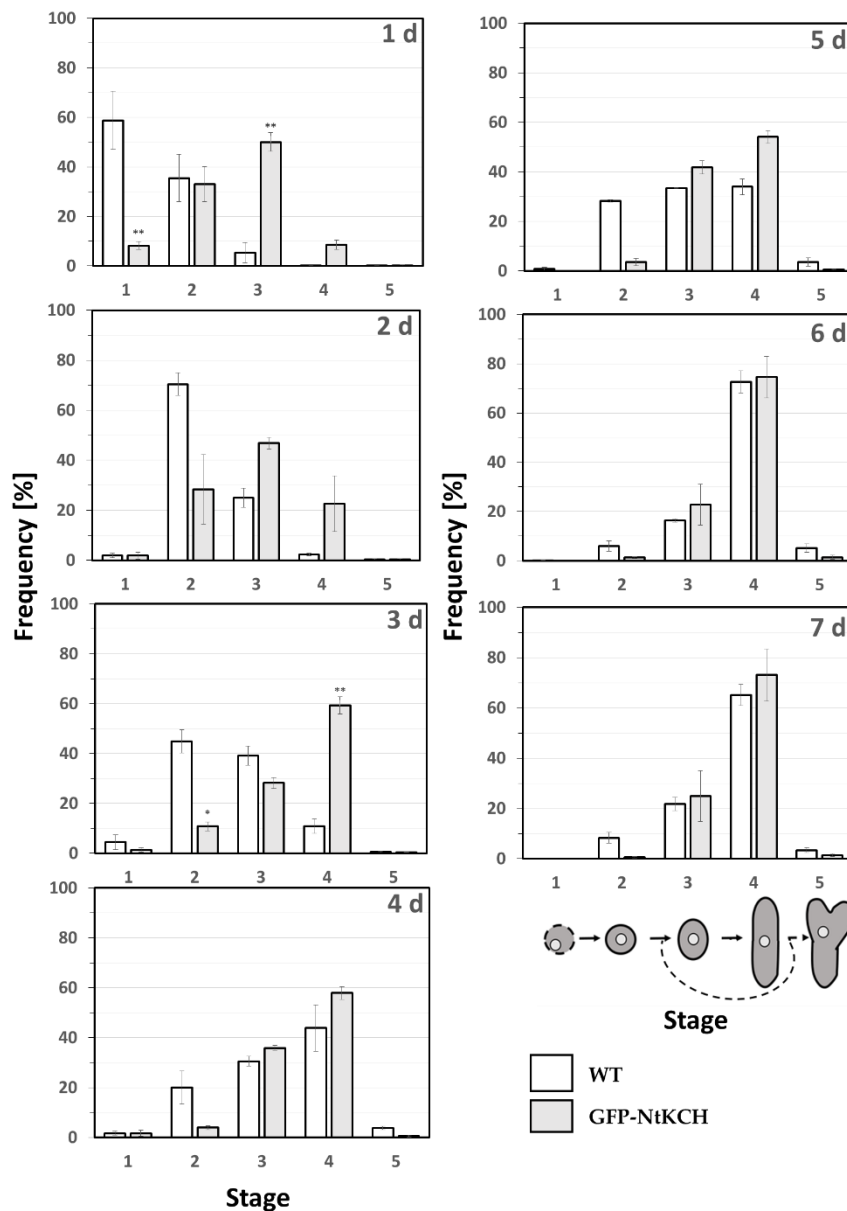
3.3.3.1 Overexpression of the class XIV kinesin KCH promotes both axis formation as well as axis manifestation

Motor proteins, which run along the cytoskeleton, play a pivotal role for cell elongation and organelle movement. Since microtubules as well as actin filaments participate in nuclear positioning, the class-XIV kinesin NtKCH as cross-linker of these cytoskeletal elements is interesting. Therefore, regeneration in a GFP-NtKCH overexpressor line was compared to the regeneration of non-transformed wildtype cells (Figure 3.10).

Similar to the Lifact-psRFP cell line, the early phases of regeneration were promoted in the GFP-NtKCH overexpression line. At day 1, less than 10% of the transgenic cells were in stage 1, in comparison to about 60% in non-transformed cells. GFP-NtKCH cells in stage 3 were already predominant after 1 d, which means that most of the cells had built an axis by this time. Around 10% had even developed further to stage 4, which was not the case for non-transformed cells. During day 2 and 3 after regeneration, the frequency of cells in stage 4 increased rapidly in the GFP-NtKCH line compared to the non-transformed line. At day 3, already 60% of the cells were elongated, i.e. they had expressed their axis, whereas only 10% of the non-transformed cells had reached this stage 4. At days 4 and 5, the kinesin overexpression line showed a higher frequency of cells in stage 4 compared to non-transformed cells. At days 6 and 7, the regeneration pattern of the transgenic line and the non-transformed line had approximated. In contrast to the Lifact-psRFP, no tripolar cells were observed during regeneration of GFP-NtKCH.

Overall, the regeneration was clearly faster in the GFP-NtKCH overexpression line, which can be attributed to an accelerated axis formation. Whereas axis manifestation was delayed upon overexpression of Lifact-psRFP, the overexpression of GFP-NtKCH did not impair axis manifestation, which is evident from the efficient progression into stage 4 and the absence of aberrant tripolar structures.

It should be mentioned that the overexpression of OsKCH, a heterologous KCH from rice, has also been tested. The effect of GFP-OsKCH was comparable to that of GFP-NtKCH, but the amplitude of the effect was less pronounced (see Appendix Figure 5.8 p.101).



3.3.3.2 Elimination of microtubules impairs axis formation

Due to the fact that the KCH runs along microtubules, which play a pivotal role in axis formation and nuclear migration, the effect of eliminating microtubules via 500 nM Oryzalin was tested (see Figure 3.11).

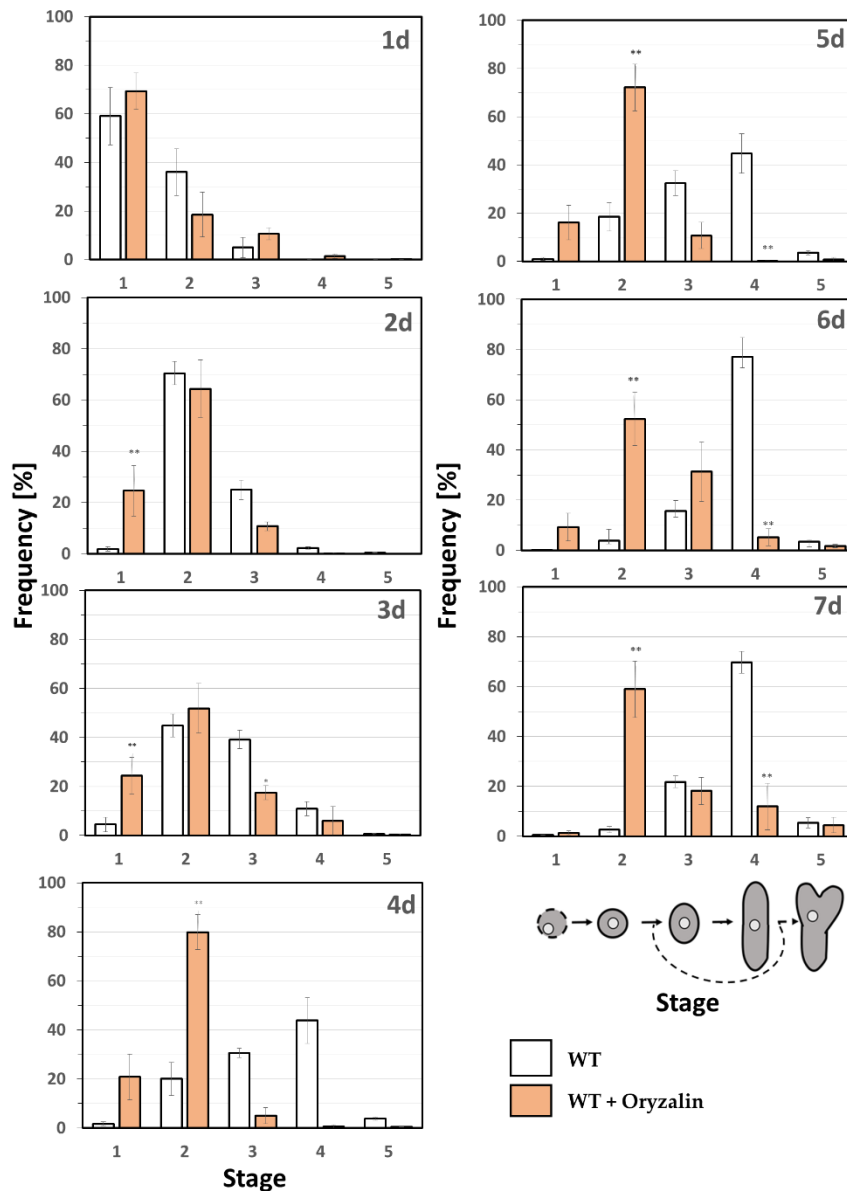
Compared to the untreated wildtype cells, the early progression of regeneration was significantly delayed in the Oryzalin treated cell line, from two days after regeneration the many of protoplasts remained in stage 1: At day 2 and 3 still 20% of the Oryzalin treated cells lacked a cell wall, whilst 40% of non-treated cells already advanced to stage 3 compared to only 20% in the Oryzalin treated cell line at day 3. While at day 4, the frequency of stage-4

RESULTS

cells had increased to 40% in the untreated WT cell line, hardly any Oryzalin treated cells were found to have reached stage 4. Thus, after retarded transition from stage 1 to 2, Oryzalin treated cells remained trapped in stage 2, maintaining spherical cell shape without clear identification of an axis. From day 5 on the distribution pattern remained the same for the Oryzalin treated cell line, since axis formation and elongation hardly occurred until day 7. No tripolar cells were observed during regeneration of Oryzalin treated protoplasts.

Additionally, Oryzalin treatment had also been tested in the GFP-NtKCH line in which axis formation was significantly promoted originally. However, the effect of Oryzalin overrules the promoting effect of overexpression of KCH (see Appendix Figure 5.10 p.103). Thus, the regeneration pattern of Oryzalin treated GFP-NtKCH looked nearly the same as the regeneration pattern of Oryzalin treated WT. Further it should be mentioned that the overexpression of the microtubule plus end-binding protein EB1 had no effect on axis formation (see Appendix Figure 5.9 p.102).

Overall, polarity induction as well as axis formation were significantly delayed and axis elongation hardly occurred until day 7, due to the elimination of microtubules after treatment with low concentrations of Oryzalin.



3.3.4 The interior of the nucleus and its membrane proteins affect axis formation

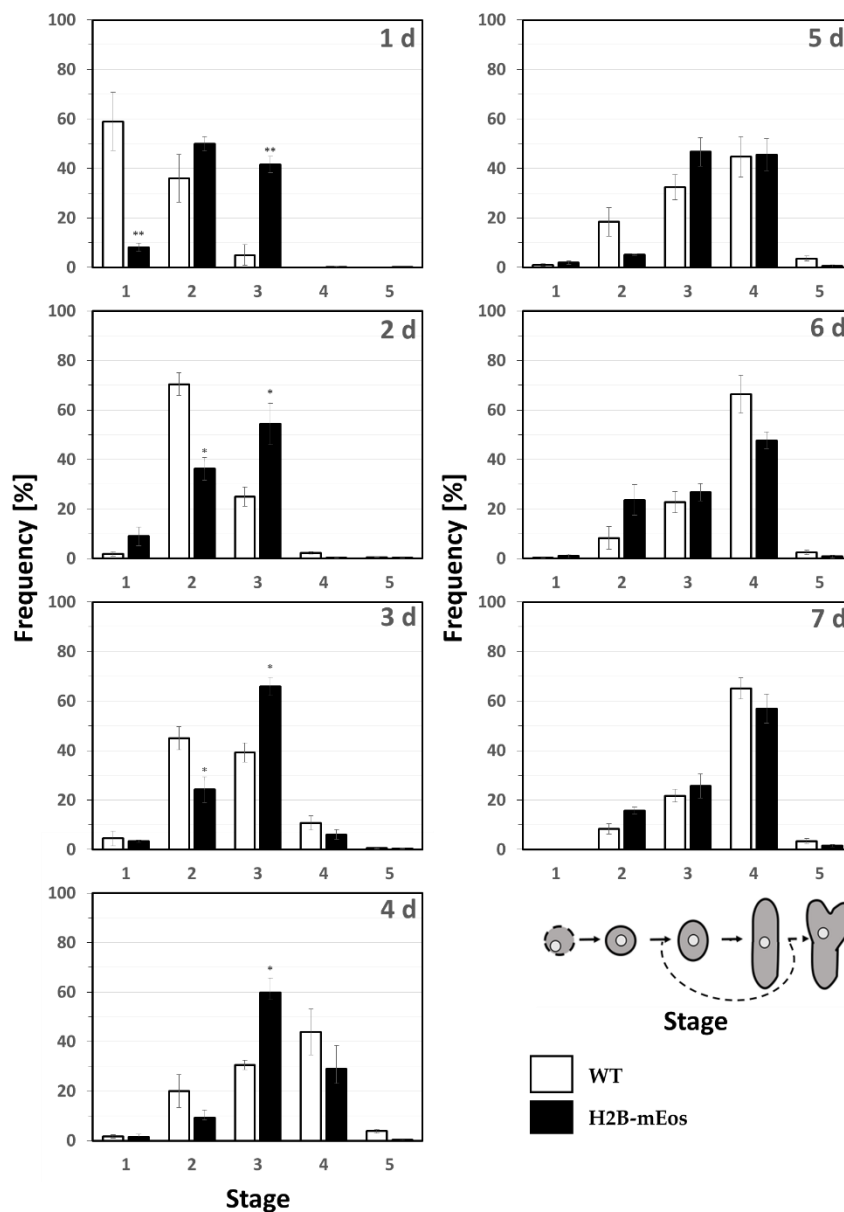
Besides the cytoskeleton accompanied by its variable dynamic and attached motor proteins within the cytoplasm, changes of intranuclear factors on their connection to the cytoskeleton could influence polarity and axis formation as well. This assumption will be tested in the following section by changing the architecture of the chromatin via overexpression of a histone in H2B-mEos and by influencing the bridge of inner nuclear factors with outer nuclear factors via overexpression of a nuclear membrane protein in the GFP-AtWIT cell line.

3.3.4.1 Overexpression of the histone marker H2B-mEos promotes axis formation, but delays axial cell expansion

Since plants lack a canonical nuclear lamina, polarity formation is expected to depend not only on extranuclear factors or the activity of motor proteins, but also on the intranuclear architecture. Hence, a cell line was tested in which a labelled histone (H2B-mEos) was overexpressed to probe for potential effects of intranuclear architecture on the regeneration pattern (Figure 3.12).

The early progression of regeneration was promoted in the H2B-mEos line, since already one day after regeneration; the majority of protoplasts had reached stage 2 and 3. At the same time, already around 40% of the cells had advanced to stage 3 in comparison to only about 5% in the non-transformed cell line. Although the frequency of stage 3 rose even further during the second day, this was not followed by an increased frequency of stage 4. While at day 3, the frequency of stage-3 cells had increased to 60%, only 5% of cells were found to have reached stage 4, which was even less than the value for non-transformed cells (10%), that derived from a significantly lower level of stage-3 precursors. Thus, H2B-mEos cells remained temporarily trapped in stage 3, maintaining an ovoid cell shape with a delay of elongation growth. Although significantly delayed, this elongation ensued eventually. The frequency distributions for day 5, 6 and 7 progressively approached those of the non-transformed cell line, only with a somewhat smaller frequency of transformed cells at stage 4 compared to non-transformed cells. However, despite the delay in cell expansion, barely any tripolar structures were observed in the H2B-mEos or in the non-transformed line. Additionally, low concentrations of the cell wall blocker 2,3 Dichlorobenzonitrile (DCB) were tested in regenerating H2B-mEos protoplasts (see Appendix Figure 5.11 p.104). Besides a delay in cell wall synthesis, the application of DCB in non-transformed BY-2 WT also showed tripolar structures. Treatment of DCB in H2B-mEos resulted in a delay in cell wall synthesis solely without the occurrence of tripolar structures. Thus, the effect of tripolar structures as a result of DCB was rescued by using H2B-mEos protoplasts instead of WT.

Overall, in H2B-mEos, cell wall synthesis and axis formation at the early phases of regeneration was promoted, and the initial steps of axis manifestation proceeded normally. However, the strong cell elongation driving the transition of stage 3 to stage 4 was delayed.



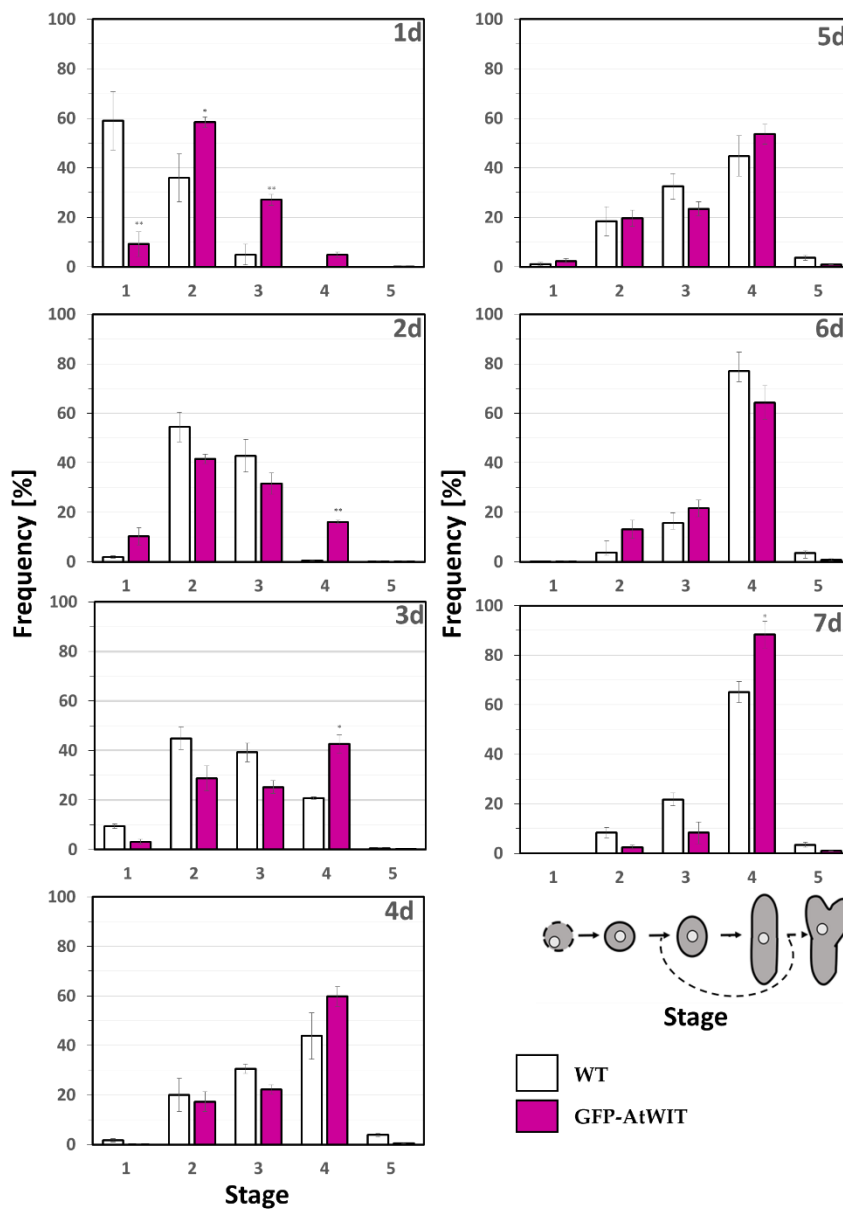
3.3.4.2 Overexpression of the nuclear membrane marker GFP-AtWIT promotes axis formation

Nuclear membrane proteins create a bridge between the interior of the nucleus and the cytoskeleton via motor proteins. Since the WIT protein originally isolated from *Arabidopsis thaliana* links the nuclear membrane to the cytoskeleton the regeneration in a GFP-AtWIT overexpressor line was compared to the regeneration of non-transformed wildtype cells (Figure 3.13).

RESULTS

Similar to the H2B-mEos cell line, the early phases of regeneration were promoted in the GFP-AtWIT overexpression line. At day 1, about 10% of the transgenic cells were in stage 1 in comparison to about 60% in non-transformed cells. By this time around 40% of the cells had advanced to stage 3, i.e. they built an axis, in comparison to only about 5% in the non-transformed cell line. Some 5% had even developed further to stage 4 which was not the case for non-transformed cells. During day 2 and 3 after regeneration, the frequency of cells in stage 4 quickly increased from 10% to 40% in the GFP-AtWIT line compared to 0% to 20% in the non-transformed line. At day 4, already 60% of the cells were elongated, i.e. they had expressed their axis, whereas only 40% of the non-transformed cells had reached this stage 4. At days 5 and 6, no significant difference was observed between the regeneration pattern of the nuclear membrane protein overexpression line and the non-transformed cell line. At day 7, more than 80% of transgenic cells had been classified to the final regeneration stage 4. Additionally, no tripolar cells were observed during regeneration of GFP-AtWIT.

Overall, the regeneration was clearly faster in the GFP-AtWIT overexpression line, which can be attributed to an accelerated axis formation. Whereas axis elongation was delayed upon overexpression of H2B-mEos, the overexpression of GFP-AtWIT did not impair axial expansion, which is evident from the fast progression into stage 4.



3.3.5 Summing up

Different treatments as well as different overexpression lines influencing the cytoskeleton, its motor proteins, the interior of the nucleus, and the nuclear membrane, caused different effects in cell wall synthesis, axis formation, and cell elongation during regeneration of BY-2 protoplasts. To summarize these, the outcome of the third result part is listed in the following table and explained below (Table 3.2).

Lifact-psRFP acting on the perinuclear basket promoted two steps (cell wall synthesis and axis formation). However, failure in axis manifestation had been shown. Treatment with low

RESULTS

concentration of Phalloidin which stabilizes actin filaments revealed a similar effect. However, it promoted all steps of regeneration. Low concentration of Latrunculin B, known for its destabilization effect upon actin filaments, caused a delay in cell wall synthesis, but not in axis formation nor cell elongation compared to the untreated WT control. In combination with Lifeact-psRFP, the effect was abolished. Overexpression of the motor plus IQ-domain of myosin XI (GFP-Myo M+IQ) led to enhanced cell wall synthesis, axis formation and cell elongation. The same was observed for the overexpression line of TailN of myosin XI (GFP-Myo TailN). Here, cell wall synthesis, axis formation and cell elongation were promoted as well.

The kinesin overexpression lines GFP-NtKCH as well as GFP-OsKCH caused a significantly faster cell wall synthesis, axis formation and cell elongation compared to the non-transformed WT. Treatment with Oryzalin, which eliminates microtubules, resulted in a significant delay in cell wall synthesis as well as axis formation. Axis elongation rarely occurred after Oryzalin treatment.

Overexpression of the core histone H2B fused to mEos led to faster cell wall synthesis and axis formation compared to the non-transformed WT. However, cell elongation was delayed in H2B-mEos. Overexpression of a nuclear membrane protein promoted all three steps (cell wall synthesis, axis formation and cell elongation) in GFP-AtWIT.

Table 3.2 Summary of the third result part - intracellular factors of polarity and axis formation

The overexpression lines or the cytoskeletal drugs acting on different locations within the cell are listed together with their respective effect in cell wall synthesis, axis formation, and cell elongation. Promotion is indicated by (+), delay is indicated by (-), and no influence is indicated by (o) compared to the non-transformed and untreated BY-2 WT. The table is ordered as follows: actin plus motor protein, microtubules plus motor protein, and inner nucleus plus nuclear membrane separated via dashed lines.

POINT OF ACTION	OVEREXPRESSION/ TREATMENT	CELL WALL SYNTHESIS	AXIS FORMATION	CELL ELONGATION
PERINUCLEAR ACTIN BASKET	Lifeact-psRFP	+	+	-
ACTIN FILAMENTS	Phalloidin	+	+	+
ACTIN FILAMENTS	Latrunculin B	-	o	o
MYOSIN XI	GFP-Myo M+IQ	+	+	+

MYOSIN XI	GFP- Myo TailN	+	+	+
KINESIN KCH	GFP-NtKCH	+	+	+
MICROTUBULES	Oryzalin	-	-	-
CORE HISTONE H2B	H2B-mEos	+	+	-
NUCLEAR MEMBRANE	GFP-AtWIT	+	+	+

3.4 Aligned structures of RGD peptides promote axis formation

Since the previous result part reveals that several intracellular factors clearly influence axis formation, in addition the role of extracellular factors will be addressed in this final section of the result part. To obtain a deeper understanding of the extracellular functions regarding axis formation, the role of the structural organization of RGD peptides arranged on aligned or unaligned fibers was investigated using structure-based nanotechnology. Polycaprolactone nanofibers were generated via an electrospin set-up. By rotating the collector at different speed rates, the fibers were orientated in an aligned or unaligned manner (see Appendix Figure 5.13 and Figure 5.14 pp.106). Subsequently, the scaffolds were activated by aminolysis and then immersed with the peptides (RGD or its reverse sequence DGR). Three days after regeneration on different surfaces (aligned or unaligned nanofibers with RGD, DGR or no peptides) cells were quantified and classified into four stages according to their shape (2=round, 3=oval, 4=elongated, 5=tripolar).

Figure 3.14 shows the distribution of cells grown on different surfaces. The legend on the right side depicts the six different surfaces, the legend on the bottom illustrates the regeneration stages. Cells regenerating on aligned and unaligned fibers without peptides serve as a control. The impact on axis formation of RGDs plotted on aligned or unaligned structures was compared to the control and to the reverse peptide sequence DGR.

Compared to cells regenerating on unaligned nanofibers with RGDs, axis formation was promoted in cells regenerating on aligned nanofibers with RGDs: More than 50% of the cells that were grown on discs with aligned nanofibers and plotted RGD peptides were already

RESULTS

elongated (stage 4). Less than 10% appeared still in a round shape (stage 2). This implies that most of the cells grown on aligned fiber-structures with RGDs peptides already undertook a break of radial symmetry and performed axis formation and further axis elongation. Whereas about 70% of the cells that were grown on discs with unaligned nanofibers and RGDs, were still round, i.e. most of those cells did not form an axis yet. Only some 5% of the cells on unaligned fibers reached the final stage 4, and thus were elongated.

Further, the diagram below shows that cells grown on a surface with RGDs on aligned fibers regenerate significantly faster compared to aligned fibers without peptides (untreated control): Less than 10% of the cells grown on aligned fibers without RGD reached the final elongated stage 4 compared to more than 50% of the cell grown on aligned fibers with RGD. More than 50% were still in round shape (stage 2) in cells grown on the untreated control fibers compared to less than 10% of the cells grown on aligned fibers with RGD.

Cells that were grown on fibers with the reverse sequence (DGR) showed considerably weaker effects compared to cells regenerating on RGD modified fibers. The cells on aligned organization of DGR regenerate slightly faster compared to cells on unaligned fibers with DGR: nearly 20% of the cells on aligned fibers with DGR were already elongated whereas a very low number of elongated cells were found grown on unaligned fibers with DGR (less than 1%). Nevertheless – compared to untreated nanofibers control – there is no significant evidence that DGR peptides alter the regeneration pattern.

Since no noteworthy amount of tripolar structures (stage 5) was observed for cells grown on all different surfaces, axis manifestation was not negatively affected by the extracellular structure.

It should be mentioned that cells regenerating without nanofibers on day 3 show a similar pattern compared to cells regenerating on untreated nanofibers (see WT 3d in Figure 3.6 p.41).

To conclude, only the aligned arrangement of RGDs on nanofibers but not the unaligned arrangement of RGD peptides significantly promotes axis formation compared to cells regenerating on untreated fibers or without fibers.

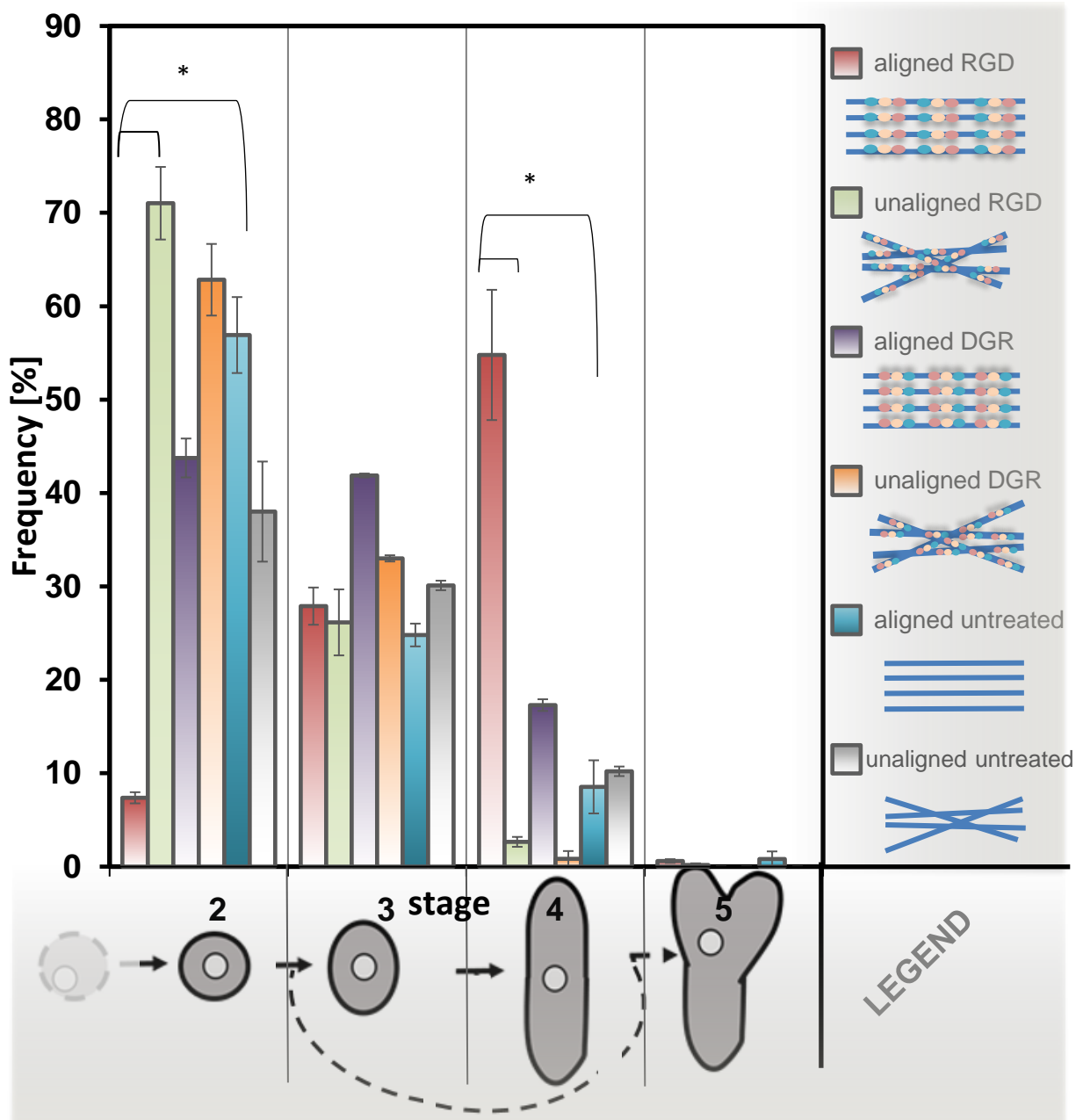


Figure 3.14 Frequency distributions of regeneration stages after three days on nanofibers

Frequency distributions of the different regeneration stages at three days after protoplast preparation of BY-2 wildtype cells on different surfaces: aligned fibers with RGD (red gradient bars), unaligned fibers with RGD (green gradient bars), aligned fibers with DGR (purple gradient bars), unaligned fibers with DGR (orange gradient bars), aligned fibers without peptides (blue gradient bars), and unaligned fibers without peptides (gray gradient bars). Stages are indicated schematically below. Explanation of respective bars together with their cartoon on the right side: blue lines indicate nanofibers, colored dots indicate RGD peptides, or in reverse direction DGR peptides. Frequency distributions were calculated from 1,000 individual cells from two independent biological replications. Error bars show standard errors of the mean (SE). Asterisks represent significance of indicated differences as tested by a paired, two-sided t-test (* $P < 5\%$).

3.5 Summary

To address the potential role of intracellular and extracellular factors for polarity and axis formation, an experimental system based on regenerating protoplasts was used, where the induction of a cell axis *de novo* can be followed by quantification of specific regeneration stages. The results

- a) revealed via time-lapse studies different nuclear migration behaviors of three overexpression lines during polarity induction and showed that the nuclear position is not a prerequisite for axis formation;
- b) presented differences in nuclear proteomes of two tested overexpression lines compared to nuclei of the non-transformed cell line via tandem MS and LFQ;
- c) showed which role intracellular factors play in axis formation investigated by comparing regeneration patterns of different overexpression lines and cytoskeletal drug treatments;
- d) indicated a significant influence of the structure of extracellular factors in axis formation tested via nano-structured aligned or unaligned fibers plotted with RGD peptides.

Contrary to the initial assumption, the results clearly revealed that nuclear position is not a prerequisite for polarity formation. Both nuclear migration and axis formation were faster compared to the non-transformed BY-2 WT as a consequence of overexpression of the perinuclear basket in the Lifact-psRFP cell line. In contrast, the nuclear migration in the histone marker line H2B-mEos and kinesin overexpression line GFP-NtKCH was delayed. Although in the latter the nucleus was still at the periphery, the cell already started to elongate. Moreover, the nuclear shape of the histone overexpressing line H2B-mEos was altered.

Proteomics of H2B-mEos and Lifact-psRFP nuclei indicate differences in their protein content compared to the nuclei of non-transformed wildtype. Histone proteins, histone linker proteins, and histone deacetylases were more abundant in the nuclei of the two transgenic cell lines than in the non-transformed cell line.

Furthermore, the results showed that overexpression of the perinuclear actin marker Lifact-psRFP, as well as stabilization of actin via Phalloidin, promoted cell wall and axis formation. However, axis manifestation was disturbed in Lifact-psRFP leading to tripolar structures.

Slight destabilization of actin via Latrunculin B caused a delay in cell wall synthesis. Latrunculin B treatment in the Lifeact-psRFP cell line showed a similar regeneration pattern compared to the untreated non-transformed BY-2 WT. Overexpression of the motor protein myosin XI running along actin led to cell wall and axis promotion as well. Overexpression of the kinesin motor protein KCH, which is able to bind to both actin and microtubules, led to faster regeneration compared to the non-transformed WT. Inhibition of microtubules via Oryzalin treatment caused incapable axial expansion and cell wall synthesis. Manipulating the interior of the nucleus via overexpression of one of the core histones H2B resulted in faster axis formation but a delay in elongation. Axis formation was promoted by the overexpression of the nuclear membrane protein AtWIT, which forms a bridge between intranuclear factors and the cytoskeleton in the cytoplasm.

Additionally, aligned structures of extracellular factors such as peptides with RGD sequences significantly promoted axis formation and elongation, compared to unaligned structures plotted with RGD peptides.

4 DISCUSSION

For all eukaryotic organisms from yeast through plants to humans, cell polarity plays an indispensable role for various cellular functions (Nick and Furuya 1992; Schmelzer 2002; Lipka and Panstruga 2005; Billadeau *et al.* 2007). Failure in cell polarity leads to tremendous consequences and can often result in diseases (Ellenbroek *et al.* 2012). Thus, understanding the mechanism behind polarity formation presents a fundamental task in basic research. In contrast to mammalian cells, directionality is a fixed characteristic of plant cells (Vöchting 1878). However, after division, cell polarity must be re-established. How cells acquire polarity and axis presents a central question of plant morphogenesis and represents the aim of this study. Therefore, the potential role of extracellular as well as intracellular candidates for axis formation was investigated by using an experimental system based on regenerating protoplasts, where the induction of a cell axis *de novo* can be followed by quantification of specific regeneration stages. Thereby the following four questions posed in the beginning were answered in this study: a) Is the position of the nucleus a prerequisite for axis formation? b) Does the nuclear proteome differ in H2B-mEos and Lifeact-psRFP compared to the non-transgenic cell line? c) Which role do intracellular factors play in axis formation? d) Does the orientation of extracellular structures affect axis formation?

Previous studies highlighted an active nuclear movement during the first preparatory phase of regenerating protoplasts (Zaban *et al.* 2013). This assumed that the nucleus – known for its role as a “great chairman” of several cellular processes – together with its particular positioning plays a major role in cell polarity formation. Against this initial hypothesis, time-lapse studies of three transgenic lines in which nuclear migration was altered, revealed that the nuclear position itself is not a prerequisite for axis formation. Additionally, biochemical approaches combined with bioinformatic quantification of nuclear proteome presented differences in histone abundance of these transgenic overexpression lines where nuclear migration was altered. Although nuclear positioning and cell axis formation were uncoupled, both phenomena are clearly dependent on the extra- and intranuclear factors. Via different overexpression lines and pharmacological approaches, this study revealed how cytoskeletal dynamics and motor proteins but also histones and nuclear membrane proteins are involved in axis formation. However, not only intracellular factors alter axis formation, as it was

demonstrated that extracellular factors such as RGD peptides are significantly involved in axis formation. Moreover, their aligned structural organization promotes axis formation, which was indicated by using structured nanofibers. Together, these results indicate that there must be a close connection between extracellular factors, the cytoskeleton, and organelle positioning.

4.1 Polarity and its link to nuclear migration

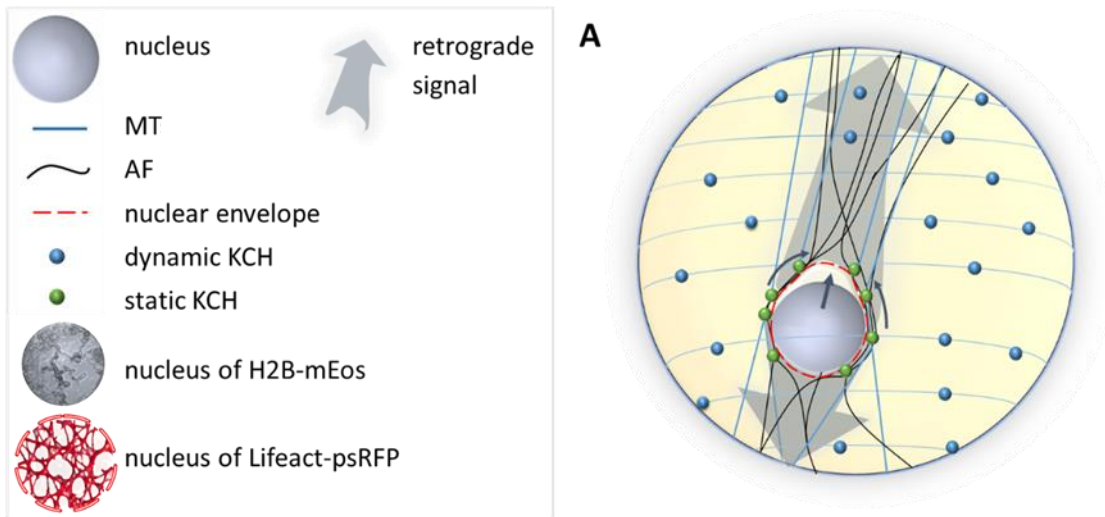
Since nuclear movement is essential for several processes in plant cells, it is important to know which role nuclear movement plays in polarity and axis formation, and to test whether a central nuclear positioning is a prerequisite for polarity and axis induction. By means of analyzing regeneration of protoplasts, it is possible to follow the induction and manifestation of a cell axis *de novo*. In order to manipulate the nuclear movement on a genetic level, three different cell lines overexpressing key players involved in nuclear positioning were used. In the Lifeact-psRFP cell line, a specific actin basket around the nucleus is labelled. In the GFP-NtKCH cell line, a motor protein acting as a cross linker of actin and microtubules was overexpressed. In the H2B-mEos cell line, a histone was overexpressed, expecting to affect intranuclear architecture. By quantification of specific regeneration stages, the temporal patterns of these overexpression lines were compared to the non-transformed line. Overexpression of the perinuclear actin marker line promoted axis formation in the beginning, but later perturbed axis manifestation, whereas overexpression of the class XIV kinesin KCH promoted both axis formation and axis manifestation. Overexpression of the histone marker promoted axis formation, but delayed cell elongation. Time-lapse studies of nuclear movement during the early stages of regeneration were used to address the question, whether a central position of the nucleus is a necessary prerequisite for the induction of axis and polarity.

4.1.1 A central position of the nucleus is not a prerequisite for polarization

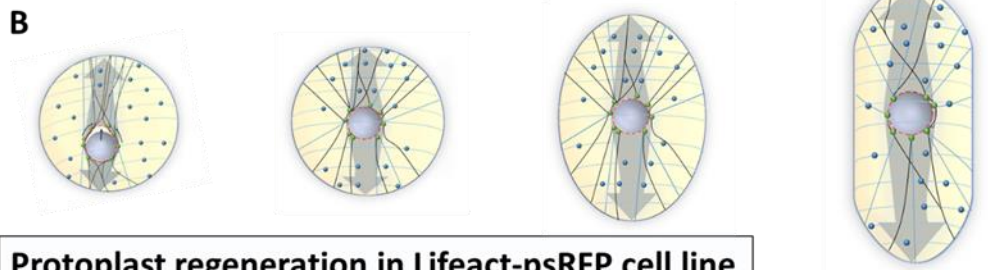
Nuclear positioning is necessary for the correct geometry of the subsequent cell division (reviewed in Smith 2001). Hence, the question arises whether a central position of the nucleus might also be a prerequisite for polarity induction. Time-lapse studies of the moving nucleus in the early stages of regeneration clearly argue against this hypothesis and demonstrate that nuclear positioning can be separated from axis formation (see Figure 3.1 p.30).

At first sight, when the nuclear migration of the Lifeact-psRFP cell line was followed, the presumed link between nuclear position and axis formation appeared to be valid. Here, the nucleus was already tethered at the cell center and axis formation started earlier compared to the non-transformed cell line (Figure 4.1 B and C). However, for the GFP-NtKCH cell line, axis formation initiated earlier than in the non-transformed line, whereas the nucleus was still not located at the cell center (Figure 4.1 B and E). Similarly, in the H2B-mEos line, axis formation had already started before the nucleus had reached the cell center (Figure 4.1 D).

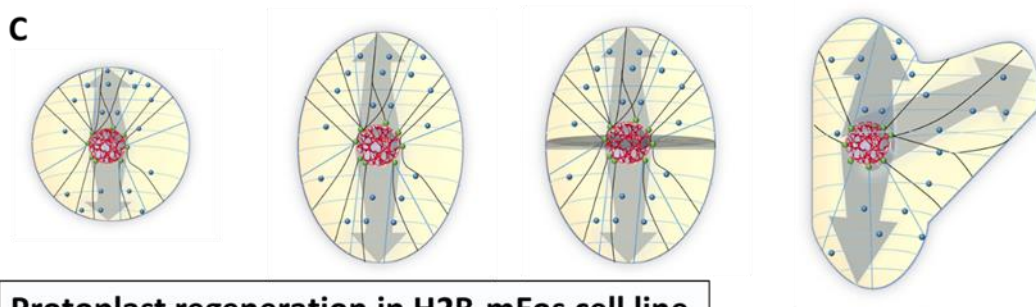
Thus, a central nuclear position is not necessary for axis formation, but rather appears to be a parallel phenomenon.



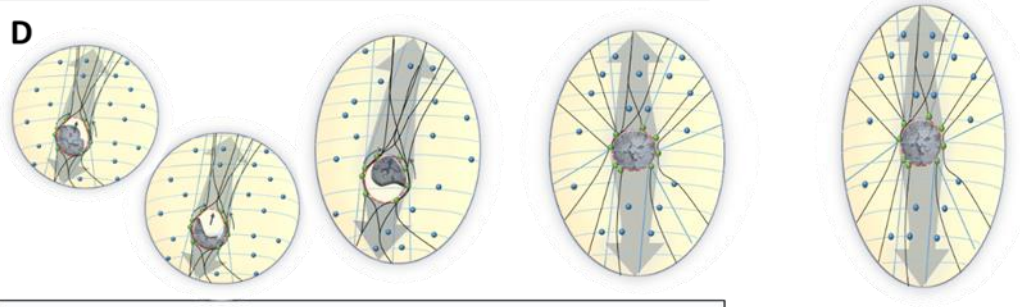
Protoplast regeneration in non-transformed cell line



Protoplast regeneration in Lifeact-psRFP cell line



Protoplast regeneration in H2B-mEos cell line



Protoplast regeneration in GFP-NtKCH cell line

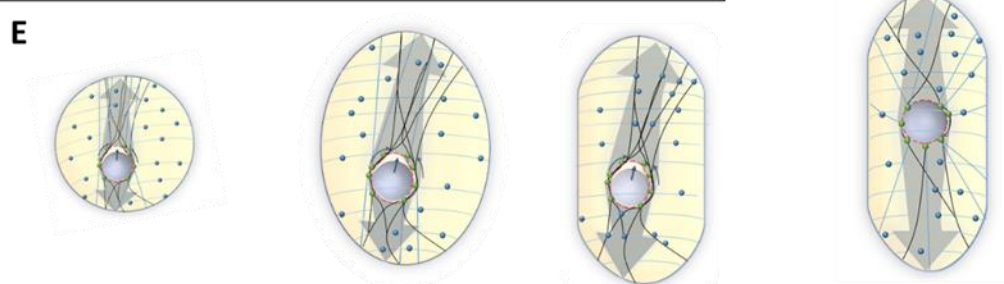


Figure 4.1 Model of nuclear migration while polarity induction and axis formation

Progression of protoplast regeneration from the onset of polarity induction (A) until elongated cells in the non-transformed cell line (B), Lifeact-psRFP cell line (C), H2B-mEos cell line (D), and GFP-NtKCH cell line (E). With the onset of polarity formation, the nucleus starts to migrate into the cell center (black arrow): Static KCHs (green spheres) decorate the perinuclear network (red dashed lines) and are connected with radial microtubules (MT, blue lines); dynamic KCHs are located in the cortex (blue spheres) and move along cortical microtubules (MT, blue horizontal lines), generating sliding forces that act on the nucleus (large gray sphere). Retrograde signals are transported from the nucleus through the cytoskeleton (actin filaments AF, microtubules MT) to targets at the plasma membrane (semi-transparent arrows). After a few hours, the nucleus has reached the cell center; the protoplast has expanded circularly, followed by axis formation, axis manifestation, and further cell elongation in which the long axis is more than twice as long as the short axis (B). Compared to the non-transformed cell line, the nucleus of the Lifeact-psRFP cell line (red basket) is already located at the cell center from the onset of polarity induction; axis formation is promoted, followed by division of protoplasts at oval stages, resulting in an increase of tripolar structures (C). The nucleus of the H2B-mEos cell line shows an abnormal nuclear architecture (gray patterned nucleus) and therefore its shape might slow down the movement. Simultaneously, axis formation already started until the nuclear shape is normal again and eventually is located at the cell center; the long cell axis is more than twice as long as the short axis, however, the cells are shorter than the non-transformed cells (D). Compared to the non-transformed cell line, axis formation in the GFP-NtKCH cell line is faster, nuclear migration is slowed down at the early phases (E).

4.1.2 Nuclear positioning depends on perinuclear actin, KCH, and chromatin structure

As mentioned in the beginning, there are two possible scenarios: 1.) Promotion or failure in axis formation could be a result of an altered nuclear position as a causal relationship or 2.) These factors act independently on both nuclear migration and axis formation at the same time. Although nuclear positioning and cell axis formation were uncoupled, both phenomena were clearly dependent on the extra- and intranuclear factors addressed by the three transgenic lines:

As plants lack a nuclear lamina meshwork, which is involved in nuclear migration and provides mechanical stability of the nucleus in animal cells (for review see Goldman *et al.* 2002), there must be structural analog to the mammalian lamina in plant cells. In fact, a perinuclear cage has been reported (Wang and Nick 1998), and is specifically visualized by the Lifeact-psRFP marker (Durst *et al.* 2014). Whereas during protoplast preparation, the G₂ nucleus loses its central position and shifts to the periphery, it remains tethered in the cell center when the protoplasts are prepared from the Lifeact-psRFP line (Figure 4.1 C), indicative of a more stable

perinuclear basket. Therefore, the perinuclear actin basket behaves as functional homolog of the nuclear lamina, but also seems to be involved in the migration of the nucleus.

Class XIV kinesins with a calponin homology domain (KCH) have been identified as important factors of premitotic nuclear positioning (Frey *et al.* 2010; Klotz and Nick 2012). In functional analogy to dyneins that convey this function in animal and fungal cells (reviewed in Morris 2000, 2003), KCH crosslink actin filaments with microtubules. The mechanically rigid microtubules can confer compression forces and could, together with the flexible actin filaments that can confer traction forces, establish a tensegral system able to sense and integrate mechanic forces between cell periphery and nucleus (reviewed in Nick 2011). As mentioned before, KCH can either occur in a free, mobile state (not linked with actin) or in a static situation cross-linked to actin (Klotz and Nick 2012). Both the nuclear migration at the onset of protoplast regeneration (see Figure 3.1 p.30), as well as premitotic nuclear positioning in walled cells (Frey *et al.* 2010) were clearly delayed.

Not only extranuclear, but also intranuclear factors were relevant for nuclear positioning. Indeed, it was shown that overexpression of a histone caused a delay of nuclear movement. This functional change is accompanied by a clear change of nuclear architecture resulting in a distorted nuclear shape during early regeneration (see Figure 3.1 p.30). This obviously changed nuclear architecture indicates that histones, in addition to their role in transcriptional activity, are important for intranuclear architecture. Although histones are highly conserved, studies showing that specific modifications and variants of histones (Verbsky and Richards 2001; Fransz and de Jong 2002; Yi *et al.* 2006; Deal and Henikoff 2011) not only contribute to several nuclear functions including DNA repair, transcription, replication, or chromosome condensation (Kouzarides 2007), but also may lead to changed chromatin architectures (Ahmad and Henikoff 2002; Smith *et al.* 2002; Talbert *et al.* 2002). There is also a clear link between position of a gene and its histone decoration: Transcriptionally active genes occupy the interior regions of the nucleus, whereas inactive genes tend to reside to the nuclear periphery (Cremer and Cremer 2010). As the DNA wraps around the highly conserved core histones forming the nucleosomes, it is to be expected that the overexpression of the H2B-mEos marker, affecting one of the four core histones, should affect DNA packaging and therefore cause to change intranuclear architecture and flexibility. The resulting higher "viscosity" should then reduce the velocity of the nucleus (Figure 4.1 D).

This was explained by the bulging model for nuclear migration from Durst *et al.* (2014). According to the bulging model, contraction of the perinuclear actin lamella might constrict the adjacent region of the nuclear envelope in such a way that it bulge outwards, and the karyoplasm would be displaced into the newly arisen space. Consequentially, a “viscous” nucleus resulting from an altered intranuclear architecture might be unable to perform the correct movement.

If this model, stating that certain overexpressions can change nuclear architecture and therefore a changed nuclear shape results in an altered nuclear migration, is valid, the protein content of those nuclei should be different compared to nuclei of non-transformed wildtype cells. This could become visible in a changed histone abundance compared to non-transformed nuclei. To test this, the nuclear proteome must be isolated, identified and compared.

4.2 Nuclear migration and its link to nuclear proteome

Indeed, when the two transgenic cell lines H2B-mEos and Lifeact-psRFP were compared to the non-transgenic line the results showed that the nuclear proteome differs (see Figure 3.3 p.33). Histones as well as histone linker proteins were more abundant in the transgenic lines than in the non-transgenic line (see Table 3.1 p.36). The core histone protein H2B was more abundant in the H2B-mEos line, which was expected since H2B is overexpressed. However, the overexpression of a histone itself might not change the entire DNA packaging. Linker proteins as well as enzymes are necessary to assist in DNA wrapping. As a matter of fact, histone linker proteins such as H1 were found more often in H2B-mEos compared to wildtype nuclei. Additionally, histone deacetylases were also found to be more abundant in H2B-mEos as in the wildtype nuclei. Histone deacetylases removes the acetyl groups on a histone, which allows the histones to wrap the DNA more tightly. This observation strengthens the hypothetical model that the nuclear architecture is completely restructured due to the overexpression of one core histone. The results indicate that not only rearrangement of histones occurred, but also the expression pattern has changed. This has never been shown so far.

However, this result should be viewed critically: it reveals a first indication rather than a proof of the hypothesis. Further investigation is required in the field of nuclear proteomics to

strengthen the hypothesis. A complete nuclear plant proteome has not been characterized so far, although it would be highly important in order to be able to understand the functions of the nucleus. Therefore, nuclear proteomics presents a promising future topic, which should be followed up on in my opinion. Bottlenecks of proteomic studies occur when it comes to the biological interpretation of big data sets. Recently, a holistic software platform called Perseus allows a viable handling of raw data (Tyanova *et al.* 2016). With this program, it is possible to create heat maps that provide a way to visualize and interpret complex data sets originally organized as matrices. It reorders the data rows of the different proteins with similar profiles closer together via Euclidian clustering, and subsequently translates the numerical matrix into color codes of heat maps making it easier to reveal patterns (see Figure 3.3 p.33).

Interestingly, the heat map of the result part showed that compared to the non-transformed cell line the same histones, histone linker proteins and enzymes found in H2B-mEos were found to be more abundant in the Lifeact-psRFP line as well (see Figure 3.4 p.34). This means that manipulating the cytoskeleton around the nucleus involves epigenetic changes. One possible explanation could be that changes in the perinuclear basket were “sensed” in a mechanical way by histones leading to epigenetic changes. This could also implicate enhanced protein import into the nucleus. Indeed, importins, which are responsible for nuclear transport, have been found more often (see Table 3.1 p.36).

A changed nuclear migration could be a result of the changed intranuclear architecture indicated by altered histone packaging; although an altered nuclear shape was microscopically not observed for Lifeact-psRFP (but for H2B-mEos). Alternatively, the modified nuclear migration could be the result of the stabilization of the perinuclear basket as described before (4.1.2 p.67). Otherwise, the changed nuclear migration compared to the non-transgenic nuclei could be the result of the combination of both phenomena.

In this theoretical assumption, the extranuclear basket sends retrograde signals - via nuclear membrane proteins - to the histones on the intranuclear side, including enhanced intranuclear protein transportation. How they are connected will be explained in the following chapter in a tensegral framework with retrograde or “echo-like” signaling.

4.3 Polarity depends on tensegrity and intracellular logistics

While the effects of perinuclear actin, KCH, and chromatin structure on nuclear movement can be understood in terms of activities around (actin, KCH) or inside (chromatin) the nucleus, the effect of these factors on polarization and axis formation has to be located at the plasma membrane. The results show that manipulation of factors that are involved in the nuclear movement also results in different regeneration patterns (Figure 4.1 p.66).

Additional intracellular factors were investigated to unravel the mechanism of cell polarity and its interconnected machinery.

It was demonstrated that overexpression of the perinuclear actin marker Lifeact-psRFP promotes axis formation, but perturbs axis manifestation (see Figure 3.6 p.41). This is surprising at first sight: Why should alterations of actin at the nuclear envelope affect actin-related processes occurring underneath the plasma membrane? This retrograde signaling from the perinuclear actin towards the plasma membrane is less surprising in the conceptual framework of a tensegral cytoskeleton. The overexpression of the Lifeact actin marker presumably causes a stabilization of the perinuclear cage or makes it more resistant against reorganization of actin filaments because of additional crosslinks, which through the radial actin cables should alter traction forces acting on the anchoring sites at the plasma membrane. This may underlie the promoted induction of asymmetry observed in the Lifeact-psRFP line. However, to translate this polarity into a new cell axis, actin dynamics is required (Zaban *et al.* 2013). Thus, reorganization of actin filaments is a prerequisite for manifestation of the reformed axis. The Lifeact-psRFP shows a high amount of premature cell division of cells in an oval stage, i.e. in cells where axis formation initiated, but axis manifestation had not yet been completed (Figure 4.1C p.66). This aborted axis manifestation is responsible for the relatively high incidence of tripolar structures. These tripolar structures derive from perturbations of simple polarities, when a second, competing pole is laid down ectopically. In contrast to a complex polarity, where both poles along an axis are defined by specific molecules or activities, the polarity of plant cells is often simple, i.e. only one pole is explicitly defined, whereas the opposing pole is simply characterized by the absence of the polarizing molecules or activities (Nick and Furuya 1992).

However, slight stabilization of actin filaments with a very low concentration of only 100 nM Phalloidin promotes induction of asymmetry and axis formation without generation of tripolar structures (see Figure 3.7 p.43). Hence, weak stabilization of actin filaments supports axis induction and elongation. With Latrunculin B treatment in Lifact-psRFP protoplasts, the stabilized nuclear basket can be destabilized and tripolar structures vanish, leading to a similar regeneration pattern as observed for untreated WT cells (see Figure 3.8 p.45). This confirms that actin filaments are stabilized in Lifact-psRFP and its resulted failure in axis manifestation can be rescued by mild destabilization. In contrast, mild destabilization with 75 nM Latrunculin B in the non-transformed cell line already inhibits cell wall formation significantly (see Figure 3.4 p.43). This inhibited effect can be explained as being a result of retarded cellulose synthase complex (CSC) trafficking along actin cables.

The CSC at the plasma membrane synthesizes cellulose. Golgi bodies, which contain CSC with cellulose synthase, move rapidly along thick actin cables (Sampathkumar *et al.* 2013). Studies have shown that if Latrunculin B is added during the primary wall synthesis in interphase *Arabidopsis* cells, the movement of Golgi bodies is impaired and the distribution of cellulose synthase at the plasma membrane is disturbed (Wightman and Turner 2008; Crowell *et al.* 2009; Gutierrez *et al.* 2009). Actin plays an important role in deposition of cell wall in many cell types including tip growing cells, such as pollen tubes or root hairs (Hu *et al.* 2003; Chen *et al.* 2007). Additionally, actin filaments seem to be necessary for the deposition of secondary wall cellulose microfibrils. The study of Wightman and Turner (2008) in developing xylem vessels showed that longitudinal actin filaments define the movement of secondary wall Golgi bodies containing cellulose synthase. Thus, if actin cables are destabilized by Latrunculin B, the trafficking of CSC containing Golgi bodies could be impaired in regenerating protoplasts and therefore cell wall synthesis is decelerated.

The transport of Golgi bodies containing CSC is a rapid process. The synthesis of the new cell wall in regenerating protoplasts normally proceeds within a few minutes (see Zaban *et al.* 2013). This calls for fast motor proteins. Fast movements at 2-7 $\mu\text{m/s}$ seem to be associated with thick actin filaments (Nebenführ *et al.* 1999; Akkerman *et al.* 2011). Class myosin XI are the fastest known motors running along actin filaments (Tominaga *et al.* 2003). In fact, overexpression of myosin XI promotes cell wall formation (see Figure 3.9 p.47). Likewise, the study by Avisar *et al.* (2008) has shown that myosin XI is required for rapid trafficking of Golgi

stacks. In addition, knockout of myosin XI genes in *A. thaliana* resulted in cessation of transport of Golgi stacks (Peremyslov *et al.* 2010). The current work revealed that overexpression of myosin XI-I in tobacco BY-2 cells in turn leads to accelerated cell wall formation, suggesting that due to faster Golgi body transport via myosins, cellulose synthase is delivered to the plasma membrane more rapidly.

Further, overexpression of myosin XI-I led to fast axis formation as well in the BY-2 protoplasts (see Figure 3.9 p.47). In moss *Physcomitrella patens*, knocking down of myosin XI resulted in a loss of cell polarity (Vidali *et al.* 2010). Also Peremyslov *et al.* 2010 provided evidence that deletion of myosin in *A. thaliana* leads to an arrest of transition from bulge initiation to polarized elongation of root hairs. This is the *argumentum e contrario* for the current findings of round protoplasts regenerating to elongated cells; the present study showed that the overexpression of myosin XI-I in turn leads to a promotion of axis formation and polarized elongation. Interestingly, myosin XI seems to be involved in F-actin organization (Peremyslov *et al.* 2010; Ueda *et al.* 2010). Hence, promoted axis formation and elongation of the regenerating protoplasts are likely a result of increased motility of organelles and vesicles, plus an enhanced actin filament structuring as a consequence of the myosin XI-I overexpression.

Conversely, new discussions arise which theorize that myosin XI is not able to bind organelles directly, but only carries specific transport vesicles along actin filaments (Buchnik *et al.* 2015). This would lead to a cytoplasmic flow that propels the passive movement of other organelles. Another scenario would be that the organelles bind to the transport vesicles attached to myosin XI (Peremyslov *et al.* 2013). Clear evidence that plant myosins XI directly bind to Golgi bodies seems a trivial analytical approach but is still missing. Nevertheless, evidence mentioned above is provided that the transport of Golgi bodies is impaired by myosin.

Axis formation and elongation also require a close interplay of both actin filaments and microtubules. While KCH overexpression delays nuclear migration, cell elongation is stimulated (Figure 4.1 E p.66). Promoted cell elongation at simultaneously retarded nuclear migration has also been found for walled cells overexpressing KCH (Frey *et al.* 2010). The retarded nuclear migration is probably caused by elevated cross-linking of microtubules with the perinuclear actin basket (Klotz and Nick 2012), whereas the stimulated cell elongation is

linked with a second sub-population of KCH kinesins associated with cortical microtubules and uncoupled from actin (Klotz and Nick 2012; Kühn *et al.* 2013), which preferentially binds to tyrosinated (dynamic) microtubules (Schneider *et al.* 2015). Although the effect of KCH overexpression resembles that of the Lifeact-psRFP marker with respect to the retarded nuclear movement, the two overexpression lines clearly differ with respect to axis manifestation (promoted for the KCH line, impaired for the Lifeact-psRFP line), and the incidence of tripolar cells (observed only in the Lifeact-psRFP, but not in the KCH lines).

Since KCH binds to microtubules, the principal role of microtubules in polarity and axis formation should be discussed as well at this point. To control cell axis, cortical microtubules must be ordered into parallel arrays, accompanied by cell elongation in a direction perpendicular to microtubule orientation and a progressive alignment of cellulose texture with microtubules. In expanding cylinders, mechanic tension is anisotropic (with transverse doubled over longitudinal tension), such that cylindrical plant cells are expected to widen rather than to elongate (Preston 1955). By transverse deposition of cellulose microfibrils, plant cells can override this mechanic anisotropy and reinforce elongation growth (Green 1980). The previous publication of Zaban *et al.* (2013) has shown that the stabilization of microtubules via overexpression of AtTuB6 led to a faster polarity induction and axis formation. It was shown that, due to overexpression of AtTuB6, microtubules were stabilized, and axis formation was promoted, which requires more efficient alignment of microtubule arrays. A similar promotion of microtubule alignment after treatment had been reported earlier after treatment with Taxol (Kuss-Wymer and Cyr 1992). Thus, alignment of cortical microtubules can proceed efficiently with stable microtubules, indicative of a mechanism that is based on mutual sliding. Also for auxin-dependent microtubule reorientation, initial direction-dependent disassembly and reassembly is followed by a second phase, where microtubules coalign and harbor mainly detyrosinated α -tubulin, a marker for microtubule stability (Wiesler *et al.* 2002). To address the role of microtubule dynamics in the system, destabilization of microtubules was induced via Oryzalin treatment, which eliminates microtubules due to their turnover, which was followed by a delay in polarity induction and axis formation. Furthermore, it was shown that Oryzalin-treated protoplasts were not able to elongate (see Figure 3.11 p.51). Additionally, when Oryzalin was applied to GFP-NtKCH, the effect was similar to that of Oryzalin in WT (see Appendix Figure 5.10 p.103). Thus,

overexpression of the KCH motor protein does not rescue the delay in polarity induction and axis formation since the microtubule railways of KCHs are destroyed by Oryzalin.

Contrary to what would be expected, overexpression of the microtubule end binding protein EB1 does not affect axis formation. As mentioned in the beginning, microtubule associated proteins (MAP) can influence microtubule dynamics. EB1 is known for its stabilizing function of microtubules (Mimori-Kiyosue *et al.* 2000). Previous studies have shown that stabilization of microtubules promotes cell wall synthesis and axis manifestation depended on microtubule dynamics (Zaban *et al.* 2013). However, no effect on axis formation was observed in EB1-GFP (see Appendix Figure 5.9 p.102). Thus, the impact on MT dynamics might not reside in the EB1-GFP cell line to any significant extent.

As mentioned before, thick actin cables are probably necessary for the transport of CSC and thus mild destabilization already delays cell wall synthesis. Additionally, microtubules are necessary for the correct positioning and movement of cellulose synthase in the plasma membrane (Paredes *et al.* 2006; Li *et al.* 2012). Hence, elimination of microtubules causes only a delay in cell wall synthesis for Oryzalin-treated protoplasts as a result of alteration of the initial trajectory of CSC (see Figure 3.11 p.51). However, cell wall synthesis was still possible without microtubules, whereas axis formation was blocked completely due to the elimination of microtubules via Oryzalin.

Axial cell expansion is delayed in H2B-mEos (see Figure 4.1 D p.66), which means that nuclear architecture conveys a signal to axis elongation. Notably, also walled cells of H2B-mEos are significantly shorter compared to the non-transformed cell line (data not shown). It is conceivable that the signal from the interior of the nucleus acts on cytoskeletal targets at the periphery. Also for animal cells a functional relationship between lamins and histones has been reported (Taniura *et al.* 1995). Since the plant nucleus harbors deep grooves, invaginations and even perforations that are maintained by actin (Collings *et al.* 2000), changes of intranuclear architecture are expected to alter the organization of the cytoskeleton.

Overexpression of both the perinuclear actin marker Lifeact-psRFP, as well as the kinesin GFP-NtKCH promoted the re-establishment of the cell wall. Thus, although the nuclear positioning itself seems to be dispensable for polarity induction, factors that influence nuclear migration

might also influence polarity formation. The resulting model assumes that retrograde signals are required for polarity induction, which are transduced (transported) through the cytoskeleton to the periphery of the cell and act on cytoskeletal targets at the plasma membrane (Figure 4.1 p.66). Interestingly, also the overexpression of the histone marker H2B-mEos leads to faster formation of the cell wall, indicating that intranuclear architecture modulates the retrograde signaling from the nucleus to the plasma membrane (see Figure 3.12 p.53). However, decelerating cell wall formation via mild treatment with DCB overwrites the promoting effect in H2B-mEos (see Appendix Figure 5.11 p.104). The nature of this retrograde signal remains to be elucidated. It might be a molecule transported along the cytoskeleton, for instance by interference with vesicle flow by the actin basket, which means chemical signaling. Alternatively, it might be a mechanical signal conveyed by cytoskeletal tensegrity, comparable to recent findings in animal cells, where the perinuclear region was found to be affected due to mechanical stimulation at the cell periphery (Shao *et al.* 2015). Either way, there must be a physical link between the interior of the nucleus to the cytoskeleton in order to convey the signal to the plasma membrane. Indeed, nuclear membrane proteins are connected to histones and the cytoskeleton via myosin XI (Tamura *et al.* 2013). The results of the present study revealed that overexpression of one of the nuclear membrane proteins WIT – as a part of the nuclear SUN WIT WIP complex – promoted cell wall synthesis and cell axis formation (see Figure 3.13 p.55).

Keeping tensegral signaling in mind, an explanatory approach for these findings can be illustrated via the following interconnected model (Figure 4.2): Overexpression of the core histone H2B assumed to change the DNA packaging. Thus, chromatin distribution might be changed. Probably, this affects the connectivity of SUN at the nuclear membrane. One potential assumption would be that more SUN proteins were then recruited to the inner nuclear membrane, due to the rearrangement of chromatin that brings more chromatin to the nuclear periphery. Together with WIT and WIP a nuclear membrane bridge is formed. Due to the prevalent bindings, more myosin XI might be recruited to the outer nuclear membrane proteins (this phenomenon would be similar to the observed effect of overexpression of WIT or myosin XI.). Myosin XI binds to actin filaments surrounding the nucleus. If more myosin XI are able to bind to the nuclear actin basket, actin stability would be affected. Therefore, the nuclear basket would be slightly stabilized (similar to observed effects of direct actin

stabilization via Phalloidin or overexpression of Lifeact-psRFP). This affects tensegrity of the cytoskeleton. The signal would be transported faster through actin and connected microtubules to the plasma membrane (as observed for the overexpression of KCH).

Consequently, figure 4.2 illustrates that all these factors are connected with each other. In terms of the tensegral framework it can be concluded that if one factor is altered the whole signaling pathway is manipulated as a result of various chain reactions. Overexpression of one of these factors improves the connection and thus alters cytoskeletal dynamic by sending an echo-like signal, which is responded by the intranuclear side. However, besides the tensegral model also the potential role of a chemical signaling should be kept in mind. Also, in my view a combination of the two models is most likely.

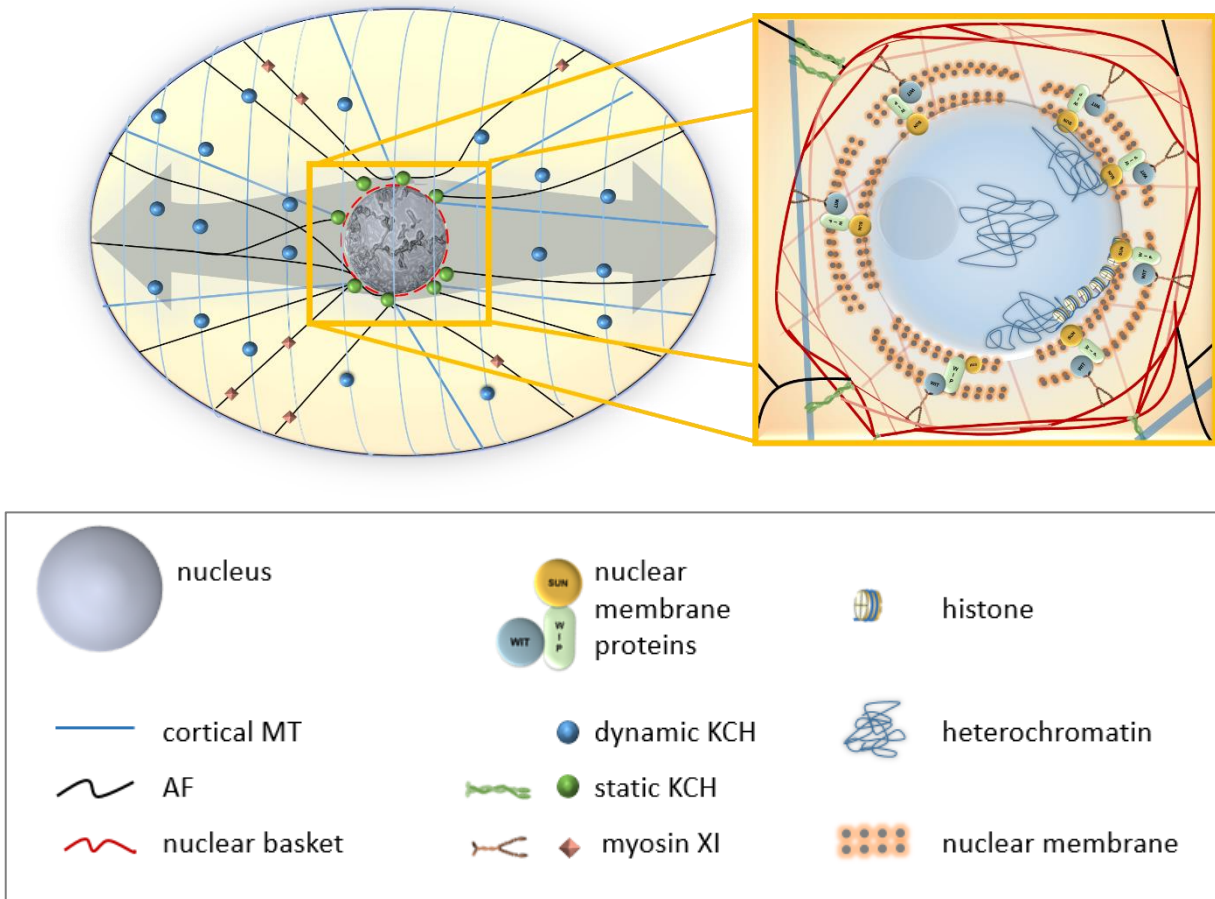


Figure 4.2 Simplified model of cell polarity in the background of a tensegral framework

Left: A plant cell is expanding in a polarized manner. Dots (blue/green: KCH, red: myosin XI) indicate motor proteins moving along respective cytoskeletal “railways” (blue: microtubules; black/red: actin filaments). The direction of expansion and its connected retrograde signaling from the nucleus to the plasma membrane is visualized via gray arrows.

Right: A more detailed section of the nucleus and its perinuclear surrounding. From intranuclear to extranuclear: Within the nucleus (blue) heterochromatin is mainly located at the nuclear periphery

organized by core histones. In the nuclear membrane (separated by nuclear pores) nuclear membrane protein complexes build of SUN (yellow) WIP (light green), and WIT (light blue) are imbedded. They are the link between histones and the cytoskeleton with the help of the motor protein myosin XI (red). Myosin XI binds to WIT and is connected to the nuclear basket. The nuclear basket is composed of actin filaments (red lines). Kinesins (green) are binding to actin filaments and walking along microtubules (blue).

4.4 Polarity and its link to external structures

As stated above, retrograde signals from the plasma membrane are transported through the cytoskeleton to the nucleus. But what is the purpose of this transfer of the signal to the nucleus? Why does a plant cell need to change its polarity? Since plants cannot run away from a changing environment, they have to adapt. This means they must constantly sense their environment and react to, for instance, stress or pathogen attacks. This is also the case on the cellular level.

In animal cells the extracellular matrix (ECM) serves as a sensitive sensory panel. Transmembrane proteins such as integrins act as mechanoreceptors. Their dimers bind to components of the ECM consisting of collagen, elastin, fibronectin, lamins and proteoglycans. These recruit cytoskeletal adaptors to build an adhesion complex and finally control cytoskeletal organization (Rooney and Streuli 2011) and thus affect cytoskeletal tensegrity. For cell migration, the structure and organization of the ECM plays an important role. This has been demonstrated recently by altering fibronectin patterning on surfaces (Autenrieth *et al.* 2016).

As mentioned in the introduction, neither integrins nor fibronectins have been found in plants. However, several studies are consistent with the fact that an ECM might be present in plants as well. ECM-like structures have been revealed in *Brassica napus*, supposed to stabilize morphological polarity (Dubas *et al.* 2014). Further, the appearance of hechtian strands in plants assumes that proteins exist with an adhesion function for signaling. Recently, bioinformatic studies have shown that only the sub-domains but not the full-length of adhesion proteins yield high level of sequence homology between plants and mammals (Langhans *et al.* 2017). This suggests that plant and mammalian cells share common functions for adhesion of plasma membrane and ECM, but feature different combinations of adhesion machineries. The plant adhesion machinery might be constructed of plasma membrane-associated proteins connected to the cell wall. They bind to proteins with intracellular

domains, such as formins, which are able to link the plasma membrane to actin or microtubules (for reviews see Cvrčková *et al.* 2014; Liu *et al.* 2015).

Furthermore, RGD peptides – recognition sides for mammalian integrins – seem to alter plant cell behavior as well: in the tobacco BY-2 protoplast system, RGD peptides promote axis formation and manifestation (Zaban *et al.* 2013). The current study revealed that not only does the presence of RGD peptides itself promote axis formation but furthermore, its structural orientation significantly impacts on axis formation (see Figure 3.14 p.59). Cells that were grown on aligned nanofibers with RGD peptides regenerate faster compared to cells grown on unaligned nanofibers with RGD peptides. However, the structure of the nanofibers itself does not influence the regeneration. This becomes clear if the distribution of cells regenerating on untreated nanofibers (either aligned or unaligned) are compared to the distribution of cells regenerating without any surface (comparison Figure 3.14 p.59 to Figure 3.6 3d WT p.41). Thus, the results have provided evidence for the assumption that extracellular structures change cytoskeletal behavior. How RGDs influence the cytoskeletal organization can be understood in terms of tensegrity and its influence on the cytoskeleton by interfering with the so-called cytoskeleton plasma membrane cell wall continuum. This has been explained in previous studies (Baluška *et al.* 2003; Zaban *et al.* 2013).

As discussed before, the formation of cell axis requires an orientation of cortical microtubules into parallel arrays. This is accompanied by cell elongation in a direction perpendicular to microtubule orientation. Reorganization of actin filaments is also necessary for axis formation. If ECM peptides such as RGD peptides are organized in an aligned manner, cytoskeletal elements might indirectly bind via recruited adapter molecules. This binding to aligned arranged peptides could promote cytoskeletal reorientation and thus result in a faster axis formation (Figure 4.3 A and C) in contrast to protoplasts regenerating on unaligned arranged peptides (Figure 4.3 B and D). In this process, the horizontal or vertical direction of aligned nanofibers does not influence the orientation of cell elongation. However, this assumption has not been proven yet and should be quantically analyzed in the future. Further investigation in combination with cytoskeletal drug treatment might strengthen this hypothesis and could reveal whether actin or/and microtubules are necessarily involved in the binding via adapter molecules to aligned orientated RGD peptides.

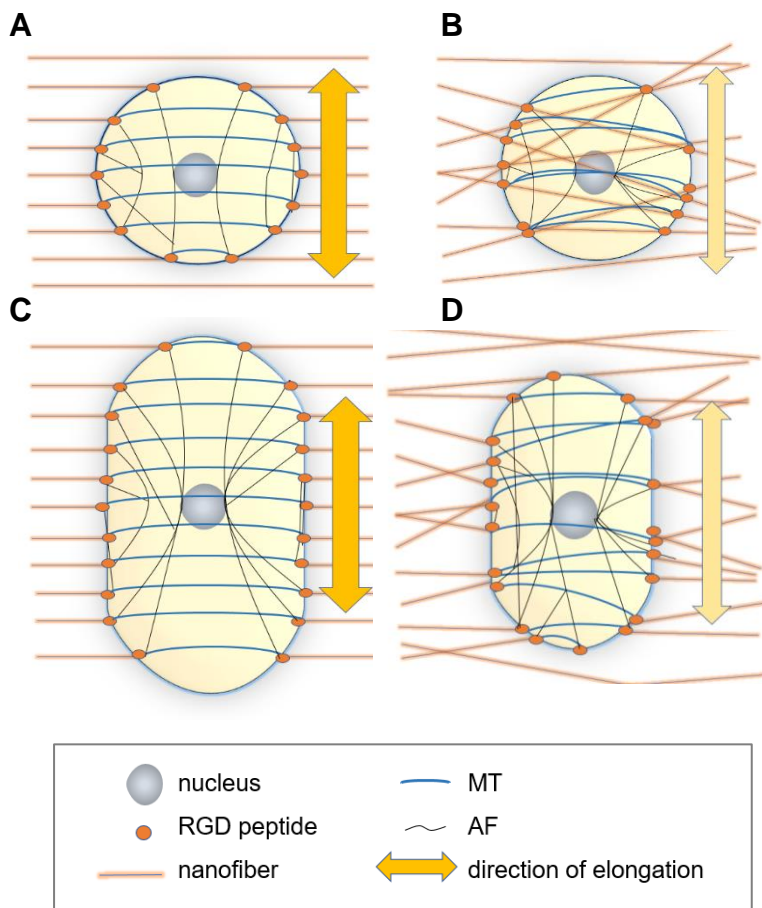


Figure 4.3 2D-view draft of regenerating protoplasts on nanofibers with RGD peptides

This sketch illustrates the regeneration of protoplasts on aligned (A, C) and unaligned (B, D) nanofibers. Figure legend is displayed below. RGD peptides (orange dots) were plotted on nanofibers (orange lines). Microtubules (MT, blue) and actin filaments (AF, black) are connected indirectly to RGD peptides via linker molecules (not illustrated). Cells elongate in the vertical direction of microtubules and same orientation of actin filaments. Protoplasts on aligned fibers with RGD peptides regenerate faster (C, big yellow arrow) compared to unaligned fibers with RGD peptides (D, small yellow arrow).

This new tool has just been established in plant cell biology but the approach seems very promising to gain more insights into the role of ECM in polarity formation. The first results revealed that the aligned orientation of RGD peptides clearly promotes axis formation. The model above could explain the mode of action of protoplasts regenerating on aligned nanofibers with RGD peptides.

However, the following question remains: Since plant cells do not migrate, why is the structural organization of extracellular components even important? This can be explained by the fact that plant cells *in vivo* are not separate but are oriented in a directional tissue. Therefore, plant cells adjust their axis in a way that resulting mechanical tensions in the tissue will be minimized. This requires an alignment of their axis of growth to minimize mechanical tensions in the turgescent tissue. One speculative assumption could be that the plant cell mechanosenses its environment by plasma membrane proteins influencing tensegrity and thus “responds” to the external pattern by fast reorganization of the cytoskeleton in order to minimize the mechanical tension.

4.5 Conclusion and the ECHO of cell polarity

In order to understand the mode of action of cell polarity formation, the potential role of extracellular as well as intracellular candidates for axis formation was investigated by using overexpression lines or cytoskeletal drugs. This experimental system was based on regenerating protoplasts, where the induction of a cell axis *de novo* can be followed by quantification of specific regeneration stages.

To conclude, the results have clearly shown that – contrary to initial assumptions – a central nuclear position is not a prerequisite for axis formation. However, nuclear positioning depends on perinuclear actin, KCH and chromatin structure leading to a model for nuclear migration and axis formation (Figure 4.1 p.66). Moreover, label-free quantification via tandem mass spectrometry indicated that the intranuclear architecture can be manipulated via overexpression, leading to changes in histone abundance. Together with time-lapse studies, this suggests that an altered nuclear migration might be a result of a changed intranuclear architecture indicated by altered histone packaging.

Further, both phenomena (nuclear migration and axis formation) depend on factors affecting cytoskeletal tensegrity and chromatin structure. Although the central nuclear position *per se* is not required for axis formation, the results show that if this organelle positioning is altered, polarity formation is affected as well. The present findings were integrated into a second model, where retrograde signals are required for polarity induction and dependent on the close interplay of several tested intracellular factors (Figure 4.2 p.77). These retrograde signals travel via the cytoskeleton from the nucleus towards targets at the plasma membrane. Manipulation of cytoskeletal dynamics due to drug treatment or overexpression of motor proteins might affect intracellular “logistics” such as the transport of Golgi bodies containing CSC. Since the cytoskeleton is connected to the nucleus via motor proteins, nuclear membrane proteins and histones alter this retrograde signaling pathway as well. If one of the tested intracellular factors is manipulated the whole signaling pathway might be affected as a result of chain reactions.

Additionally, it was demonstrated that apart from intracellular factors, extracellular candidates such as RGD peptides influence polarity formation. The results have shown that

aligned orientation of extracellular components significantly promotes axis formation. A possible mode of action for protoplast regeneration on aligned nanofibers with RGD peptides was illustrated via a third model (Figure 4.3 p.80). Thus, although plant cells do not migrate like animal cells, the structural organization of extracellular components is important for axis formation. One possible explanatory approach could be related to the fact that plant cells *in vivo* have to adjust their axis in a way that resulting mechanical tensions within a directional tissue will be minimized. Therefore, the plant cell mechanosenses its environment by plasma membrane proteins influencing tensegrity. Thus, the regenerating protoplasts “respond” to the aligned external pattern by fast reorganization of the cytoskeleton in order to minimize the mechanical tension.

Further, it should be kept in mind that mechanical signaling is assumed to correlate with chemical signaling plus its distribution of molecules. For instance, plant hormones such as auxin influence cell polarity together with the polar distribution of auxin-efflux carriers such as pin-formed proteins (PIN). These are associated with the actin cytoskeleton and thus affect cytoskeletal tensegrity (Maisch and Nick 2007; Nick 2010).

To understand details of cell polarity formation and resolve the puzzle which factors regulate cell polarity, it is worthwhile to look at the bigger picture.

Taken the results together, plant cell polarity depends on four key players:

- 1.) **E**xtracellular components and their organization (see 4.4, pp.78), which affect the
- 2.) **C**ytoskeleton with its motor proteins (see 4.3 pp.70) that are connected to the plasma membrane. The cytoskeletal elements are both impaired and responsible for the distribution of
- 3.) **H**ormones such as auxin or other signaling molecules (for review see Nick 2010).

Finally, the organization and movement of

- 4.) **O**rganelles such as the nucleus (see 4.1 pp.46) are manipulated.

To put it in a nutshell: Plant cell polarity depends on an **ECHO**-principle (see Figure 4.4 p.84).

This ECHO principle implies a pathway from extracellular signals towards the nucleus via the cytoskeleton in combination with hormones or other signaling proteins. Strikingly, the model supported by data from this work additionally assumes that the nucleus itself might respond to those signals: Differences in histone packaging act on the cytoskeleton and thus intranuclear signals are transported to the plasma membrane (see Figure 3.12 p.53). Moreover, the results have shown that if the nuclear basket was manipulated, histone distribution was altered as well and so was axis formation (see Table 3.1 p.36 and Figure 3.6 p.41). Overexpression of core histones influences the behavior on the plasma membrane, possibly by acting on the cytoskeleton around the nucleus via motor proteins attached to nuclear membrane proteins. Received at the nucleus, extracellular signals were “echoed” back to the plasma membrane.

Hence, the idea of ECHO also illustrates its retrograde behavior: Extracellular signals or changes could be referred through the cytoskeleton and molecules to the organelles. In turn, responding signals from the nucleus could be transported through the cytoskeleton to the plasma membrane as a feedback.

Alterations on one of the four key players would provoke a chain reaction on the other key players. This assumes that there should persist a constant *actio et reactio* between the intra- and extracellular situation. Is this exclusively the case for plant cells? The clear answer is no. Various studies have shown that apart from the green kingdom, the ECHO effect with its homolog representative molecules can be observed for all eukaryotic organisms (see Figure 4.4). Detailed description of every respective candidate of ECHO for each kingdom would go beyond the scope of this dissertation and is therefore briefly summarized in the additional table together with one selected review or latest publication each (Appendix Table A 5.3 p.108).

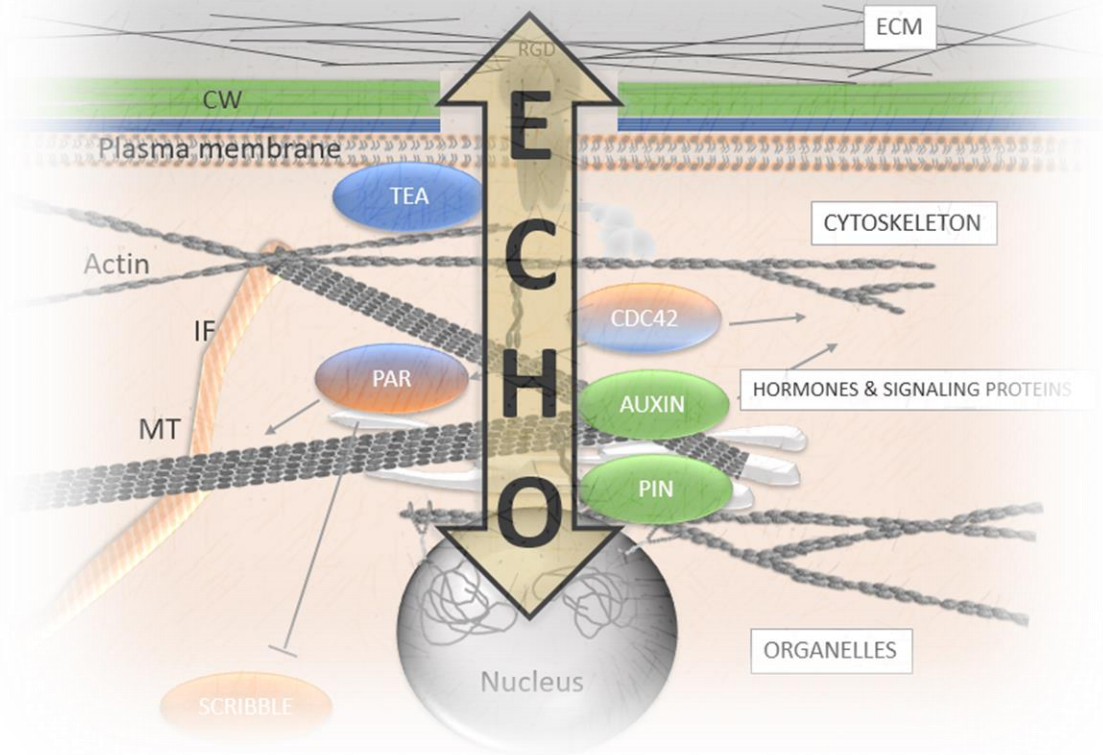


Figure 4.4 Sketch of the ECHO concept of cell polarity

Regardless of the specific eukaryotic organism one can observe that four factors (listed on the right) interacting with each other are involved in polarity formation of a cell: The extracellular matrix (ECM), the cytoskeleton, hormones and other signaling molecules (some representatives: Tea, CDC42, PAR, SCRIBBLE, AUXIN, PIN) and the positioning of organelles (summarized in short: ECHO). The ECHO principle hypothesizes that signals from outside are recognized by potential transmembrane proteins via RGD recognition sides and are transported via the cytoskeleton with the help of signaling molecules towards the organelles, which in turn give feedback through the cytoskeleton to the plasma membrane towards the outside of the cell (visualized by arrow heads in both directions). Thus, this feedback communication between the nucleus and the outside can be illustrated like the effect of an “responding” echo. Parts which are exclusively for plants are highlighted in green (CW=cell wall of plants, Auxin, PIN), parts which have been observed only for animals are colored in orange (IF=intermediate filaments, SCRIBBLE), and for fungi are colored in blue (cell wall of fungi, TEA).

4.6 Outlook

With reference to the ECHO concept defined in the previous chapter, one key player is represented by the cytoskeleton (Figure 4.4). The work of this thesis has indicated that the organization of the cytoskeleton plays a pivotal role in polarity formation. The term “skeleton” in cytoskeleton can be misleading since the cytoskeleton is not a rigid structure. As discussed in the chapter above, particularly in the tensegral framework, the dynamic of actin or microtubules is essential for correct axis formation. This has been indicated in the current study via cytoskeletal drugs and overexpression lines. However, cytoskeletal drugs act ubiquitously in the cell. But what if cytoskeletal dynamics differ within the cell? To which degree is a filament stabilized? Does the dynamic of a filament change during the regeneration? A future challenge will be the quantification of stabilization degree; leading to question the method of choice to uncover and detect differences in cytoskeletal dynamics.

4.6.1 How to make intracellular dynamic visible and measurable?

A well-known technique to detect kinetics within a cell is fluorescence recovery after photobleaching. This method uses fluorescent probes and high-powered laser to bleach a region of interest. Subsequently, images are taken with low light intensity to record the redistribution of molecules via the recovery of the fluorescence within the living cell (Axelrod *et al.* 1976). However, it cannot be excluded that the harsh bleaching affects the molecules and alters their kinetic behavior. Therefore, the group of Dr. Mathur invented a much gentler technique to follow the mobility of cellular molecules (Wozny *et al.* 2012). For this innovative method, a photoconvertible probe such as mEos should be chosen and fused to the respective protein. The region of interest (ROI) is then photoconverted and the recovery of the non-photoconverted molecules followed over time.

For example, to compare different actin dynamics of two sides of the same cell, mEos can be fused to the actin binding probe Lifeact. The region of interest (ROI) is irradiated with violet-blue light. This results then in a photoconversion from green to red emission spectrum (Figure 4.5 A). Finally, images are taken and the green and red values plotted over time. The calculated green to red ratio can be compared for one part of the cell with the other part (Figure 4.5 B). Hereby, conclusions about differences in cytoskeletal dynamics within a cell are possible.

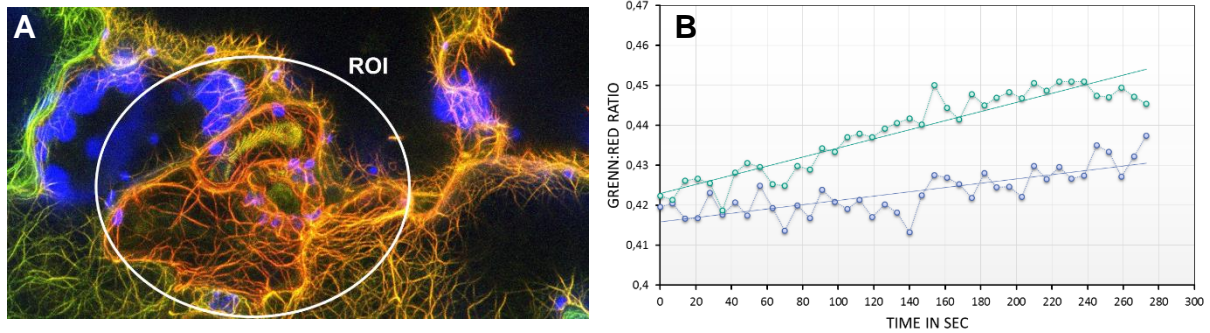


Figure 4.5 Example for color recovery after photoconversion of Lifeact-mEos in *A. thaliana*

(A) Image of a time-lapse movie of an *Arabidopsis thaliana* leaf transformed with Lifeact-mEos. Blue: false-colored chloroplasts, Green: non-photoconverted actin filaments. Orange: photoconverted actin filaments. The region of interest (ROI) can be split into two parts and then the green to red ratio can be plotted over time separately (B). The RGB values can be calculated on a standard eight-bit scale of 0 to 255 stretching across the region of interest (ROI). Green line: left side of the ROI, blue line: right side of the ROI. Image taken at the department of molecular cell biology at the University of Guelph, Ontario, Canada. Data analysis was performed via Image J. The appendix 5.6 (pp.109) provides a more detailed description of the used protocol.

4.6.2 Translation to the protoplast system

Using color recovery after photoconversion in the protoplast system enables, for instance, measurement of actin dynamics during regeneration (Figure 4.6). The degree of stabilization of actin filaments might be different regarding the position of the nucleus before axis formation. Further, with a photoconverted probe such as mEos fused to KCH, it becomes possible to track the location and the motion speed of two different sub-populations of KCH during cell wall synthesis and axis formation.

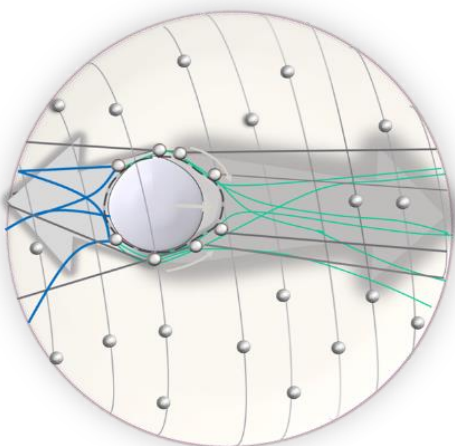


Figure 4.6 Draft of actin dynamics in Lifeact-mEos BY-2 protoplast during regeneration

Regenerating protoplast and the moving nucleus plus the retrograde signaling towards the plasma membrane (gray arrows). In addition, schematically drawn are the cytoskeleton (lines) and its motor proteins (dots). Actin dynamic differs within the cell during re-establishing the cell wall and axis formation regarding its location (blue filaments, left hand side compared to green filaments, right hand side).

Another recently investigated method to measure cytoskeletal dynamics is based on quantitative analysis of cytoskeletal kymograms (QuACK). Together with variable angle epifluorescence microscopy and spinning disc confocal microscopy differences in actin dynamics have been successfully displayed in *A. thaliana* formin mutants via this new technique (Cvrčková and Oulehlová 2017).

Overall, this work has contributed to partially decode plant cell polarity and axis formation. However, the mechanism of cell polarity formation is still far from being understood completely. The presented results motivate and support further research via novel nanostructure based ECM-pattern analysis, new microscopic tools, and broad bioinformatic analysis in the field of nuclear proteomics and should stimulate further investigations, which would help to refine the model of plant cell polarity step by step.

5 APPENDIX

5.1 Vectors of myosin lines

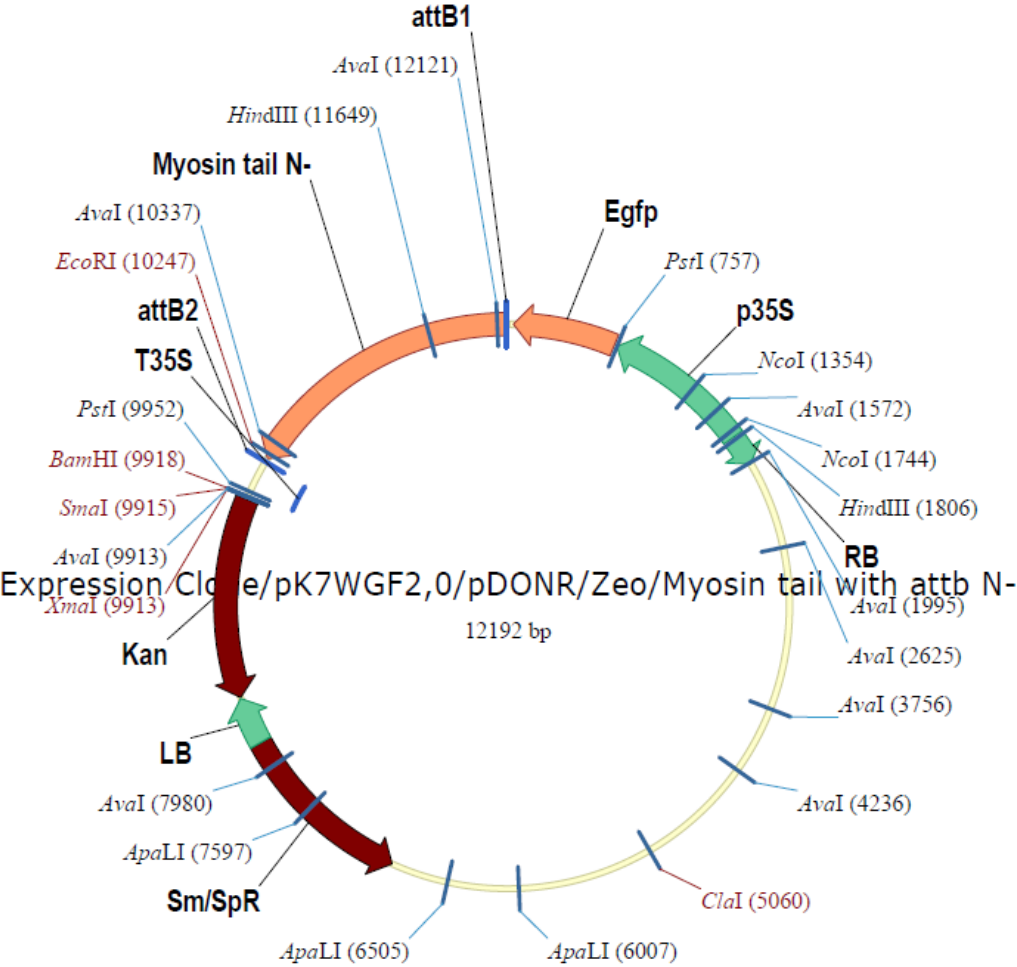


Figure 5.1 Vector GFP- myosin XI TailN

From Dr. Qiong Liu

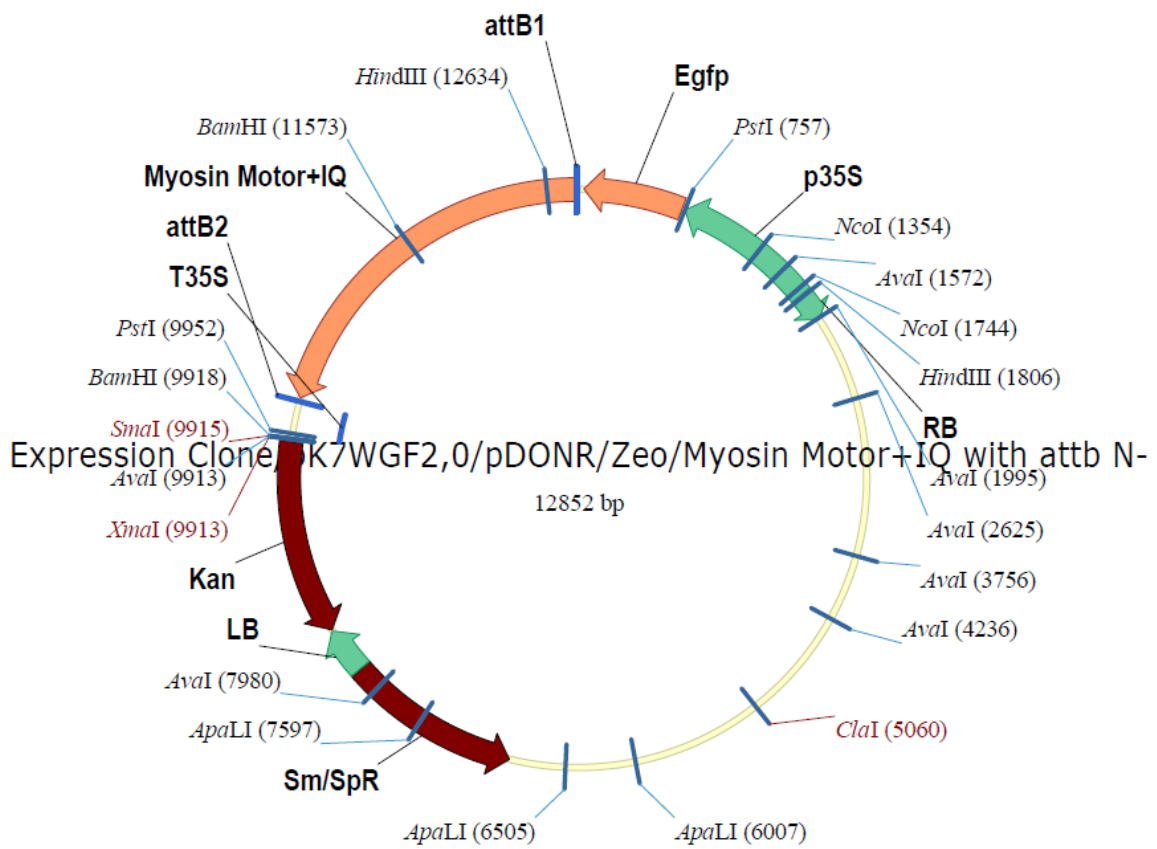


Figure 5.2 Vector GFP-Myo XI M+IQ
From Dr. Qiong Liu

5.2 Protein analysis of BY-2 WT, H2B-mEos, and Lifeact-psRFP nuclei

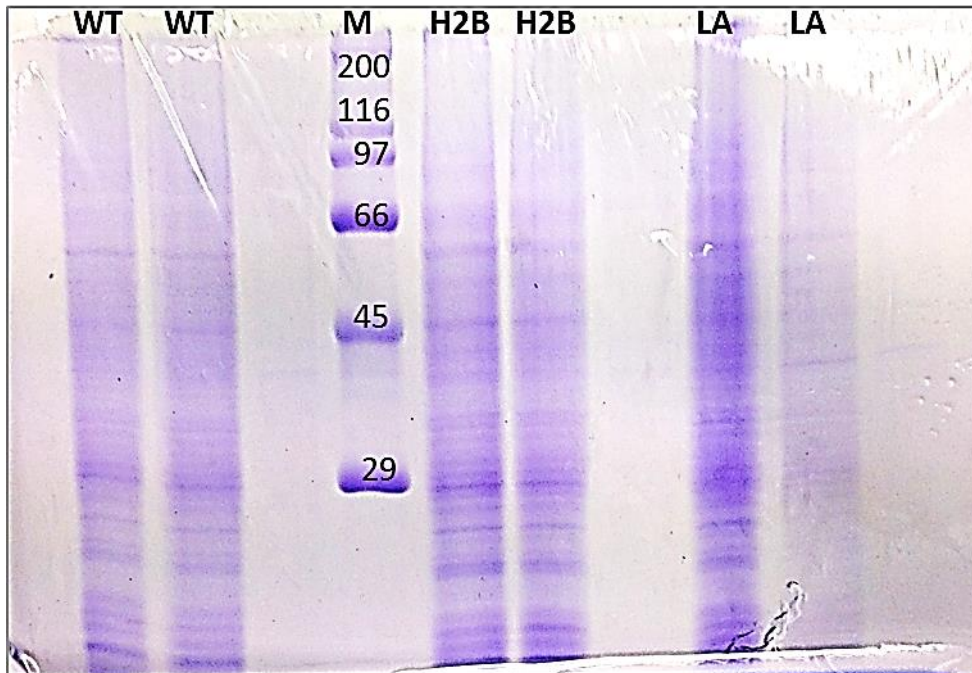
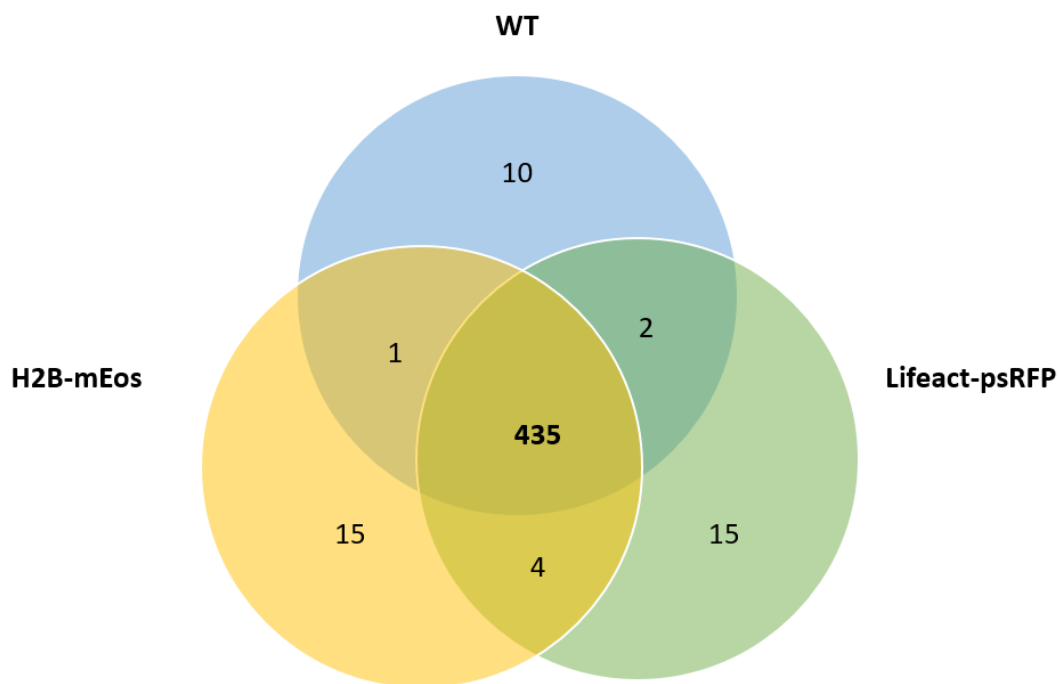


Figure 5.3 SDS PAGE of isolated nuclei

From left to right: wildtype (WT), wildtype (WT), high molecular weight marker (M) in kDa (for composition see Material and Methods), H2B-mEos (H2B), H2B-mEos (H2B), Lifeact-psRFP (LA), Lifeact-psRFP (LA).



Number of proteins identified: **482**

Common proteins used for further analysis: **435**

Figure 5.4 Venn diagram of identified proteins via tandem MS

The diagram depicts common and unique proteins. Only a small number of proteins was identified as unique proteins: 10 proteins were exclusively found in wildtype nuclei (WT, blue), 15 proteins were exclusively identified in transgenic nuclei each; Lifeact-psRFP nuclei (green) and H2B-mEos nuclei (orange). In WT and Lifeact-psRFP two common proteins were identified, WT and H2B-mEos share one common protein, and Lifeact-psRFP and H2B-mEos four common proteins. Proteins, which were identified in only one or two samples are listed below and were filtered out during data processing. 435 proteins were identified as common proteins for all three samples. These proteins were used for further analysis.

Table A 5.1 FASTA Headers of discarded proteins identified solely in WT (10), Lifeact-psRFP (15), H2B-mEos (15), WT+Lifeact-psRFP (2), WT+H2B-mEos (1) or H2B-mEos+Lifeact-psRFP (4)

Left to right: Tr = UniProtKB/TrEMBL, FASTA, OS= Name of Organism, PE= Protein Existence, the numerical value which describes the evidence for the existence of the proteins, SV= Sequence Version, version number of the sequence, generated with UniProt (2017).

WT	10
>tr A0A0K0XR75 A0A0K0XR75_TOBAC	Sorting nexin 1-like protein OS=Nicotiana tabacum GN=ATG20 PE=2 SV=1
>tr A0MWC2 A0MWC2_TOBAC	Apyrase-like protein OS=Nicotiana tabacum GN=APY1 PE=2 SV=1
>tr A7WPK7 A7WPK7_TOBAC	Putative uncharacterized protein C365 OS=Nicotiana tabacum GN=C365 PE=2 SV=1
>tr D9IP68 D9IP68_TOBAC	Pto-like protein (Fragment) OS=Nicotiana tabacum PE=2 SV=1
>tr I1Z1X7 I1Z1X7_TOBAC	Glycosyltransferase (Fragment) OS=Nicotiana tabacum GN=IRX10 PE=2 SV=1;
>tr I1Z1X8 I1Z1X8_TOBAC	Glycosyltransferase (Fragment) OS=Nicotiana tabacum GN=IRX10 PE=2 SV=1
>tr Q3LHS9 Q3LHS9_TOBAC	DNA polymerase OS=Nicotiana tabacum GN=Ntpoll-like2 PE=2 SV=1
>tr Q8S9H3 Q8S9H3_TOBAC	Minichromosome maintenance protein 3 (Fragment) OS=Nicotiana tabacum PE=2 SV=1
>tr Q93X37 Q93X37_TOBAC	Proteasome endopeptidase complex (Fragment) OS=Nicotiana tabacum GN=a5 PE=2 SV=1
>tr Q949G2 Q949G2_TOBAC	Ferrochelatase OS=Nicotiana tabacum GN=FeCh PE=2 SV=1
>tr A0A067ZTA7 A0A067ZTA7_TOBAC	Rab5.2 isoform OS=Nicotiana tabacum PE=2 SV=1
WT+Lifeact-psRFP	2
>tr A0A076KWG4 A0A076KWG4_TOBAC	CLB1 OS=Nicotiana tabacum PE=2 SV=1
>tr A0A097BU01 A0A097BU01_TOBAC	Mitochondrial-like 60S ribosomal protein L2 OS=Nicotiana tabacum PE=2 SV=1
Lifeact-psRFP	15
>tr D0VEA8 D0VEA8_TOBAC	Methyltransferase (Fragment) OS=Nicotiana tabacum PE=2 SV=1
>tr P93378 P93378_TOBAC	Tumor-related protein OS=Nicotiana tabacum PE=2 SV=1
>tr Q40511 Q40511_TOBAC	Heat shock protein 70 (Fragment) OS=Nicotiana tabacum GN=Nthsp70 PE=2 SV=1
>tr Q5MA04 Q5MA04_TOBAC	Ribosomal protein S3 OS=Nicotiana tabacum GN=rps3 PE=3 SV=2;
>tr A0A0M4JNE9 A0A0M4JNE9_TOBAC	Ribosomal protein S3 OS=Nicotiana tabacum GN=rps3 PE=3 SV=1
>tr Q84KS8 Q84KS8_TOBAC	Purple acid phosphatase OS=Nicotiana tabacum GN=PAP PE=2 SV=1
>tr Q8GSC4 Q8GSC4_TOBAC	DNA topoisomerase 2 OS=Nicotiana tabacum PE=2 SV=1
>tr Q8GUA3 Q8GUA3_TOBAC	Vacuolar invertase OS=Nicotiana tabacum GN=vi PE=2 SV=2
>tr Q8W402 Q8W402_TOBAC	Sucrose synthase (Fragment) OS=Nicotiana tabacum GN=SUSY PE=2 SV=1
>tr Q94FM5 Q94FM5_TOBAC	Elicitor-inducible cytochrome P450 OS=Nicotiana tabacum GN=CYP73A27 PE=2 SV=1;
>tr Q94FM4 Q94FM4_TOBAC	Elicitor-inducible cytochrome P450 OS=Nicotiana tabacum GN=CYP73A28 PE=2 SV=1
>tr Q9M6E6 Q9M6E6_TOBAC	Polyadenylate-binding protein OS=Nicotiana tabacum GN=PABP PE=2 SV=1;
>tr Q9M6E5 Q9M6E5_TOBAC	Poly(A)-binding protein (Fragment) OS=Nicotiana tabacum GN=PABP1 PE=2 SV=1
>tr Q9MB97 Q9MB97_TOBAC	Cytosine-5-methyltransferase OS=Nicotiana tabacum GN=NtMET1 PE=2 SV=1
>tr Q9SQI5 Q9SQI5_TOBAC	Centrin OS=Nicotiana tabacum GN=CEN1 PE=2 SV=1;
>tr Q9SQI4 Q9SQI4_TOBAC	Centrin OS=Nicotiana tabacum GN=CEN2 PE=2 SV=1
>tr Q9ZP39 Q9ZP39_TOBAC	Alpha-expansin OS=Nicotiana tabacum GN=Nt-EXPA1 PE=2 SV=1;
>tr Q9ZP38 Q9ZP38_TOBAC	Alpha-expansin OS=Nicotiana tabacum GN=Nt-EXPA2 PE=2 SV=1

>tr|Q9ZRD2|Q9ZRD2_TOBAC NTGP3 OS=Nicotiana tabacum GN=rac2 PE=2 SV=1
>tr|Q4LB98|Q4LB98_TOBAC Putative glutathione S-transferase (Fragment) OS=Nicotiana tabacum GN=GST1 PE=2 SV=1
H2B-mEos+WT 1

>tr|A0A077D7Q1|A0A077D7Q1_TOBAC 54 kDa signal recognition particle 2 OS=Nicotiana tabacum PE=2 SV=1
H2B-mEos 15

>tr|D2CNC8|D2CNC8_TOBAC Subtilase (Fragment) OS=Nicotiana tabacum GN=SBT1.2B PE=2 SV=1;>tr|D2CNC6|D2CNC6_TOBAC Subtilase OS=Nicotiana tabacum GN=SBT1.2A PE=4 SV=1
>tr|I7B1E5|I7B1E5_TOBAC Clathrin heavy chain 2 (Fragment) OS=Nicotiana tabacum GN=CHC2 PE=2 SV=1
>tr|P93360|P93360_TOBAC 4-coumarate:CoA ligase (Fragment) OS=Nicotiana tabacum PE=2 SV=1
>tr|Q9AT53|Q9AT53_TOBAC Glycosyltransferase (Fragment) OS=Nicotiana tabacum GN=togt2 PE=2 SV=1;>tr|P93364|P93364_TOBAC Glycosyltransferase OS=Nicotiana tabacum GN=IS10a PE=2 SV=1
>tr|Q93WZ1|Q93WZ1_TOBAC Endoglucanase OS=Nicotiana tabacum GN=Cel7 PE=2 SV=1;>tr|Q0H8W0|Q0H8W0_TOBAC Endoglucanase OS=Nicotiana tabacum GN=Cel7 PE=3 SV=1
>tr|Q40511|Q40511_TOBAC Heat shock protein 70 (Fragment) OS=Nicotiana tabacum GN=Nthsp70 PE=2 SV=1
>tr|Q6EIX9|Q6EIX9_TOBAC Potyviral capsid protein interacting protein 1 OS=Nicotiana tabacum GN=CPIP1 PE=2 SV=1
>tr|Q6Q8A0|Q6Q8A0_TOBAC Phosphotransferase OS=Nicotiana tabacum GN=Hxk6 PE=2 SV=1
>tr|Q75WV4|Q75WV4_TOBAC N protein (Fragment) OS=Nicotiana tabacum GN=N PE=2 SV=1
>tr|Q75ZE1|Q75ZE1_TOBAC 14-3-3 d-2-AS protein OS=Nicotiana tabacum GN=14-3-3 d-2 PE=2 SV=1;>tr|Q75ZE2|Q75ZE2_TOBAC 14-3-3 d-2 protein OS=Nicotiana tabacum GN=14-3-3 d-2 PE=2 SV=1
>tr|Q8GT44|Q8GT44_TOBAC Putative rac protein OS=Nicotiana tabacum GN=rac4 PE=2 SV=1
>tr|Q8RU72|Q8RU72_TOBAC Glucosyltransferase OS=Nicotiana tabacum GN=NtGT3 PE=2 SV=1
>tr|Q8SF03|Q8SF03_TOBAC Dicarboxylate/tricarboxylate carrier (Fragment) OS=Nicotiana tabacum GN=dtc2 PE=2 SV=1;>tr|Q9FSF4|Q9FSF4_TOBAC Mitochondrial 2-oxoglutarate/malate carrier protein OS=Nicotiana tabacum GN=momc1 PE=2 SV=1
>tr|Q9FEV9|Q9FEV9_TOBAC Microtubule-associated protein MAP65-1a OS=Nicotiana tabacum GN=map65-1a PE=2 SV=1
>tr|W0KRH1|W0KRH1_TOBAC Superoxide dismutase OS=Nicotiana tabacum PE=2 SV=1
H2B-mEos+Lifeact-psRFP 4

>tr|A0A076FN11|A0A076FN11_TOBAC Glucose-6-phosphate isomerase OS=Nicotiana tabacum GN=GPI PE=2 SV=1
>tr|A0A077D837|A0A077D837_TOBAC Glutathione synthetase OS=Nicotiana tabacum PE=2 SV=1
>tr|A0A077DCK9|A0A077DCK9_TOBAC Carbonic anhydrase OS=Nicotiana tabacum PE=2 SV=1;>tr|Q9LW91|Q9LW91_TOBAC Carbonic anhydrase (Fragment) OS=Nicotiana tabacum GN=carbonic anhydrase PE=2 SV=1
>tr|A0A0R4WFQ1|A0A0R4WFQ1_TOBAC Mannose-binding lectin OS=Nicotiana tabacum GN=MBL2 PE=2 SV=1

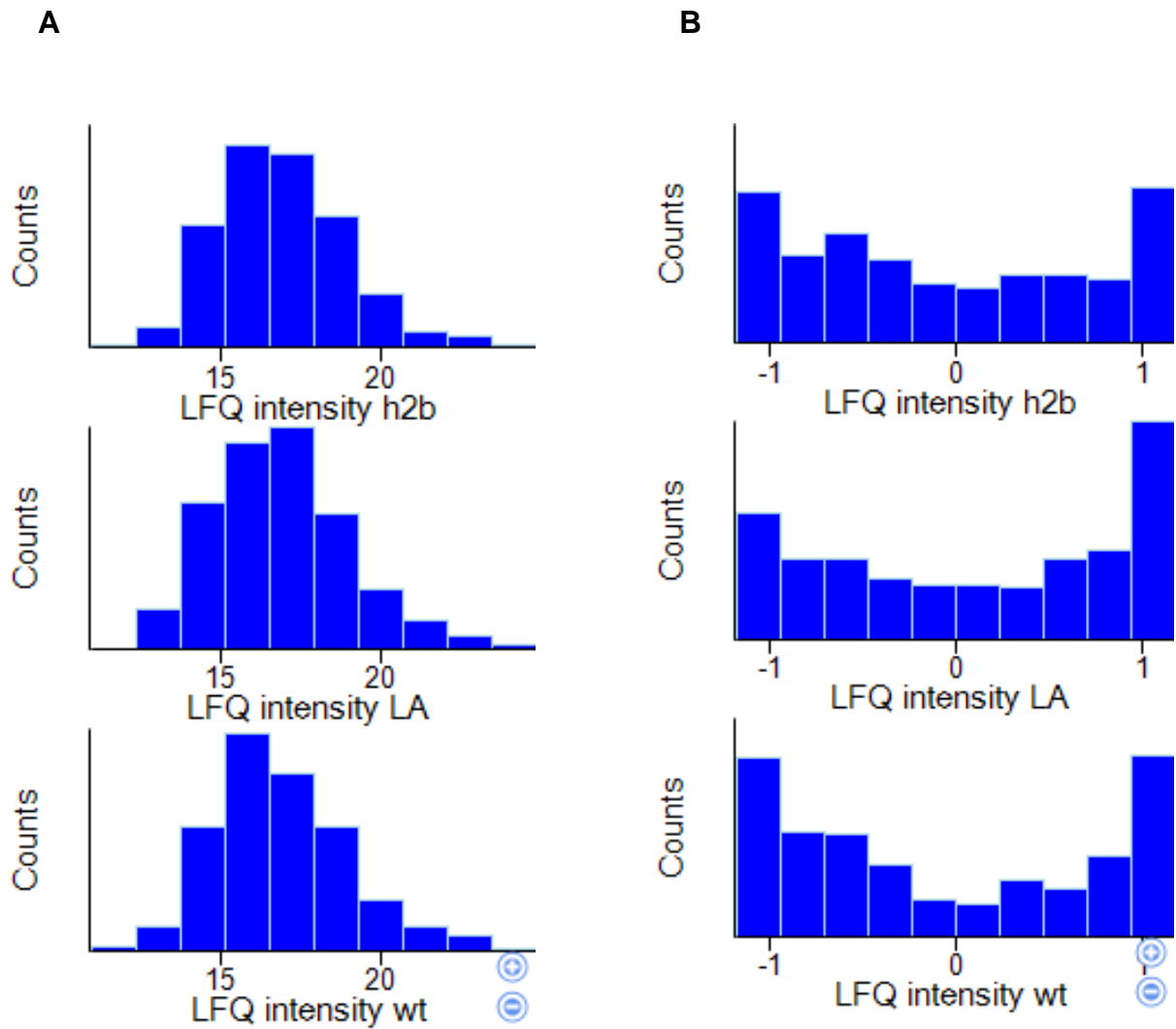


Figure 5.5 Histogram of LFQ intensities

Distribution of proteins intensities in H2B-mEos (h2b), Lifeact-psRFP (LA) and wildtype (wt) after transformation (A) and z-normalization (B).

Table A 5.2 FASTA Headers of chosen Cluster ②

Left to right: Tr = UniProtKB/TrEMBL, FASTA, OS= Name of Organism, PE= Protein Existence, the numerical value which describes the evidence for the existence of the proteins, SV= Sequence Version, version number of the sequence, generated with UniProt (2017).

>tr W8SRJ3 W8SRJ3_TOBAC ATP synthase subunit beta OS=Nicotiana tabacum PE=2 SV=1
>tr W8SI43 W8SI43_TOBAC Farnesyl pyrophosphate synthase 1 OS=Nicotiana tabacum PE=2 SV=1
>tr R9R4F9 R9R4F9_TOBAC Nectarin I (Fragment) OS=Nicotiana tabacum GN=Nec1 PE=2 SV=1;>tr S4TH40 S4TH40_TOBAC PDGLP1 (Fragment) OS=Nicotiana tabacum PE=2 SV=1
>tr Q9ZR68 Q9ZR68_TOBAC Aquaporin 1 OS=Nicotiana tabacum GN=aqp1 PE=2 SV=1;>tr A0A0D3L6R2 A0A0D3L6R2_TOBAC Tonoplast intrinsic protein 1 OS=Nicotiana tabacum GN=TIP1 PE=2 SV=1
>tr Q9ZNX0 Q9ZNX0_TOBAC NAD-dependent isocitrate dehydrogenase OS=Nicotiana tabacum PE=2 SV=1
>tr Q9TNL9 Q9TNL9_TOBAC Stromal ascorbate peroxidase OS=Nicotiana tabacum PE=2 SV=1;>tr Q9XPR6 Q9XPR6_TOBAC Thylakoid-bound ascorbate peroxidase OS=Nicotiana tabacum PE=2 SV=1
>tr Q9SWA4 Q9SWA4_TOBAC Histone H1C OS=Nicotiana tabacum GN=H1c PE=2 SV=1;>tr Q8H6B7 Q8H6B7_TOBAC Histone H1D OS=Nicotiana tabacum GN=H1d PE=2 SV=1;>tr Q8H0G8 Q8H0G8_TOBAC Stress-inducible H1 histone-like protein OS=Nicotiana tabacum GN=A10 PE=2 SV=1
>tr Q9SLS1 Q9SLS1_TOBAC Histone H1 OS=Nicotiana tabacum GN=NtH1 PE=2 SV=1;>tr Q40509 Q40509_TOBAC Histone H1 OS=Nicotiana tabacum GN=H1C12 PE=2 SV=1
>tr Q9MB97 Q9MB97_TOBAC Cytosine-5-methyltransferase OS=Nicotiana tabacum GN=NtMET1 PE=2 SV=1
>tr Q9M6E6 Q9M6E6_TOBAC Polyadenylate-binding protein OS=Nicotiana tabacum GN=PABP PE=2 SV=1;>tr Q9M6E5 Q9M6E5_TOBAC Poly(A)-binding protein (Fragment) OS=Nicotiana tabacum GN=PABP1 PE=2 SV=1
>tr Q9FSF7 Q9FSF7_TOBAC O-linked GlcNAc transferase like (Fragment) OS=Nicotiana tabacum GN=glcNAc-like PE=2 SV=1
>tr Q948K3 Q948K3_TOBAC 14-3-3 protein OS=Nicotiana tabacum GN=D75 PE=2 SV=1
>tr Q947H4 Q947H4_TOBAC Aldose 1-epimerase OS=Nicotiana tabacum GN=NCAPP2 PE=2 SV=1
>tr Q93X38 Q93X38_TOBAC Proteasome endopeptidase complex (Fragment) OS=Nicotiana tabacum GN=a4 PE=2 SV=1
>tr Q93X35 Q93X35_TOBAC Proteasome subunit alpha type (Fragment) OS=Nicotiana tabacum GN=a6 PE=2 SV=1
>tr Q8W3Z9 Q8W3Z9_TOBAC Invertase (Fragment) OS=Nicotiana tabacum GN=NtINV PE=2 SV=1
>tr Q8SF04 Q8SF04_TOBAC Dicarboxylate/tricarboxylate carrier OS=Nicotiana tabacum GN=dtc1 PE=2 SV=1
>tr Q8GZV0 Q8GZV0_TOBAC Obtusifoliol-14-demethylase OS=Nicotiana tabacum GN=CYP51 PE=2 SV=1;>tr Q8GVD5 Q8GVD5_TOBAC Obtusifoliol-14-demethylase OS=Nicotiana tabacum GN=NtCYP51-2 PE=2 SV=1
>tr Q84KZ2 Q84KZ2_TOBAC Purple acid phosphatase OS=Nicotiana tabacum GN=PAP PE=2 SV=1
>tr Q84KS8 Q84KS8_TOBAC Purple acid phosphatase OS=Nicotiana tabacum GN=PAP PE=2 SV=1
>tr Q7M242 Q7M242_TOBAC Glutamate synthase (Ferredoxin) (Clone C(35)) (Fragment) OS=Nicotiana tabacum PE=4 SV=1
>tr Q75ZE5 Q75ZE5_TOBAC 14-3-3 a-1 protein OS=Nicotiana tabacum GN=14-3-3 a-1 PE=2 SV=1;>tr Q75ZD8 Q75ZD8_TOBAC 14-3-3 f-1 protein OS=Nicotiana tabacum GN=14-3-3 f-1 PE=2 SV=1;>tr Q75XU9 Q75XU9_TOBAC 14-3-3 f-2 protein (Fragment) OS=Nicotiana tabacum GN=14

>tr Q75ZE3 Q75ZE3_TOBAC 14-3-3 c-2 protein OS=Nicotiana tabacum GN=14-3-3 c-2 PE=2 SV=1;>tr Q5KTN5 Q5KTN5_TOBAC 14-3-3 c-1 protein OS=Nicotiana tabacum GN=14-3-3 c-1 PE=2 SV=1;>tr Q948K2 Q948K2_TOBAC 14-3-3 protein (Fragment) OS=Nicotiana tabacum GN=D5 PE=
>tr Q75ZE1 Q75ZE1_TOBAC 14-3-3 d-2-AS protein OS=Nicotiana tabacum GN=14-3-3 d-2 PE=2 SV=1;>tr Q75ZE2 Q75ZE2_TOBAC 14-3-3 d-2 protein OS=Nicotiana tabacum GN=14-3-3 d-2 PE=2 SV=1
>tr Q75ZD4 Q75ZD4_TOBAC 14-3-3 i-1 protein OS=Nicotiana tabacum GN=14-3-3 i-1 PE=2 SV=1
>tr Q71V35 Q71V35_TOBAC ATP synthase subunit beta (Fragment) OS=Nicotiana tabacum GN=atpB PE=3 SV=1;>tr A0A140G1S2 A0A140G1S2_TOBAC ATP synthase subunit beta OS=Nicotiana tabacum GN=atpB PE=3 SV=1
>tr Q6T6H9 Q6T6H9_TOBAC Inosine-5-phosphate dehydrogenase (Fragment) OS=Nicotiana tabacum GN=guaB PE=2 SV=1
>tr Q6E2S8 Q6E2S8_TOBAC RNA polymerase II (Fragment) OS=Nicotiana tabacum GN=RPB2 PE=4 SV=1
>tr Q67C43 Q67C43_TOBAC Glutamate dehydrogenase alpha subunit (Fragment) OS=Nicotiana tabacum GN=gdh1 PE=2 SV=1
>tr Q5QJB2 Q5QJB2_TOBAC Harpin binding protein 1 OS=Nicotiana tabacum GN=HrBP1 PE=2 SV=1
>tr Q5MA04 Q5MA04_TOBAC Ribosomal protein S3 OS=Nicotiana tabacum GN=rps3 PE=3 SV=2;>tr A0A0M4JNE9 A0A0M4JNE9_TOBAC Ribosomal protein S3 OS=Nicotiana tabacum GN=rps3 PE=3 SV=1
>tr Q5M9V4 Q5M9V4_TOBAC ATP synthase subunit alpha OS=Nicotiana tabacum GN=atp1 PE=3 SV=2;>tr A0A0M4JJI5 A0A0M4JJI5_TOBAC ATP synthase subunit alpha OS=Nicotiana tabacum GN=atp1 PE=3 SV=1;>tr Q6E2W3 Q6E2W3_TOBAC ATP synthase subunit alpha (Fragment) OS=Nic
>tr Q43798 Q43798_TOBAC Inorganic pyrophosphatase OS=Nicotiana tabacum GN=ppa PE=2 SV=1;>tr Q43801 Q43801_TOBAC Inorganic pyrophosphatase OS=Nicotiana tabacum PE=2 SV=1
>tr Q40487 Q40487_TOBAC Peroxidase OS=Nicotiana tabacum PE=2 SV=1
>tr Q40486 Q40486_TOBAC Peroxidase OS=Nicotiana tabacum PE=2 SV=1
>tr Q40483 Q40483_TOBAC Cdc2 protein OS=Nicotiana tabacum GN=cdc2 PE=2 SV=1;>tr Q9FUR4 Q9FUR4_TOBAC Cyclin-dependent kinase A:4 (Fragment) OS=Nicotiana tabacum GN=CdkA:4 PE=2 SV=1;>tr Q40484 Q40484_TOBAC Cdc2 homolog OS=Nicotiana tabacum PE=2 SV=1;>tr Q404
>tr Q25C91 Q25C91_TOBAC Tobacco fibrillar protein homolog OS=Nicotiana tabacum GN=NtFib1 PE=2 SV=1
>tr Q1W0X2 Q1W0X2_TOBAC Mitochondrial import receptor-like protein (Fragment) OS=Nicotiana tabacum PE=2 SV=1
>tr Q0MW94 Q0MW94_TOBAC 1-deoxy-D-xylulose-5-phosphate reductoisomerase OS=Nicotiana tabacum GN=DXR PE=2 SV=1
>tr P93378 P93378_TOBAC Tumor-related protein OS=Nicotiana tabacum PE=2 SV=1
>tr P93353 P93353_TOBAC Hin1 protein OS=Nicotiana tabacum GN=hin1 PE=2 SV=1;>tr Q9M663 Q9M663_TOBAC Harpin inducing protein OS=Nicotiana tabacum GN=hin1 PE=2 SV=1
>tr O82151 O82151_TOBAC Beta-D-glucan exohydrolase OS=Nicotiana tabacum PE=2 SV=1
>tr O24157 O24157_TOBAC Nascent polypeptide associated complex alpha chain (Fragment) OS=Nicotiana tabacum PE=2 SV=1
>tr O22402 O22402_TOBAC Guanosine nucleotide diphosphate dissociation inhibitor OS=Nicotiana tabacum GN=GDI PE=2 SV=1
>tr I6QBI4 I6QBI4_TOBAC BOP1 OS=Nicotiana tabacum PE=2 SV=1;>tr I6QFZ0 I6QFZ0_TOBAC BOP3 OS=Nicotiana tabacum PE=2 SV=1;>tr I6QA31 I6QA31_TOBAC BOP4 OS=Nicotiana tabacum PE=2 SV=1
>tr I1Z1X7 I1Z1X7_TOBAC Glycosyltransferase (Fragment) OS=Nicotiana tabacum GN=IRX10 PE=2 SV=1;>tr I1Z1X8 I1Z1X8_TOBAC Glycosyltransferase (Fragment) OS=Nicotiana tabacum GN=IRX10 PE=2 SV=1
>tr G9MD86 G9MD86_TOBAC Heat shock protein 90 OS=Nicotiana tabacum GN=NtHsp90er-1 PE=2 SV=1

APPENDIX

>tr F6N7C2 F6N7C2_TOBAC Zeta-carotene desaturase OS=Nicotiana tabacum PE=2 SV=1;>tr A0A067YEL0 A0A067YEL0_TOBAC Zeta-carotene desaturase OS=Nicotiana tabacum GN=ZDS PE=2 SV=1
>tr E1U7Y2 E1U7Y2_TOBAC Type 2 histone deacetylase a OS=Nicotiana tabacum GN=HD2a PE=2 SV=1
>tr D6RUV9 D6RUV9_TOBAC ARGONAUTE 1 OS=Nicotiana tabacum GN=AGO1 PE=2 SV=1
>tr D6PZY8 D6PZY8_TOBAC RNA-binding glycine-rich protein OS=Nicotiana tabacum GN=RGP-3 PE=2 SV=1;>tr Q9T2M1 Q9T2M1_TOBAC RNA binding protein (Fragment) OS=Nicotiana tabacum PE=4 SV=1;>tr J7G5U5 J7G5U5_TOBAC RNA-binding glycine-rich protein OS=Nicotiana tab
>tr D0VEA8 D0VEA8_TOBAC Metyltransferase (Fragment) OS=Nicotiana tabacum PE=2 SV=1
>tr C8CJE5 C8CJE5_TOBAC Farnesyl pyrophosphate synthase (Fragment) OS=Nicotiana tabacum GN=fps PE=2 SV=1
>tr C3PTS5 C3PTS5_TOBAC Aspartic protease OS=Nicotiana tabacum PE=2 SV=1
>tr A9CM22 A9CM22_TOBAC Voltage-dependent anion channel OS=Nicotiana tabacum GN=NtVDAC3 PE=2 SV=1
>tr A8J6V0 A8J6V0_TOBAC Histone H2B OS=Nicotiana tabacum GN=NtH2B2 PE=2 SV=1
>tr A2SXR4 A2SXR4_TOBAC Uricase OS=Nicotiana tabacum PE=2 SV=1
>tr A1XEI4 A1XEI4_TOBAC CYP98A33v1 OS=Nicotiana tabacum PE=2 SV=1;>tr A1XEI5 A1XEI5_TOBAC CYP98A33v1 OS=Nicotiana tabacum PE=2 SV=1
>tr A0JCI0 A0JCI0_TOBAC Ubiquinol oxidase OS=Nicotiana tabacum GN=AOX PE=2 SV=1
>tr A0A0M4K6A0 A0A0M4K6A0_TOBAC Ribosomal protein L5 OS=Nicotiana tabacum GN=rpl5 PE=4 SV=1;>tr Q5MA46 Q5MA46_TOBAC Ribosomal protein L5 OS=Nicotiana tabacum GN=rpl5 PE=4 SV=2;>tr A0A172CTD5 A0A172CTD5_TOBAC Ribosomal protein L5 OS=Nicotiana tabacum GN=rpl
>tr A0A0A8JBT3 A0A0A8JBT3_TOBAC Alpha-L-Arabinofuranosidase/beta-D-Xylopyrianosidase (Fragment) OS=Nicotiana tabacum PE=2 SV=1
>tr A0A097BU01 A0A097BU01_TOBAC Mitochondrial-like 60S ribosomal protein L2 OS=Nicotiana tabacum PE=2 SV=1
>tr A0A077DCK9 A0A077DCK9_TOBAC Carbonic anhydrase OS=Nicotiana tabacum PE=2 SV=1;>tr Q9LW91 Q9LW91_TOBAC Carbonic anhydrase (Fragment) OS=Nicotiana tabacum GN=carbonic anhydrase PE=2 SV=1
>tr A0A077D9P0 A0A077D9P0_TOBAC 40S ribosomal protein S17-like protein OS=Nicotiana tabacum PE=2 SV=1
>tr A0A077D849 A0A077D849_TOBAC Eukaryotic translation initiation factor 5A OS=Nicotiana tabacum PE=2 SV=1
>tr A0A076L4P6 A0A076L4P6_TOBAC Importin subunit alpha OS=Nicotiana tabacum PE=2 SV=1
>tr A0A076KXA2 A0A076KXA2_TOBAC Putative alfin-like transcription factor OS=Nicotiana tabacum PE=2 SV=1
>tr A0A075F1U0 A0A075F1U0_TOBAC Constitutive plastid-lipid associated protein OS=Nicotiana tabacum GN=CHRD PE=2 SV=1
>tr A0A068JFR6 A0A068JFR6_TOBAC Triosephosphate isomerase OS=Nicotiana tabacum PE=2 SV=1

5.3 Regeneration analysis – Additional diagrams and figures

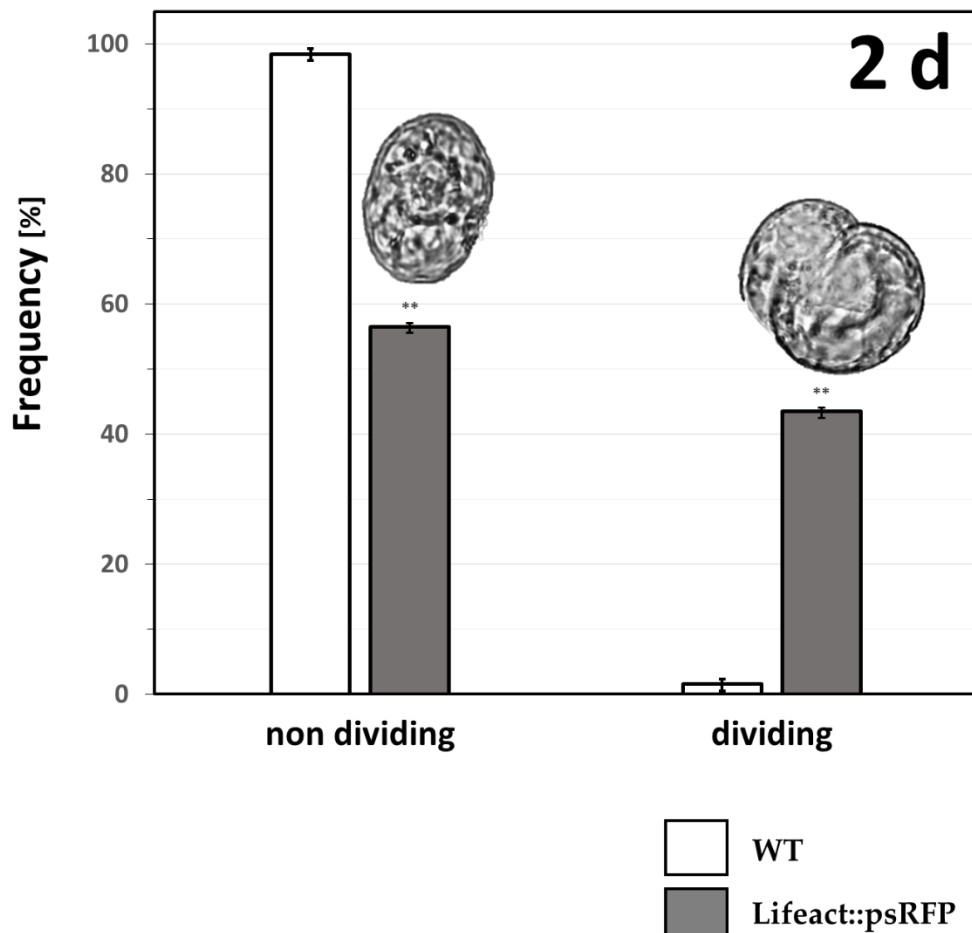


Figure 5.6 Frequency distribution of cell division in BY-2 Lifeact-psRFP

Frequency distribution of cell division two days after protoplast preparation in BY-2 Lifeact-psRFP protoplasts (gray bars) compared to non-transformed BY-2 protoplasts (WT, white bars). Frequency distributions have been calculated from 2,000 individual cells. Error bars show standard errors of the mean (SE). Asterisks represent significance of indicated differences as tested by a paired, two-sided t-test (**P < 1%).

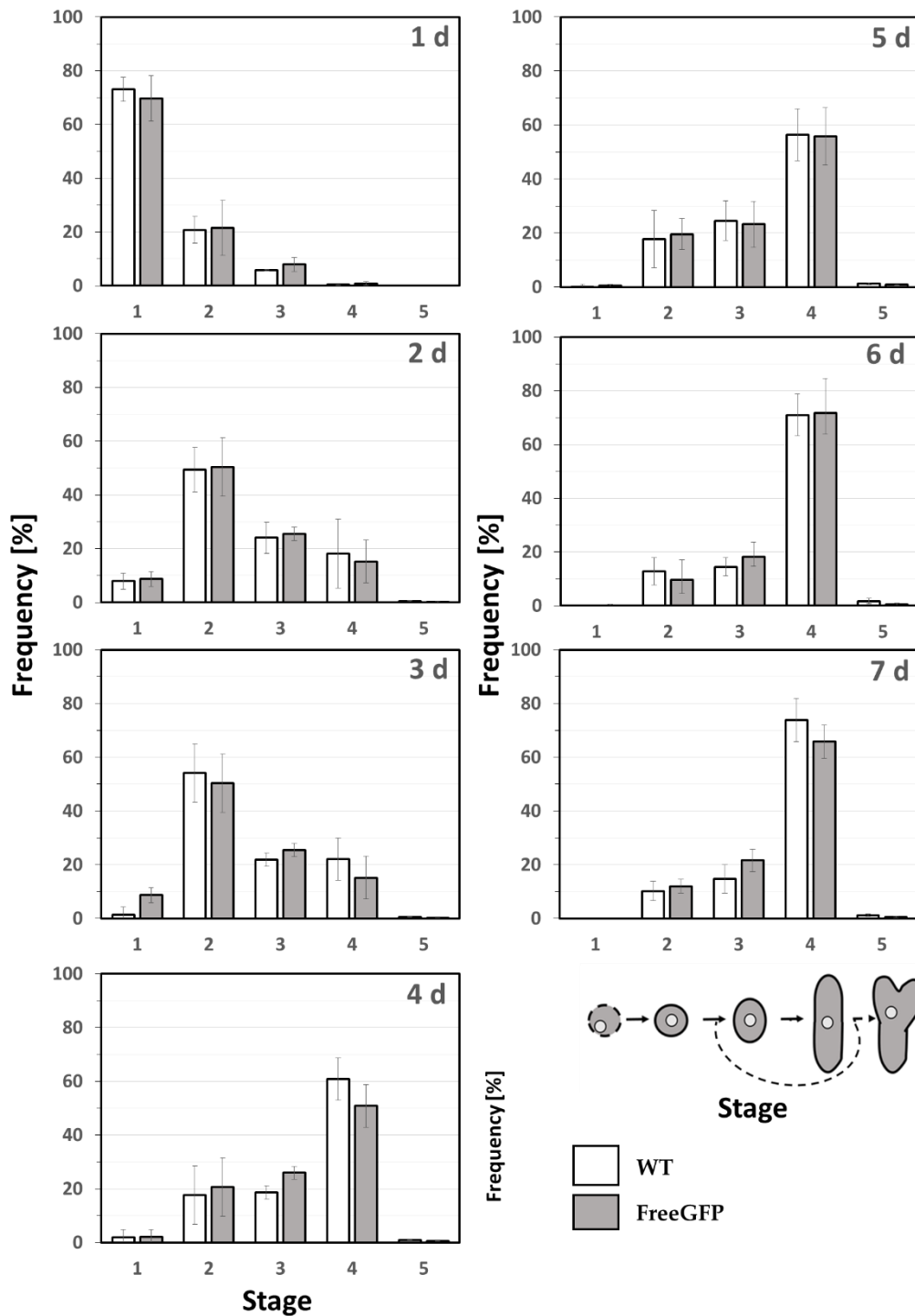


Figure 5.7 Frequency distributions of regeneration stages in BY-2 free GFP

Frequency distributions of the different regeneration stages for different time points after protoplast preparation in BY-2 free GFP (light gray bars) compared to non-transformed BY-2 protoplasts (WT, white bars). Stages are indicated schematically. Frequency distributions were calculated from 3,000 individual cells per time point from three independent biological replications. Error bars show standard errors of the mean (SE). Asterisks represent significance of indicated differences as tested by a paired, two-sided t-test (*P < 5%, **P < 1%).

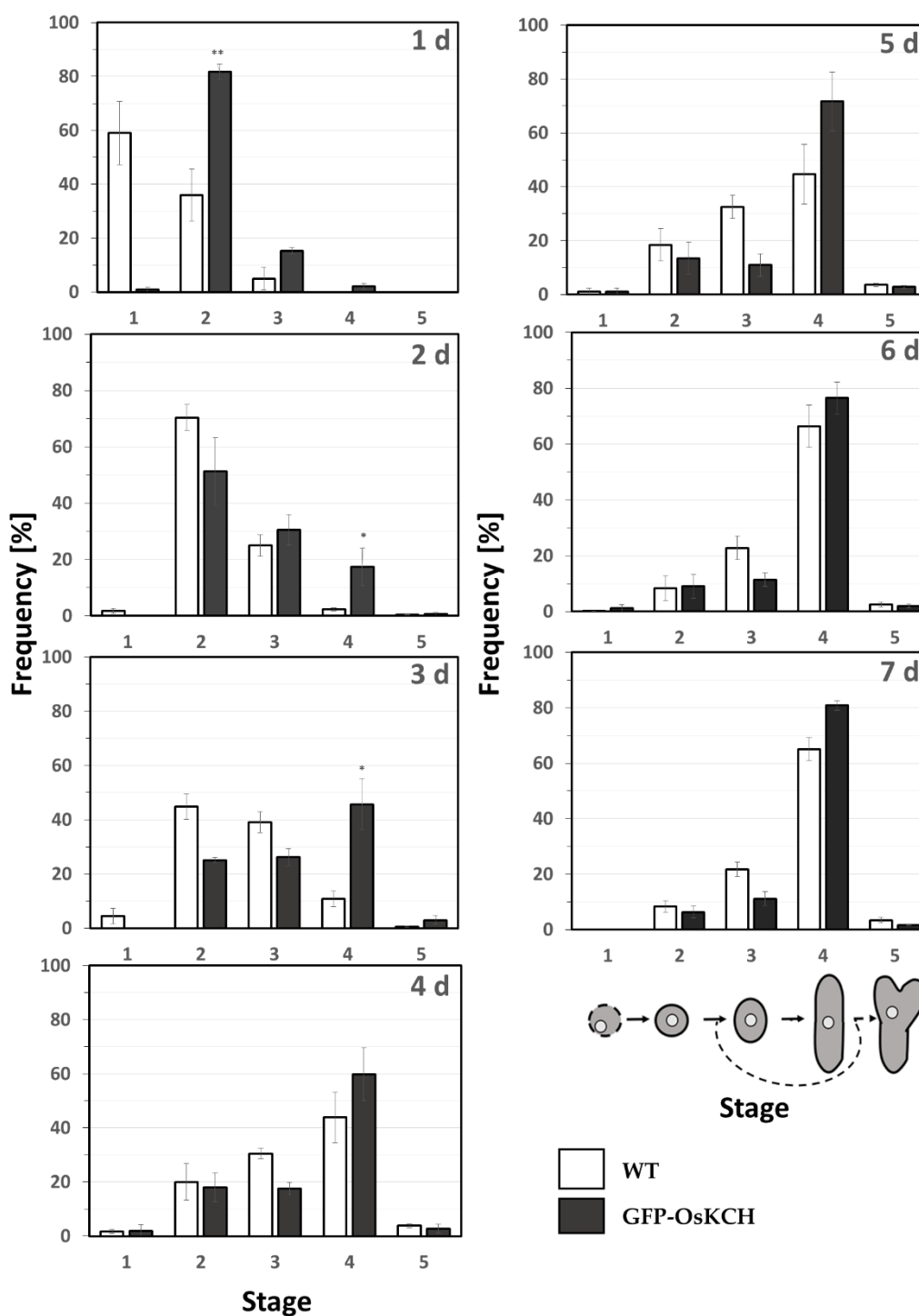


Figure 5.8 Frequency distributions of regeneration stages in BY-2 GFP-OsKCH

Frequency distributions of the different regeneration stages for different time points after protoplast preparation in BY-2 GFP-OsKCH (dark gray bars) compared to non-transformed BY-2 protoplasts (WT, white bars). Stages are indicated schematically. Frequency distributions were calculated from 3,000 individual cells per time point from three independent biological replications. Error bars show standard errors of the mean (SE). Asterisks represent significance of indicated differences as tested by a paired, two-sided t-test (* $P < 5\%$, ** $P < 1\%$).

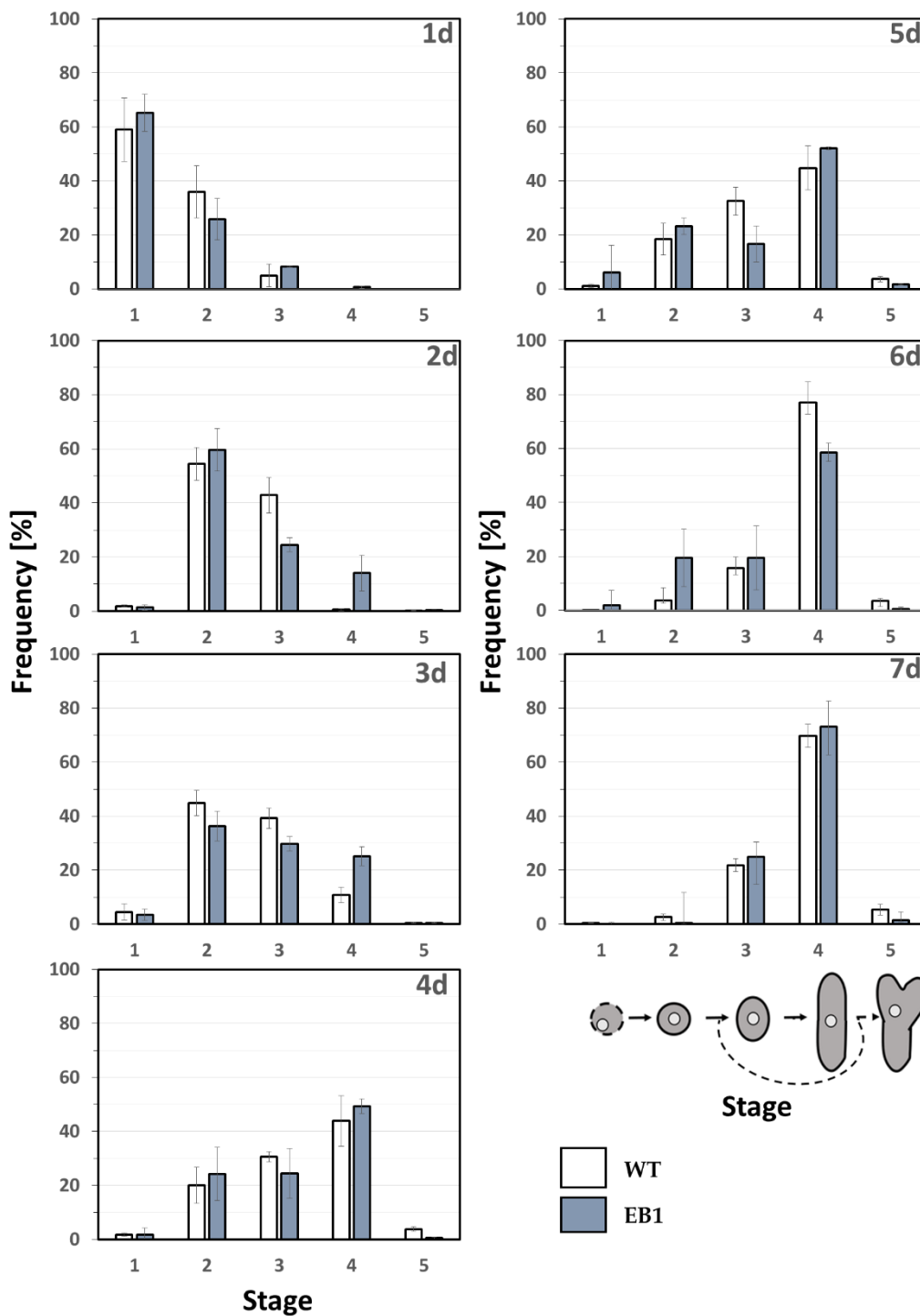


Figure 5.9 Frequency distributions of regeneration stages in BY-2 GFP-EB1

Frequency distributions of the different regeneration stages for different time points after protoplast preparation in BY-2 GFP-EB1 (light blue bars) compared to non-transformed BY-2 protoplasts (WT, white bars). Stages are indicated schematically. Frequency distributions were calculated from 3,000 individual cells per time point from three independent biological replications. Error bars show standard errors of the mean (SE). Asterisks represent significance of indicated differences as tested by a paired, two-sided t-test (*P < 5%, **P < 1%).

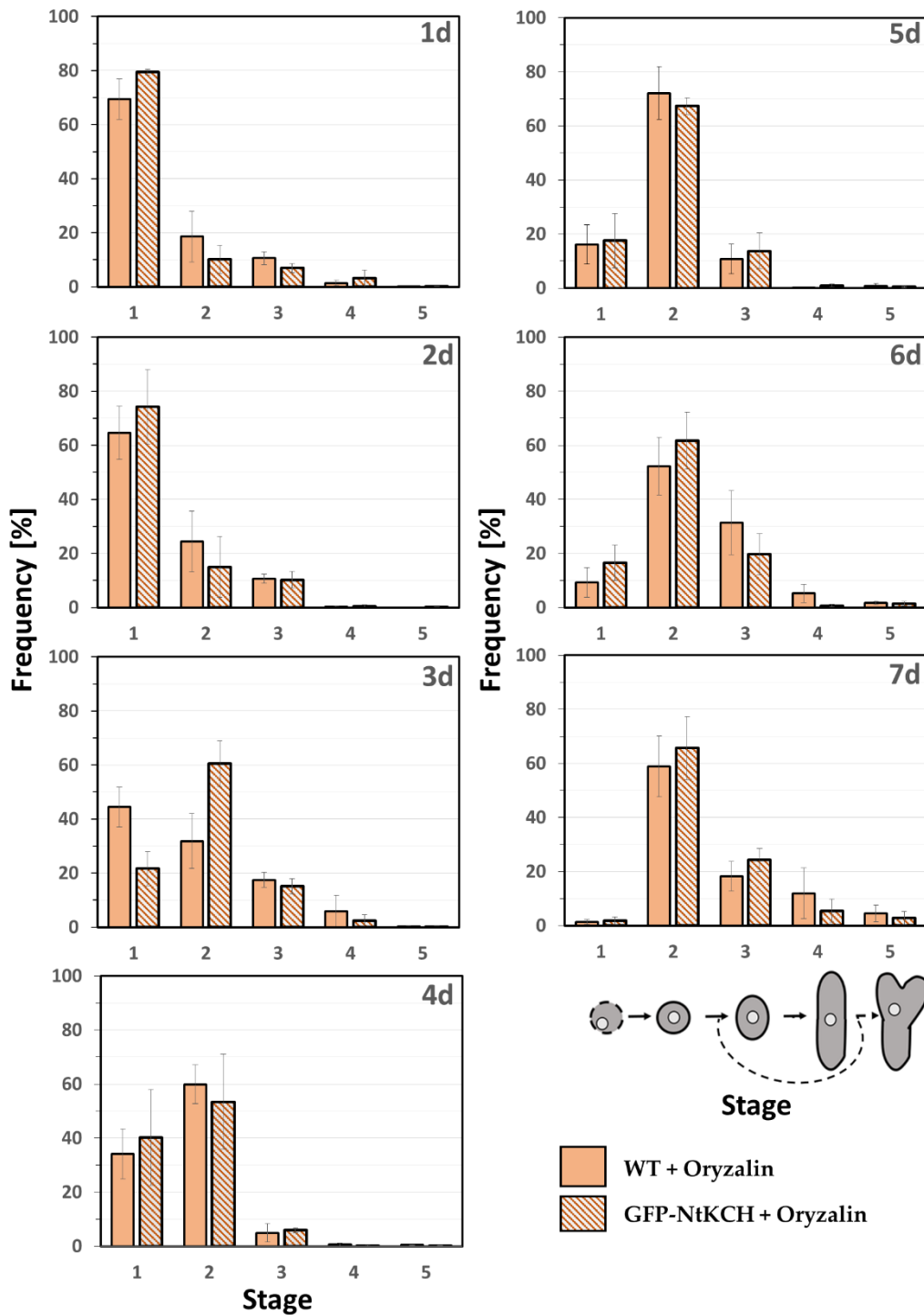


Figure 5.10 Frequency distributions of regeneration stages in Oryzalin treated GFP-NtKCH

Frequency distributions of the different regeneration stages for different time points after protoplast preparation in 100nM Oryzalin treated BY-2 GFP-NtKCH (orange bars) compared to non-transformed 100 nM Oryzalin treated WT BY-2 protoplasts (patterned orange bars). Stages are indicated schematically. Frequency distributions were calculated from 3,000 individual cells per time point from three independent biological replications. Error bars show standard errors of the mean (SE). Asterisks represent significance of indicated differences as tested by a paired, two-sided t-test (*P < 5%, **P < 1%).

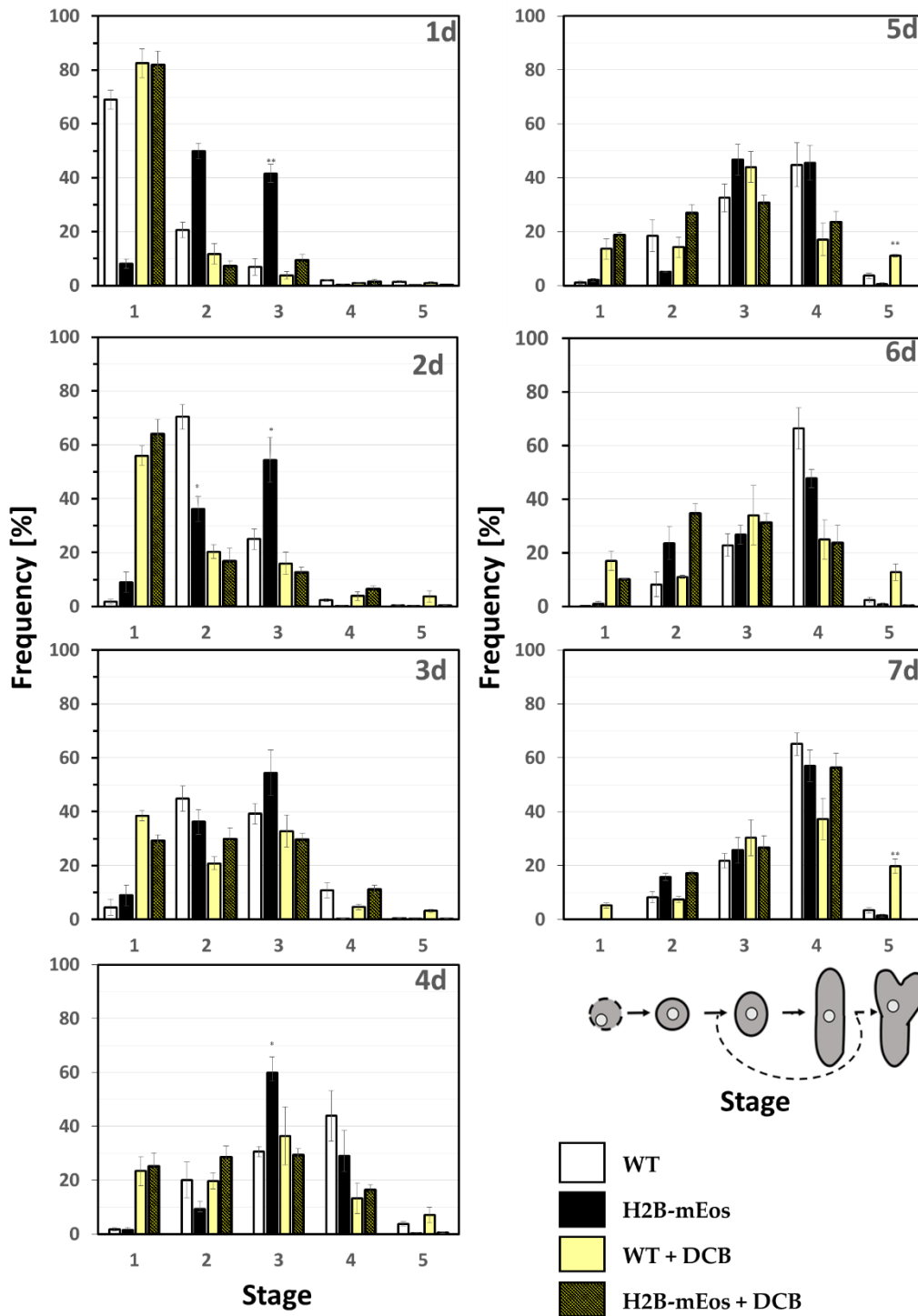


Figure 5.11 Frequency distributions of regeneration stages in DCB treated BY-2 WT and H2B-mEos

Frequency distributions of the different regeneration stages for different time points after protoplast preparation in DCB treated BY-2 WT (light yellow bars) and H2B-mEos (dark yellow bars) protoplasts compared to non-transformed and non-treated BY-2 WT (WT, white bars) as well as non-treated H2B-mEos (black bars) protoplasts. Stages are indicated schematically. Frequency distributions were calculated from 3,000 individual cells per time point from three independent biological replications. Error bars show standard errors of the mean (SE). Asterisks represent significance of indicated differences as tested by a paired, two-side t-test (*P < 5%, **P < 1%).

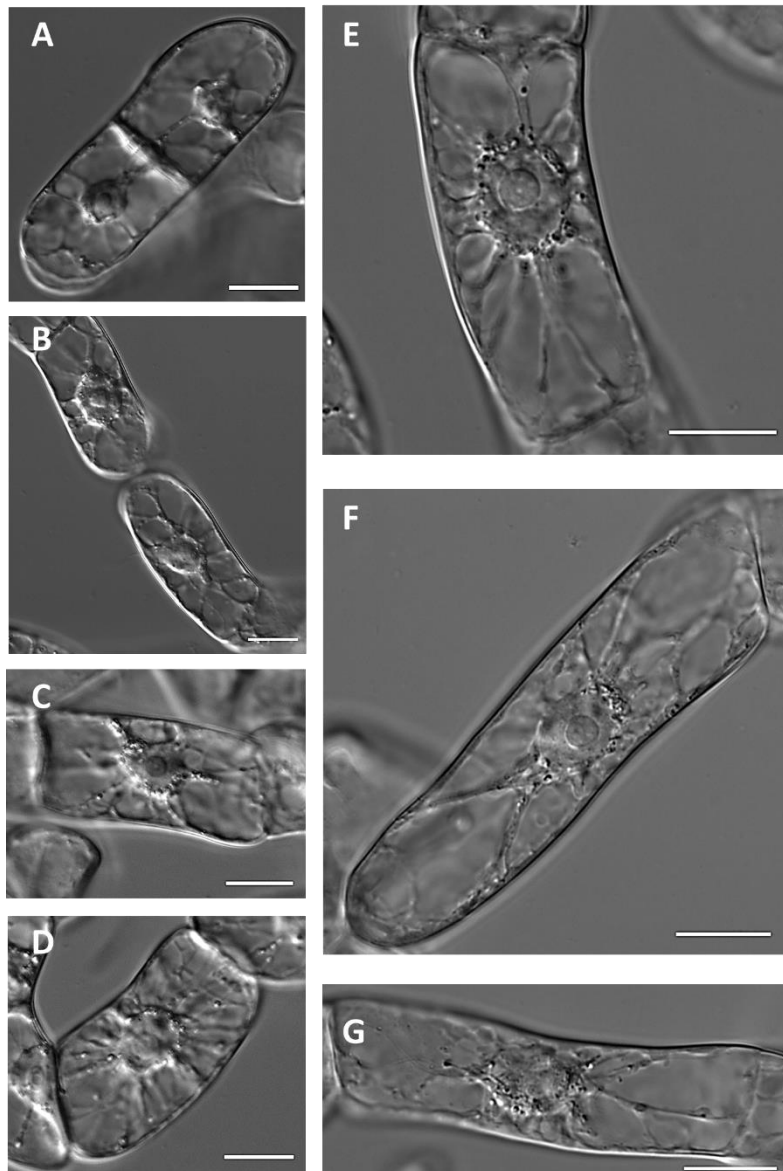


Figure 5.12 Images of BY-2 cells at the peak of proliferation

Representative images of BY-2 cells 3 d after subcultivation (A-G). Nuclei are in the cell center. Scale bars: 20 μm .

5.4 SEM analysis of aligned and unaligned nanofibers

Nanofibers were kindly provided by Dr. Renee Goreham from The Alan MacDiarmid Institute, School of Chemical and Physical Sciences; Victoria University of Wellington, New Zealand.

After producing the nanofibers, they were investigated by Dr. Renee Gorham via an electron microscope as described in the following: “The morphology and composition of the electrospun nanofibers were examined by scanning electron microscopy (SEM) using a JEOL 6500 F field-emission scanning electron microscope equipped with an energy-dispersive spectroscopy (EDS) analysis system. Individual fibers mats were mounted on aluminum specimen stubs with double-sided carbon adhesive tape and sputter-coated, first with a platinum layer and then carbon, to provide a conductive layer in order to reduce the build-up of charges on the surface of the sample. The samples were viewed at sequential magnifications under secondary electron and backscatter conditions.”

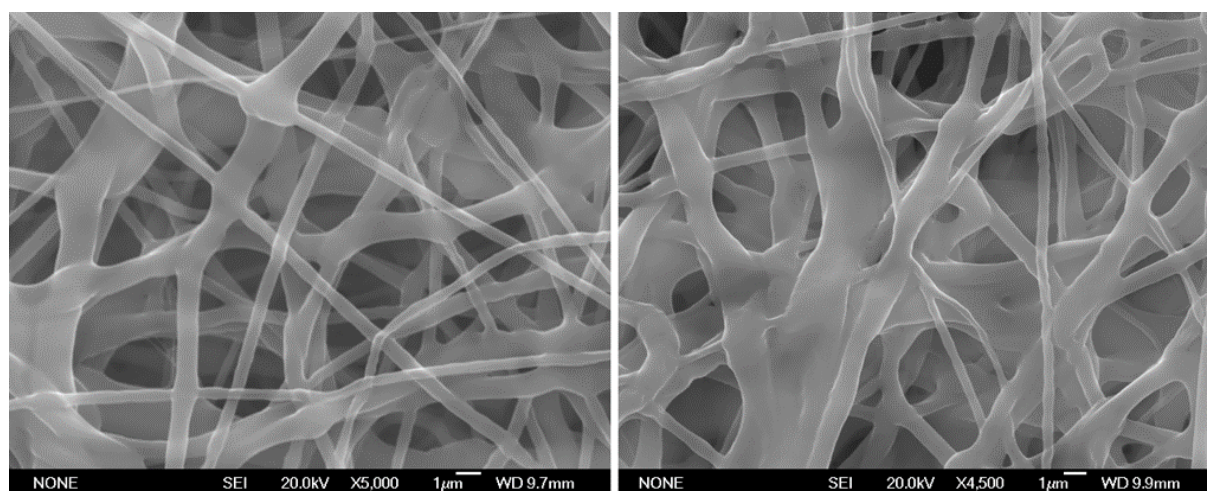


Figure 5.13 SEM images of nanofiber structures

SEM images at 5000x magnification of the nanofiber structures produced using the 12% solution of PCL at 21 kV (left) and 15 kV (right). Note the belt-formation in the bottom left quadrant of the 15 kV image.

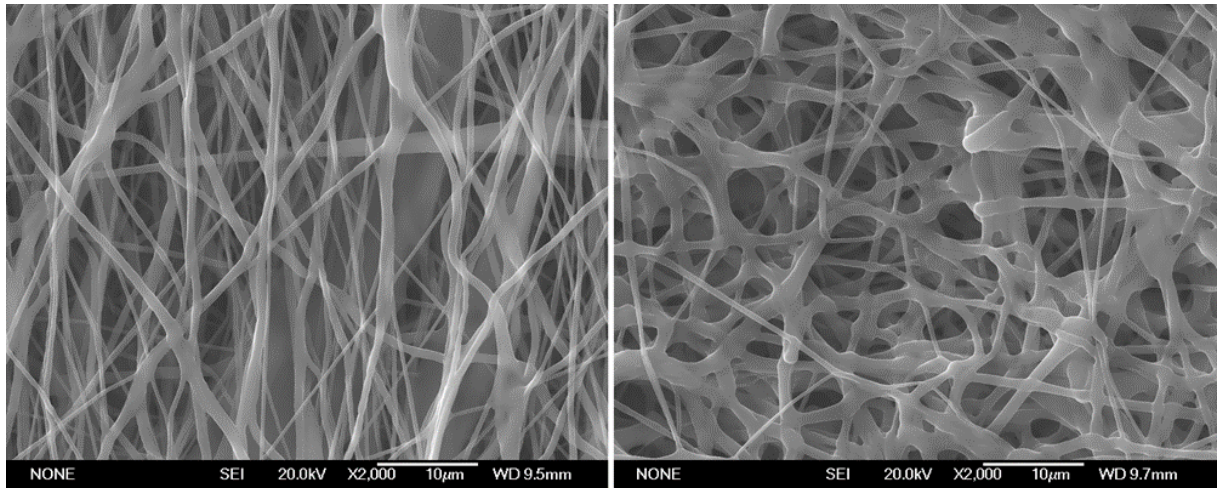


Figure 5.14 SEM images of aligned nanofiber structures

SEM images at 2000x magnification demonstrating the alignment of nanofibers produced using a rotational speed of 1400 rpm (left) and 140 rpm (right). Note the general up/down alignment generated using the higher rotational speed.

5.5 ECHO research – Four key players, three kingdoms, two mechanisms, one concept

The role of four key players, which are the extracellular matrix, cytoskeleton, hormones and other molecules, and organelles (short: ECHO) is explored for three kingdoms (animals, plants and fungi) in the background of a combination of mechanically and chemically driven mechanisms leading to the so-called ECHO-concept of cell polarity. The idea of ECHO illustrates also the retrograde behavior of the cellular signaling.

Table A 5.3 Overview of the ECHO concept of cell polarity in eukaryotic kingdoms

Left to right are the representative proteins of the respective key player (top down: extracellular matrix, cytoskeleton, hormones and other signaling molecules, organelles) found in animals (red), plants (green) and fungi (blue). Additionally, corresponding literature is given in brackets.

FAKTORS	ANEMALIA	PLANT	FUNGI
EXTRACELLULAR MATRIX	Fibronectin recognized by Integrin, ECM (Autenrieth <i>et al.</i> 2016)	RGD motif recognition and ECM like structures (Liu <i>et al.</i> 2015)	ECM recognition by integrin like structures (Cornillon <i>et al.</i> 2006)
CYTOSKELETON	AF, MT, intermediate filaments, dynein, kinesin, myosin nuclear lamina (Ingber 2003 a+b)	MT, AF, kinesin and minus-end directed kinesins, myosin, nuclear basket (Nick 2011)	AF, MT, myosin, dynein, kinesin (Manck <i>et al.</i> 2015)
HORMONES AND OTHER SIGNALING MOLECULES	PAR, SCRIBBLE, CRUMBS, CDC42. Rho GTPase (Mazel 2017)	Auxin and PIN (Nick 2010) RAP	PAR, TEA, CDC42, Rho, polarity factors (Mata and Nurse 1997)
ORGANELLES	ER, centriole, nucleus, Golgi apparatus (Gomes <i>et al.</i> 2005)	plastids, (Delfosse <i>et al.</i> 2015) nuclear migration (indirect)	probably nucleus (Fischer 1999)

5.6 Supplemental experimental procedure

Method for growing *Arabidopsis* seeds and subsequent imaging

Seeds from Lifact-mEos *Arabidopsis thaliana* were kindly provided by Dr. Jaideep Mathur at the UoG.

Stable transgenic lines were generated using *Agrobacterium tumefaciens* (strain GV3101)-mediated floral dip transformation (Clough and Bent 1998).

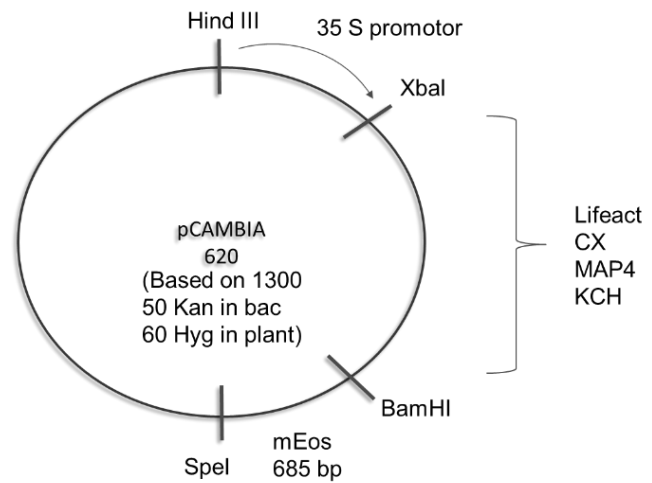


Figure 5.15 Construct

pCambia with fluorescent mEos protein and BamHI and XbaI gateway to insert requested Lifact, CX, MAP4 or KCH under control of a 35 S promoter

Method for growing the seeds was adopted from J. Mathur:

Seeds were grown on 1% agar-gelled Murashige and Skoog 1962 medium supplemented with 3% sucrose and with pH 5.8. Plants were raised in a growth chamber at 21°C and a 16 h/8 h light/dark regime using cool-white light at 80 to 100 $\mu\text{mol m}^{-2} \text{s}^{-1}$.

Microscopy and imaging following instructions from J. Mathur:

Images were taken via 40x/0.8 water-immersion objective under a Leica TCS-SP5 confocal laser-scanning microscope with a 488-nm argon laser and a 543-nm helium-neon laser. Fluorescence emission collection was at 490 to 510 nm for GFP, 570 to 620 nm for RFP, and 626 to 763 nm for chlorophyll. Photoconversion of mEos was performed manually by controlling the diaphragm on the Leica DM6000CS microscope and using the epifluorescent lighting through a D filter cube (Leica UV/violet; Ex, BP 355–425; dichroic, 455; Em, LP 470 nm).

Data analysis according to Mathur *et al.* 2010 and Wozny *et al.* 2012:

The RGB values can be calculated on a standard eight-bit scale of 0 to 255 stretching across the region of interest (ROI) and analyzed via the RGB profiler (<http://rsbweb.nih.gov/ij/plugins/rgb-profiler.html>) plug-ins from ImageJ version 1.40g (<http://rsbweb.nih.gov/ij/>). For every time point the RGB value was calculated and subsequently plotted over time.

6 ACKNOWLEDGEMENTS

This work was supported by the Landesgraduiertenförderung (LGF) PhD fellowship of the state of Baden-Württemberg for two years.

The stay at the University of Guelph in Canada was funded by the Research Travel Grant of the Karlsruhe House of Young Scientists (KHYS) of the KIT.

For all the support during my stay in Canada and the provided constructs and seeds I would like to thank Dr. Jaideep Mathur from the Department of Molecular Cell Biology at the University of Guelph.

The proteomics were performed by Dr. Achim Treumann and Dr. Andrew Porter from the Department of Proteomics and Proteome analysis, Newcastle University, UK.

Nanofibered RGD structures were provided by Prof. Dr. Thomas Nann and Dr. Renee Goreham from the Alan MacDiarmid Institute, Victoria University of Wellington, New Zealand.

Further, I would like to thank the Deutsche Forschungsgemeinschaft (DFG) for funding my publication "Break of symmetry in regenerating tobacco protoplasts is independent of nuclear positioning".

7 REFERENCES

- Ahmad K, Henikoff S (2002)** Histone H3 variants specify modes of chromatin assembly. *Proc Natl Acad Sci* 99: 16477-16484.
- Akhmanova A, Steinmetz MO (2015)** Control of microtubule organization and dynamics: Two ends in the limelight. *Nat Rev Mol Cell Biol.* 16:711–726.
- Akhtar N, Streuli CH (2013)** An integrin-ILK-microtubule network orients cell polarity and lumen formation in glandular epithelium. *Nat Cell Biol.* 15:17–27.
- Akkerman M, Overdijk EJR, Schel JHN, Emons AMC, Ketelaar T (2011)** Golgi body motility in the plant cell cortex correlates with actin cytoskeleton organization. *Plant Cell Physiol.* 52:1844–1855.
- Autenrieth TJ, Frank SC, Greiner AM, Klumpp D, Richter B, Hauser M, Lee S-I, Levine J, Bastmeyer M (2016)** Actomyosin contractility and RhoGTPases affect cell-polarity and directional migration during haptotaxis. *Integr Biol (Camb).* 8:1067–1078.
- Avisar D, Prokhnevsky AI, Makarova KS, Koonin EV, Dolja VV (2008)** Myosin XI-K Is Required for Rapid Trafficking of Golgi Stacks, Peroxisomes, and Mitochondria in Leaf Cells of *Nicotiana benthamiana*1WOA. *Plant Physiol.* 146:1098–1108.
- Axelrod D, Koppel DE, Schlessinger J, Elson E, Webb WW (1976)** Mobility measurement by analysis of fluorescence photobleaching recovery kinetics. *Biophys J.* 16:1055–1069.
- Azimifar SB, Nagaraj N, Cox J, Mann M (2014)** Cell-type-resolved quantitative proteomics of murine liver. *Cell Metab.* 20:1076–1087.
- Baluška F, Samaj J, Wojtaszek P, Volkmann D, Menzel D (2003)** Cytoskeleton-plasma membrane-cell wall continuum in plants. Emerging links revisited. *Plant Physiol.* 133:482–491.
- Bartova E, Krejci J, Harnicarova A, Galiova G, Kozubek S (2008)** Histone modifications and nuclear architecture: a review. *J Histochem Cytochem* 56: 711-721.
- Billadeau DD, Nolz JC, Gomez TS (2007)** Regulation of T-cell activation by the cytoskeleton. *Nat Rev Immunol* 7:131–143.
- Bombardelli L, Carpenter ES, Wu AP, Alston N, DelGiorno KE, Crawford HC (2010)** Pancreas-specific ablation of beta1 integrin induces tissue degeneration by disrupting acinar cell polarity. *Gastroenterology.* 138:2531-40.

- Buchnik L, Abu-Abied M, Sadot E (2015)** Role of plant myosins in motile organelles: Is a direct interaction required? *J Integr Plant Biol* 57:23–30.
- Calikowski TT, Meulia T, Meier I (2003)** A proteomic study of the arabidopsis nuclear matrix. *J Cell Biochem* 90:361–378.
- Chen T, Teng N, Wu X, Wang Y, Tang W, Samaj J, Baluska F, Lin J (2007)** Disruption of actin filaments by latrunculin B affects cell wall construction in *Picea meyeri* pollen tube by disturbing vesicle trafficking. *Plant Cell Physiol* 48:19–30.
- Clough SJ, Bent AF (1998)** Floral dip: A simplified method for *Agrobacterium*-mediated transformation of *Arabidopsis thaliana*. *Plant J.* 16:735–743.
- Collings DA, Carter CN, Rink JC, Scott AC, Wyatt SE, Allen NS (2000)** Plant nuclei can contain extensive grooves and invaginations. *Plant Cell* 12: 2425-2440.
- Cornillon S, Gebbie L, Benghezal M, Nair P, Keller S, Wehrle-Haller B, Charette SJ, Brückert F, Letourneur F, Cosson P (2006)** An adhesion molecule in free-living *Dictyostelium* amoebae with integrin beta features. *EMBO Rep.* 7:617–621.
- Cox J, Mann M (2008)** MaxQuant enables high peptide identification rates, individualized p.p.b.-range mass accuracies and proteome-wide protein quantification. *Nat Biotechnol.* 26:1367–1372.
- Cremer T, Cremer M (2010)** Chromosome territories. *Cold Spring Harb Perspect Biol* 2:1-22.
- Crisp M, Liu Q, Roux K, Rattner JB, Shanahan C, Burke B, Stahl PD, Hodzic D (2006)** Coupling of the nucleus and cytoplasm: Role of the LINC complex. *J Cell Biol* 172:41–53.
- Crowell EF, Bischoff V, Desprez T, Rolland A, Stierhof Y-D, Schumacher K, Gonneau M, Höfte H, Vernhettes S (2009)** Pausing of Golgi Bodies on Microtubules Regulates Secretion of Cellulose Synthase Complexes in *Arabidopsis* W. *The plant cell* 21:1141–1154.
- Cvrčková F, Oulehlová D, Žárský V (2014)** Formins: Linking cytoskeleton and endomembranes in plant cells. *Int J Mol Sci.* 16:1–18.
- Cvrčková F, Oulehlová D (2017)** A new kymogram-based method reveals unexpected effects of marker protein expression and spatial anisotropy of cytoskeletal dynamics in plant cell cortex. *Plant Methods.* 13:19.
- Deal RB, Henikoff S (2011)** Histone variants and modifications in plant gene regulation. *Curr Opin Plant Biol* 14: 116-122.

- Delfosse K, Wozny MR, Jaipargas E-A, Barton KA, Anderson C, Mathur J (2015)** Fluorescent Protein Aided Insights on Plastids and their Extensions: A Critical Appraisal. *Front Plant Sci.* 6:1253.
- Dubas E, Custers J, Kieft H, Wędzony M, van Lammeren AAM (2014)** Characterization of polarity development through 2- and 3-D imaging during the initial phase of microspore embryogenesis in *Brassica napus* L. *Protoplasma.* 251:103–113.
- Durst S, Hedde PN, Brochhausen L, Nick P, Nienhaus GU, Maisch J (2014)** Organization of perinuclear actin in live tobacco cells observed by PALM with optical sectioning. *J Plant Physiol* 171: 97-108.
- Ellenbroek SIJ, Iden S, Collard JG (2012)** The Rac activator Tiam1 is required for polarized protrusional outgrowth of primary astrocytes by affecting the organization of the microtubule network. *Small GTPases.* 3:4–14.
- Etienne-Manneville S, Hall A (2001)** Integrin-mediated activation of Cdc42 controls cell polarity in migrating astrocytes through PKCzeta. *Cell.* 106:489–498.
- Fischer R (1999)** Nuclear movement in filamentous fungi. *FEMS Microbiol Rev.* 23:39–68.
- Fransz PF, de Jong JH (2002)** Chromatin dynamics in plants. *Curr Opin Plant Biol* 5: 560-567.
- Frey N, Klotz J, Nick P (2009)** Dynamic bridges--a calponin-domain kinesin from rice links actin filaments and microtubules in both cycling and non-cycling cells. *Plant Cell Physiol.* 50:1493–1506.
- Frey N, Klotz J, Nick P (2010)** A kinesin with calponin-homology domain is involved in premitotic nuclear migration. *J Exp Bot* 61: 3423-3437.
- Fuchs J. (2011)** Characterization and application of photoswitchable fluorescent proteins for nanoscopy. Karlsruhe, Germany: Karlsruhe Institute of Technology [PhDthesis].
- Goldman RD, Gruenbaum Y, Moir RD, Shumaker DK, Spann TP (2002)** Nuclear lamins: building blocks of nuclear architecture. *Genes Dev* 16: 533-547.
- Gomes ER, Jani S, Gundersen GG (2005)** Nuclear movement regulated by Cdc42, MRCK, myosin, and actin flow establishes MTOC polarization in migrating cells. *Cell.* 121:451–463.
- Goodner B, Quatrano RS (1993)** Fucus embryogenesis: A model to study the establishment of polarity. *Plant Cell* 5: 1471-1481.
- Green PB (1980)** Organogenesis - a biophysical view. *Ann Rev Plant Physiol.* 31: 51-82.

- Griffis AH, Groves NR, Zhou X, Meier I (2014)** Nuclei in motion: movement and positioning of plant nuclei in development, signaling, symbiosis, and disease. *Front Plant Sci* 5: 129.
- Gutierrez R, Lindeboom JJ, Paredez AR, Emons AMC, Ehrhardt DW (2009)** Arabidopsis cortical microtubules position cellulose synthase delivery to the plasma membrane and interact with cellulose synthase trafficking compartments. *Nat Cell Biol.* 11:797–806.
- Hable WE, Hart PE (2010)** Signaling mechanisms in the establishment of plant and fucoid algal polarity. *Mol Reprod Dev* 77: 751-758.
- Hu Y, Zhong R, Morrison WH3, Ye Z-H (2003)** The Arabidopsis RHD3 gene is required for cell wall biosynthesis and actin organization. *Planta.* 217:912–921.
- Ingber DE (2003a)** Tensegrity I. Cell structure and hierarchical systems biology. *J Cell Sci.* 116:1157–1173.
- Ingber DE (2003b)** Tensegrity II. How structural networks influence cellular information processing networks. *J Cell Sci.* 116:1397–1408.
- Jiang D, Berger F (2017)** Histone variants in plant transcriptional regulation. *Biochim Biophys Acta.* 1860:123–130.
- Katsuta J, Shibaoka H (1988)** The Roles of the cytoskeleton and the cell-wall in nuclear positioning in tobacco BY-2 cells. *Plant Cell Physiol* 29: 403-413.
- Khan M, Takasaki H, Komatsu S (2005)** Comprehensive phosphoproteome analysis in rice and identification of phosphoproteins responsive to different hormones/stresses. *J Proteome Res.* 4:1592–1599.
- Klotz J, Nick P (2012)** A novel actin-microtubule cross-linking kinesin, NtKCH, functions in cell expansion and division. *New Phytol* 193: 576-589.
- Kouzarides T (2007)** Chromatin modifications and their function. *Cell* 128: 693-705.
- Kühn S, Liu Q, Eing C, Wüstner R, Nick P (2013)** Nanosecond electric pulses target to a plant-specific kinesin at the plasma membrane. *J Membr Biol* 246: 927-938.
- Kuss-Wymer CL, Cyr RJ (1992)** Tobacco protoplasts differentiate into elongate cells without net microtubule depolymerization. *Protoplasma* 168: 64-72.
- Laemmli UK (1970)** Cleavage of structural proteins during the assembly of the head of bacteriophage T4. *Nature.* 227:680–685.
- Langhans M, Weber W, Babel L, Grunewald M, Meckel T (2017)** The right motifs for plant cell adhesion: What makes an adhesive site? *Protoplasma.* 254:95–108.

- Lee JL, Streuli CH (2014)** Integrins and epithelial cell polarity. *J Cell Sci.* 127:3217–3225.
- Lee KK, Starr D, Cohen M, Liu J, Han M, Wilson KL, Gruenbaum Y (2002)** Lamin dependent localization of UNC-84, a protein required for nuclear migration in *Caenorhabditis elegans*. *Mol Biol Cell* 13: 892-901.
- Lee M, Vasioukhin V (2008)** Cell polarity and cancer--cell and tissue polarity as a non-canonical tumor suppressor. *J Cell Sci.* 121:1141–1150.
- Lee SH, Dominguez R (2010)** Regulation of actin cytoskeleton dynamics in cells. *Mol Cells.* 29:311–325.
- Lenartowska M, Michalska A (2008)** Actin filament organization and polarity in pollen tubes revealed by myosin II subfragment 1 decoration. *Planta.* 228:891–896.
- Li X, Clarke K, Li K, Chen A (2012)** The pattern of cell wall deterioration in lignocellulose fibers throughout enzymatic cellulose hydrolysis. *Biotechnol Prog.* 28:1389–1399.
- Lipka V, Panstruga R (2005)** Dynamic cellular responses in plant-microbe interactions. *Curr Opin Plant Biol.* 8:625–631.
- Liu Z, Persson S, Zhang Y (2015)** The connection of cytoskeletal network with plasma membrane and the cell wall. *J Integr Plant Biol.* 57:330–340.
- Lyczak R, Gomes J-E, Bowerman B (2002)** Heads or tails: Cell polarity and axis formation in the early *Caenorhabditis elegans* embryo. *Dev Cell.* 3:157–166.
- Madden K, Snyder M (1998)** Cell polarity and morphogenesis in budding yeast. *Annu Rev Microbiol.* 52:687–744.
- Maeda H, Ishida N (1967)** Specificity of binding of hexopyranosyl polysaccharides with fluorescent brightener. *J Biochem* 62: 276-278.
- Maisch J, Nick P (2007)** Actin is involved in auxin-dependent patterning. *Plant Physiol.* 143:1695–1704.
- Maisch J, Fiserová J, Fischer L, Nick P (2009)** Tobacco Arp3 is localized to actin-nucleating sites in vivo. *J Exp Bot.* 60:603–614.
- Malone CJ, Fixsen WD, Horvitz HR, Han M (1999)** UNC-84 localizes to the nuclear envelope and is required for nuclear migration and anchoring during *C. elegans* development. *Development* 126: 3171-3181.
- Manck R, Ishitsuka Y, Herrero S, Takeshita N, Nienhaus GU, Fischer R (2015)** Genetic evidence for a microtubule-capture mechanism during polarised growth of *Aspergillus nidulans*. *J Cell Sci.* 128:3569–3582.

- Mata J, Nurse P (1997)** tea1 and the microtubular cytoskeleton are important for generating global spatial order within the fission yeast cell. *Cell*. 89:939–949.
- Mathur J, Radhamony R, Sinclair AM, Donoso A, Dunn N, Roach E, Radford D, Mohaghegh PSM, Logan DC, Kokolic K, Mathur N (2010)** mEosFP-based green-to-red photoconvertible subcellular probes for plants. *Plant Physiol*. 154:1573–1587.
- Mattanavee W, Suwantong O, Puthong S, Bunaprasert T, Hoven VP, Supaphol P (2009)** Immobilization of biomolecules on the surface of electrospun polycaprolactone fibrous scaffolds for tissue engineering. *ACS Appl Mater Interfaces*. 1:1076–1085.
- Mazel T. (2017)** Crosstalk of cell polarity signaling pathways. *Protoplasma*. 254:1241–1258.
- Mimori-Kiyosue Y, Shiina N, Tsukita S (2000)** The dynamic behavior of the APC-binding protein EB1 on the distal ends of microtubules. *Curr Biol*. 10:865–868.
- Mondal K, Sharma A (2016)** Recent advances in electrospun metal-oxide nanofiber based interfaces for electrochemical biosensing. *RSC Adv*. 6:94595–94616.
- Morris NR (2000)** Nuclear migration: From fungi to the mammalian brain. *J Cell Biol* 148: 1097-1101.
- Morris NR (2003)** Nuclear positioning: the means is at the ends. *Curr Opin Cell Biol* 15: 54-59.
- Murashige T, Skoog F (1962)** A Revised Medium for Rapid Growth and Bio Assays with Tobacco Tissue Cultures. *Physiol Plant*. 15:473–497.
- Nagata T, Takebe I (1970)** Cell wall regeneration and cell division in isolated tobacco mesophyll protoplasts. *Planta* 92: 301-308.
- Nagata T, Nemoto Y, Hasezawa S (1992)** Tobacco BY-2 cell line as the "HeLa" cell in the cell biology of higher plants. *Int Rev Cytol* 132: 1-30.
- Nebenführ A, Gallagher LA, Dunahay TG, Frohlick JA, Mazurkiewicz AM, Meehl JB, Staehelin LA (1999)** Stop-and-go movements of plant Golgi stacks are mediated by the actomyosin system. *Plant Physiol*. 121:1127–1142.
- Nick P, Furuya M (1992)** Induction and fixation of polarity - Early steps in plant morphogenesis. *Dev Growth Differ* 34: 115-125.
- Nick P (2008)** Control of cell axis. *Plant Cell Monographs*. Springer-Verlag, Berlin Heidelberg. pp. 3-46.
- Nick P (2010)** Probing the actin-auxin oscillator. *Plant Signal Behav* 5, 94-98.

- Nick P (2011)** Mechanics of the cytoskeleton. In: P. Wojtaszek, ed. *Mechanical Integration of Plant Cells and Plants*. Springer-Verlag, Berlin-Heidelberg. pp. 53-90.
- Nick P (2013)** Microtubules, signalling and abiotic stress. *Plant J.* 75:309–323.
- Paredez AR, Somerville CR, Ehrhardt DW (2006)** Visualization of cellulose synthase demonstrates functional association with microtubules. *Science.* 312:1491–1495.
- Park E, Nebenführ A (2013)** Myosin XIK of *Arabidopsis thaliana* accumulates at the root hair tip and is required for fast root hair growth. *PLoS ONE.* 8:e76745.
- Peremyslov VV, Prokhnevsky AI, Dolja VV (2010)** Class XI myosins are required for development, cell expansion, and F-Actin organization in *Arabidopsis*. *The plant cell.* 22:1883–1897.
- Peremyslov VV, Morgun EA, Kurth EG, Makarova KS, Koonin EV, Dolja VV (2013)** Identification of myosin XI receptors in *Arabidopsis* defines a distinct class of transport vesicles. *The plant cell.* 25:3022–3038.
- Petrovska B, Sebela M, Dolezel J (2015)** Inside a plant nucleus: Discovering the proteins. *J Exp Bot.* 66:1627–1640.
- Preston RD (1955)** Mechanical properties of the plant cell wall. In: W. Ruhland, ed. *Handbuch der Pflanzenphysiologie* vol. 1. Springer-Verlag, Berlin-Göttingen Heidelberg. pp. 745-751.
- Qiao F, Chang X-L, Nick P (2010)** The cytoskeleton enhances gene expression in the response to the Harpin elicitor in grapevine. *J Exp Bot.* 61:4021–4031.
- Razafsky D, Hodzic D (2009)** Bringing KASH under the SUN: The many faces of nucleocytoskeletal connections. *J Cell Biol.* 186:461–472.
- Roignot J, Peng X, Mostov K (2013)** Polarity in mammalian epithelial morphogenesis. *Cold Spring Harb Perspect Biol.* 5.
- Rooney N, Streuli CH (2011)** How integrins control mammary epithelial differentiation: A possible role for the ILK-PINCH-Parvin complex. *FEBS Lett.* 585:1663–1672.
- Rosa S, Shaw P (2013)** Insights into chromatin structure and dynamics in plants. *Biology (Basel).* 2:1378–1410.
- Sampathkumar A, Gutierrez R, McFarlane HE, Bringmann M, Lindeboom J, Emons A-M, Samuels L, Ketelaar T, Ehrhardt DW, Persson S (2013)** Patterning and Lifetime of Plasma Membrane-Localized Cellulose Synthase Is Dependent on Actin Organization in *Arabidopsis* Interphase Cells1W. *Plant Physiol.* 162:675–688.

- Saxena PK, Fowke LC, King J (1985)** An Efficient Procedure for Isolation of Nuclei from Plant Protoplasts. *Protoplasma* 128: 184-189
- Schierenberg E (1987)** Reversal of cellular polarity and early cell-cell interaction in the embryos of *Caenorhabditis elegans*. *Dev Biol.* 122:452–463.
- Schmelzer E (2002)** Cell polarization, a crucial process in fungal defence. *Trends Plant Sci.* 7:411–415. eng.
- Schneider M, Noegel AA, Karakesisoglou I (2008)** KASH-domain proteins and the cytoskeletal landscapes of the nuclear envelope. *Biochem Soc Trans.* 36:1368–1372.
- Schneider N, Ludwig H, Nick P (2015)** Suppression of tubulin detyrosination by parthenolide recruits the plant-specific kinesin KCH to cortical microtubules. *J Exp Bot* 66: 2001-2011.
- Schneider R, Persson S (2015)** Connecting two arrays: the emerging role of actin microtubule cross-linking motor proteins. *Front Plant Sci* 6: 415.
- Shao X, Li Q, Mogilner A, Bershadsky AD, Shivashankar GV (2015)** Mechanical stimulation induces formin-dependent assembly of a perinuclear actin rim. *Proc Natl Acad Sci* 112: 2595-2601.
- Smertenko A, Franklin-Tong VE (2011)** Organisation and regulation of the cytoskeleton in plant programmed cell death. *Cell Death Differ.* 18:1263–1270.
- Smith CM, Haimberger ZW, Johnson CO, Wolf AJ, Gafken PR, Zhang ZL, Parthun MR, Gottschling DE (2002)** Heritable chromatin structure: Mapping "memory" in histones H3 and H4. *Proc Natl Acad Sci* 99: 16454-16461.
- Smith LG (2001)** Plant cell division: Building walls in the right places. *Nat Rev Mol Cell Bio* 2: 33-39.
- St Johnston D, Nüsslein-Volhard C (1992)** The origin of pattern and polarity in the *Drosophila* embryo. *Cell.* 68:201–219.
- Staiger CJ, Poulter NS, Henty JL, Franklin-Tong VE, Blanchoin L (2010)** Regulation of actin dynamics by actin-binding proteins in pollen. *J Exp Bot.* 61:1969–1986.
- Starr DA (2009)** A nuclear-envelope bridge positions nuclei and moves chromosomes. *J Cell Sci.* 122:577–586.
- Starr DA (2011)** KASH and SUN proteins. *Curr Biol.* 21:R414-5
- Talbert PB, Masuelli R, Tyagi AP, Comai L, Henikoff S (2002)** Centromeric localization and adaptive evolution of an Arabidopsis histone H3 variant. *Plant Cell* 14: 1053-1066.

- Tamura K, Iwabuchi K, Fukao Y, Kondo M, Okamoto K, Ueda H, Nishimura M, Hara-Nishimura I. (2013)** Myosin XI-i links the nuclear membrane to the cytoskeleton to control nuclear movement and shape in Arabidopsis. *Curr Biol.* 23:1776–1781.
- Taniura H, Glass C, Gerace L (1995)** A chromatin binding site in the tail domain of nuclear lamins that interacts with core histones. *J Cell Biol* 131: 33-44.
- Tominaga M, Kojima H, Yokota E, Orii H, Nakamori R, Katayama E, Anson M, Shimmen T, Oiwa K. (2003)** Higher plant myosin XI moves processively on actin with 35 nm steps at high velocity. *EMBO J.* 22:1263–1272.
- Tyanova S, Temu T, Sinitcyn P, Carlson A, Hein MY, Geiger T, Mann M, Cox J (2016)** The Perseus computational platform for comprehensive analysis of (prote)omics data. *Nat Methods.* 13:731–740.
- Ueda H, Yokota E, Kutsuna N, Shimada T, Tamura K, Shimmen T, Hasezawa S, Dolja VV, Hara-Nishimura I (2010)** Myosin-dependent endoplasmic reticulum motility and F-actin organization in plant cells. *Proc Natl Acad Sci U S A.* 107:6894–6899.
- UniProt: The universal protein knowledgebase (2017)** *Nucleic Acids Res.* 45:D158-D169.
- Verbsky ML, Richards EJ (2001)** Chromatin remodeling in plants. *Curr Opin Plant Biol* 4: 494-500.
- Verde F, Mata J, Nurse P (1995)** Fission yeast cell morphogenesis: Identification of new genes and analysis of their role during the cell cycle. *J Cell Biol.* 131:1529–1538.
- Vidali L, Burkart GM, Augustine RC, Kerdavid E, Tüzel E, Bezanilla M (2010)** Myosin XI is essential for tip growth in *Physcomitrella patens*. *The plant cell.* 22:1868–1882.
- Vöchting H. (1878)** Über Organbildung im Pflanzenreich: Physiologische Untersuchungen über Wachstumsursachen und Lebenseinheiten. Bonn: Cohen.
- Wang QY, Nick P (1998)** The auxin response of actin is altered in the rice mutant Yin-Yang. *Protoplasma* 204: 22-33.
- Wiesler B, Wang QY, Nick P (2002)** The stability of cortical microtubules depends on their orientation. *Plant J* 32: 1023-1032.
- Wightman R, Turner SR (2008)** The roles of the cytoskeleton during cellulose deposition at the secondary cell wall. *Plant J.* 54:794–805.
- Wilhelmsen K, Ketema M, Truong H, Sonnenberg A (2006)** KASH-domain proteins in nuclear migration, anchorage and other processes. *J Cell Sci.* 119:5021–5029.

References

- Wodarz A, Nathke I (2007)** Cell polarity in development and cancer. *Nat Cell Biol.* 9:1016–1024.
- Wozny M, Schattat MH, Mathur N, Barton K, Mathur J (2012)** Color recovery after photoconversion of H2B::mEosFP allows detection of increased nuclear DNA content in developing plant cells. *Plant Physiol* 158: 95-106.
- Yi H, Sardesai N, Fujinuma T, Chan CW, Veena, Gelvin SB (2006)** Constitutive expression exposes functional redundancy between the Arabidopsis histone H2A gene HTA1 and other H2A gene family members. *Plant Cell* 18: 1575-1589.
- Yuan S, Xiong G, Wang X, Zhang S, Choong C (2012)** Surface modification of polycaprolactone substrates using collagen-conjugated poly(methacrylic acid) brushes for the regulation of cell proliferation and endothelialisation. *J. Mater. Chem.* 22:13039.
- Zaban B, Maisch J, Nick P (2013)** Dynamic actin controls polarity induction de novo in protoplasts. *J Integr Plant Biol* 55: 142-159.
- Zhou X, Graumann K, Evans DE, Meier I (2012)** Novel plant SUN-KASH bridges are involved in RanGAP anchoring and nuclear shape determination. *J Cell Biol.* 196:203–211.
- Zhou X, Meier I (2013)** How plants LINC the SUN to KASH. *Nucleus* 4:206–215.

Publikationen

Durst S, Hedde PN, Brochhausen L, Nick P, Nienhaus GU, Maisch J (2014) Organization of perinuclear actin in live tobacco cells observed by PALM with optical sectioning. *J Plant Physiol* 171: 97-108.

Teile dieser Arbeit wurden publiziert in:

Brochhausen L, Maisch J, Nick P (2016) Break of symmetry in regenerating tobacco protoplasts is independent of nuclear positioning. *J Plant Physiol* 58: 799-812.